DOCTORAL THESIS

Title	**Biodegradable Poly-(*D,L*-lactide) and Poly-(*D,L*-lactide-*co*-glycolide) Nanoparticles for Photodynamic Therapy**
Presented by	**Ester Boix Garriga**
Centre	**IQS School of Engineering**
Department	**Analytical and Applied Chemistry**
Supervised by	**Prof. Santi Nonell Marrugat** **Dr. Mª Lluïsa Sagristá Gratovil**

“Inténtalo. Fracasa.

No importa.

Inténtalo otra vez.

Fracasa de nuevo.

Fracasa mejor.”

Samuel Beckett

“Nuestra gran debilidad es siempre la renuncia.

El único camino cierto para lograrlo es volver a intentarlo una vez más.”

Thomas Alva Edison

“Success consists of going from failure to failure without loss of enthusiasm.”

Winston Churchill

Acknowledgments

Primer de tot vull agrair al Dr. Santi Nonell l'oportunitat d'haver pogut desenvolupar aquesta tesi i d'haver confiat en mi. Gràcies, Santi, per la paciència i dedicació durant aquests anys, per haver-me transmès el teu esperit, qualitat i passió científiques, i també per haver-me ajudat a volar.

També vull agrair a les meves codirectores de tesi, les Dres. Ma Lluïsa Sagristá i Margarita Mora, l'oportunitat d'haver pogut desenvolupar bona part de la meva tesi al seu laboratori i la seva gran ajuda en els camps dels nanovehicles i dels cultius cel·lulars.

I would also like to express my best gratitude to Prof. Ross W. Boyle and Prof. Norbert Lange, for accepting me as a student in their laboratory, for their warm welcome, and for transmitting to me their vast knowledge on synthesis, nanovehicles and photodynamic therapy. A special thanks to Prof. Lange for trusting me and being delighted to accept me for two extra months in his group.

Als Drs. Salvador Borrós, Carlos Semino, Iñaki Borrell, Xavier Batllori, Francesc Broto i Jordi Abellà i a tots els seus col·laboradors i investigadors, que m'han permès utilitzar les seves instal·lacions i els seus equips per poder realitzar certs experiments que sinó no haurien estat possibles. A la Dra. Judith Báguena per tota la confiança dipositada en mi durant les auxiliaries del laboratori de segon. I a la Sra. Núria Ruiz pel seu servei de pesada de mostres i d'espectroscòpia infraroja.

También quiero agradecer a la Dra. Ángeles Villanueva y a todo el equipo de la Universidad Autónoma de Madrid la realización y dedicación en los experimentos de localización subcelular y mecanismo de muerte celular. Gracias también a Pili, cuando viniste a Barcelona y me enseñaste los protocolos de fijación y tinción celular así como a distinguir los distintos mecanismos de muerte celular según la morfología de las células. Gracias a ti y también a Mireia por haberme dado la oportunidad de trabajar con vosotras en el proyecto del 3D, y por haber compartido esos largos días (y noches) de ardua investigación.

Un especial agraïment es mereixen els meus companys de fotoquímica. Als més veterans, Adaya, María i Rubén, gràcies per la vostra paciència i per haver-me ajudat en els meus primers passos en la fotoquímica. I als més "nous", què us he de dir que no sapigueu... Oriol, Bea, Joaquim i Roger, gràcies per omplir el laboratori d'alegria fins i tot en els moments més difícils. Gràcies per haver estat al meu costat i per la vostra incontestable ajuda en innombrables ocasions. I als companys de sala, els "compus", especialment al Roger Estrada, l'Àlex i l'Eli, gràcies per la vostra amistat i companyerisme.

Als companys del laboratori de Vehiculització de Fàrmacs de la UB, Ana, Begoña, Fèlix i Joan Carles. Moltes gràcies per la vostra càlida acollida al laboratori i la vostra ajuda en els moments necessaris. Sense vosaltres aquest camí hagués estat molt més difícil.

I would also like to thank my labmates from the laboratories where I have developed my internships. Dr. Francesca Bryden, thank you very much for having taught me all your expertise in the synthesis of porphyrins and their conjugation to biological molecules, and thank you as well for helping me over the distance with the synthetic procedures concerning our collaboration. Thank you as well to you, Lauren and Louis for having readily accepted me in your lab, and specially, for helping me with the moving rooms at the beginning of my stay ☺. I would also like to thank Ms Huguette Savoie for her valuable help in gel electrophoresis as well as in her disposition to complete some additional experiments regarding the nanoparticles with conjugated photosensitizers. A special thanks to Alberto, the colleague of the neighboring lab, for having introduced me to his scientist friends, with whom we shared many lunches and dinners. Another special thanks to Beppe for your support and your help and sharing with me some special moments over the last month in Hull.

To my colleagues in Geneva… what can I say? Thank you all for you warm welcome and your help. Karine, thank you very much for supervising me during my first three months in Geneva. Your expertise but also your scientific mentality have been very valuable to become the scientist who I am now. Andréj, many thanks for shining a light in the synthesis when I was completely stuck and for teaching me some key aspects in product manipulation that have been really helpful. Viktorija, I think there is nothing you do not know yet… an enormous thanks for sharing with me my time in Geneva, for your unconditional friendship and support in the worst moments. I hope this is only the start of a very good relationship. Karolina, you deserve a special acknowledgment as well for having taken care of the last purification step of my conjugates and sending them to Barcelona, and also for all your help during my stay (and our lunches together☺). Jordan, many thanks for our scientific discussions as well as for your unconditional help in the lab. Céline, Nathalie(s), Pierre, Cédric, Tiziana, Katrine, Stella, Christian, Damei, Vineetha, Marco and a long etcetera of colleagues: as I said, many thanks for welcoming me in your group and also in your social life. Merci spécialement à Florence von Ow pour toute l'aide bureaucratique pendant mes séjours à Genève. Thank you as well to Markus, for the special moments shared and for your comprehension during my hard-working period.

Moltes gràcies a la meva amiga de la infància Anna Reche. Buf… quantes coses que hem arribat a passar tu i jo. Sobretot vull agrair-te la paciència i el suport durant tot aquest llarg camí. Tot arriba, i al final t'hauré de donar la raó (tu ja saps de què parlo ☺). A la meva colla d'amics de

Sant Feliu, Caldes, Palau, us vull agrair també l'interès que sempre heu mostrat cap a la meva tesi i els ànims que m'heu donat per seguir endavant. Sempre ajuda sentir-se valorat pels amics. I a l'Arantxa, que tot i que no ens veiem gaire, sé que puc comptar amb tu. Moltes gràcies pel kit per preparar-me pel dia D, m'ha ajudat molt durant aquestes setmanes d'escriptura.

A les meves "noietes" de la UB, especialment a l'Anna i la Nathaly. Gràcies per escoltar-me en els moments en què ho necessitava i per la vostra empenta quan ha estat necessària.

Vull agrair al tango, sí, al tango, haver-me ajudat a canalitzar els moments més durs de la tesi. A mis profesores de tango, en especial a Eugenia Deanna y Silvia Lezcano, que mediante la danza me han enseñado a confiar más en mi misma dentro y fuera del baile. Moltes gràcies també als innumerables amics, coneguts i ballarins que s'han creuat al meu camí durant tot aquest temps. Especialment el trio tanguero, Fina, Hermínia i Sol. Moltíssimes gràcies per la vostra saviesa i experiència i el vostre suport i escolta incondicionals, a més dels viatges i els moments compartits. No sé què hauria fet sense vosaltres. También quiero agradecer a Maxi, Santi, Jordi, Camila y Ana, por haberme sabido comprender. Y a Hugo... gracias por acompañarme en buena parte de este largo viaje. Gracias por las risas, las charlas y todos los momentos compartidos. También por tu escucha y tu comprensión en los momentos más difíciles, y sobre todo tu soporte en estos últimos días. Gracias por estar allí cuando te he necesitado.

També vull agrair a tota la meva família la seva comprensió durant tot aquest temps. I especialment a l'investigador pioner de la família: gràcies Cesc, per saber-me dir les paraules necessàries en els moments clau. Els teus consells m'han ajudat molt a seguir endavant.

I finalment, un dels agraïments més importants és pels meus pares, sense els quals aquesta aventura no hagués estat possible. Crec que mil paraules no serien suficients per agrair-vos tot el que heu fet per mi. Gràcies per confiar en mi, per la vostra paciència i el vostre amor incondicional, per consolar-me en els moments més durs i saber inculcar-me la confiança necessària per tirar endavant. I també per valorar els èxits i poder-los compartir amb mi.

Finalment, esmentar que el desenvolupament d'aquesta tesi ha estat possible gràcies als ajuts predoctoral FPI BES-2011-04412 i projecte CTQ2013-48767-C3-1-R del Ministerio de Economía y Competitividad, així com al suport econòmic de l'Institut Químic de Sarrià, la Universitat Ramon Llull i la Universitat de Barcelona.

ABSTRACT

This thesis reports the study of poly-(*D,L*-lactide-*co*-glycolide) (PLGA) and poly-(*D,L*-lactide) (PLA) nanoparticles and their poly-(ethylene glycol) (PEG)-coated counterparts as delivery systems for photosensitizers in photodynamic therapy.

First, the influence of the polymeric matrix and of the PEG surface coating on the physicochemical, photophysical and photobiological properties of nanoparticle suspensions containing a physically entrapped photosensitizer has been studied. PEG coating confers a higher stability to the nanoparticles in biological media containing serum proteins. Singlet oxygen produced in bare PLGA nanoparticles remains confined within them, while PEG surface coating facilitates singlet oxygen diffusion to the external medium as well as a faster drug release from the nanoparticles. In both cases, the photosensitizer localizes in lysosomes and induces cell death by apoptosis. The phototoxic effect is superior and faster for PEGylated NPs, in agreement with the singlet oxygen observations.

The role of the chemical structure of the photosensitizer on the photophysical and photobiological properties of the colloidal suspensions has been subsequently investigated. Free base photosensitizers aggregate when entrapped in the nanoparticles, whereas metallated ones are incorporated in monomeric form. When the photosensitizers are covalently conjugated to the nanoparticles, their chemical properties influence their localization in the nanoparticles and consequently, the photophysical properties of the suspension, although they remain photophysically active. Physically entrapped photosensitizers are able to induce cell mortality in cells even if they are aggregated in the nanoparticles, while covalently conjugated photosensitizers are not. This drives us to the conclusions that the delivery of the photosensitizer into the cell is crucial to achieve a photodynamic response, and that PEG-PLGA nanoparticles are not internalized by cells but they rather deliver their cargo at the cell surface, which does not occur when the photosensitizer is covalently bound to the nanoparticles.

Finally, we have explored the potential of the active targeting strategy by conjugating the cRGDfK peptide to the surface of the nanoparticles. The presence of a PEG side chain is essential to achieve an enhanced increase in the photosensitizer delivery into the cell, but unfortunately, it does not render a higher phototoxicity to the cells compared to the non-targeted nanoparticles, which suggests that a higher internalization is not the only important factor in the final outcome of photodynamic therapy.

RESUMEN

Esta tesis profundiza en el estudio de nanopartículas de poli-(*D,L*-láctido-*co*-glicólido) (PLGA) o poli-(*D,L*-láctido) (PLA) y sus homólogas recubiertas con polietilenglicol (PEG) como sistemas de vehiculización para fotosensibilizadores empleados en terapia fotodinámica.

En primer lugar se ha investigado la influencia de la matriz polimérica y del recubrimiento superficial con PEG sobre las características fisicoquímicas, fotofísicas y fotobiológicas de suspensiones con un fotosensibilizador atrapado físicamente. El recubrimiento con PEG confiere una mayor estabilidad a las nanopartículas en medio biológico. El oxígeno singlete generado en las nanopartículas de PLGA permanece confinado en su interior, mientras que la presencia de PEG facilita la difusión del oxígeno singlete al medio externo, así como una liberación más rápida del fotosensibilizador. En ambos casos, éste se localiza en los lisosomas en el interior de las células e induce muerte celular por apoptosis, lo que indica que ambos tipos de nanopartículas liberan el fotosensibilizador dentro de la célula. El efecto fototóxico es sin embargo superior y más rápido para las nanopartículas PEGiladas de acuerdo con las observaciones de oxígeno singlete.

El papel de la estructura química del fotosensibilizador en las propiedades fotofísicas y fotobiológicas de las nanopartículas también se ha investigado. Los fotosensibilizadores no metalados se agregan dentro de las nanopartículas, mientras que los metalados restan en forma monomérica. Cuando éstos se unen covalentemente a las nanopartículas, sus propiedades químicas influyen en su localización en las mismas y, en consecuencia, en las propiedades fotofísicas de la suspensión, aunque preservan sus propiedades fotofísicas. Los fotosensibilizadores encapsulados son capaces de inducir mortalidad celular aunque estén agregados dentro de las nanopartículas, mientras que los que están unidos covalentemente no lo son. Este hecho permite concluir que la liberación del fotosensibilizador dentro de la célula es crucial para lograr una respuesta fotodinámica, y que las nanopartículas de PEG-PLGA no son internalizadas por las células, sino que liberan el fotosensibilizador en la superficie celular, lo que no ocurre cuando el fotosensibilizador se une covalentemente a las nanopartículas.

Finalmente, se ha examinado el potencial de la vehiculización activa mediante la conjugación del péptido cRGDfK a la superficie de las nanopartículas. La presencia de PEG es esencial para lograr un mayor aumento en la concentración celular de fotosensibilizador. Sin embargo, dicha mayor concentración no produce una mayor fototoxicidad en comparación con las nanopartículas no marcadas, lo que sugiere que una mayor internalización no es el único factor importante en el resultado final de la terapia fotodinámica.

RESUM

Aquesta tesi aprofundeix en l'estudi de les nanopartícules de poli-(*D, L*-làctid-*co*-glicòlid) (PLGA) o poli-(*D, L*-làctid) (PLA) i les seves nanopartícules homòlogues recobertes amb polietilenglicol (PEG) com a sistemes de vehiculització per fotosensibilitzadors emprats en teràpia fotodinàmica.

En primer lloc s'ha investigat la influència de la matriu polimèrica i del recobriment superficial amb PEG sobre les característiques fisicoquímiques, fotofísiques i fotobiològiques de suspensions amb un fotosensibilitzador atrapat físicament. El recobriment amb PEG confereix una major estabilitat a les nanopartícules en medi biològic. L'oxigen singlet generat en les nanopartícules de PLGA resta confinat en el seu interior, mentre que la presència de PEG facilita la difusió de l'oxigen singlet al medi extern, així com un alliberament més ràpid del fotosensibilitzador. En ambdós casos, el fotosensibilitzador es localitza als lisosomes a l'interior de les cèl·lules i indueix la mort cel·lular per apoptosi, la qual cosa indica que ambdós tipus de nanopartícules alliberen el fotosensibilitzador dins de la cèl·lula. L'efecte fototòxic és tanmateix major i més ràpid per a les nanopartícules PEGilades d'acord amb les observacions d'oxigen singlet.

El paper de l'estructura química del fotosensibilitzador en les propietats fotofísiques i fotobiològiques de les nanopartícules també s'ha investigat. Els fotosensibilitzadors no metal·lats s'agreguen dins de les nanopartícules, mentre que els metal·lats romanen en forma monomèrica. Les seves propietats químiques també influeixen en la seva localització i, en conseqüència, en les propietats fotofísiques de les nanopartícules quan hi estan units covalentment, encara que hi siguin fotofísicament actius. Els fotosensibilitzadors encapsulats són capaços d'induir mortalitat cel·lular encara que estiguin agregats dins de les nanopartícules, mentre que els que estan units covalentment no ho són. Aquest fet permet concloure que l'alliberament del fotosensibilitzador dins de la cèl·lula és crucial per aconseguir una resposta fotodinàmica, i que les nanopartícules de PEG-PLGA no són internalitzades per les cèl·lules sinó que alliberen el fotosensibilitzador en la superfície cel·lular, cosa que no passa quan el fotosensibilitzador s'uneix covalentment a les nanopartícules.

Finalment, s'ha examinat el potencial de la vehiculització activa mitjançant la conjugació del pèptid cRGDfK a la superfície de les nanopartícules. La presència de PEG és essencial per aconseguir un major augment en la concentració cel·lular de fotosensibilitzador. No obstant això, aquesta major concentració no produeix una major fototoxicitat en comparació amb les nanopartícules no marcades, el que suggereix que una major internalització no és l'únic factor important en el resultat final de la teràpia fotodinàmica.

Table of contents

CHAPTER 1

Introduction

A general introduction to the subject of this thesis is given in this chapter, as well as the main objectives of this work. The basis of photodynamic therapy as an anticancer therapy are reviewed, together with the state of art of drug delivery systems applied to this treatment modality, especially centered in poly-(*D,L*-lactide) and poly-(*D,L*-lactide-*co*-glycolide) nanoparticles.

1.1. Photodynamic therapy of cancer: general aspects

According to the WHO estimates in 2012, cancer is the second cause worldwide of human death after cardiovascular diseases.[1,2] Furthermore, it has been estimated that only in 2012 there were 14.1 million new cases and 8.2 million of cancer deaths.[3] These data thus remark the seriousness of this medical condition and urge the scientific community to come up with new drugs or treatment methods capable of decreasing these death rates and improving life quality of patients.

Photodynamic therapy (PDT) is a clinically approved therapeutic modality for the treatment of malignant and non-malignant diseases as well as pathogenic infections. It consists on the administration of a drug, called photosensitizer (PS), followed by light exposure in the presence of oxygen. The combination of these three elements, which are not harmful *per se*, leads to reactive oxygen species (ROS) which ultimately cause cell death via apoptosis, necrosis or autophagy. Moreover, PDT not only exerts its curative effect through direct phototoxicity in tumor cells, but also through damage to tumor vasculature and through an induction of an inflammatory response that can lead to systemic immunity. The contribution of each of these mechanisms in tumor eradication is believed to depend on many variables, among them the type and dose of PS used, the time between PS and light administration, total light dose and its fluence rate or oxygen concentration in the tumor milieu.[4] Clinical studies have shown that PDT can be curative in early stage tumors, can prolong survival of patients with inoperable cancers and can significantly improve quality of life with minimal normal tissue toxicity, negligible systemic effects and lack of intrinsic or acquired resistance mechanisms.

The photodynamic treatment is a 2-stage process: first, the PS is administered to the patient either systemically or locally, in the absence of light, and is left certain time to accumulate in tumor tissue. When the ratio between PS concentration in malignant tissue respect to that in healthy tissue is considered to be maximal, light of appropriate wavelength and dose is delivered to the specific tumor area.[5] Selectivity of the treatment is thus achieved by specific PS accumulation into the tumor and localized light delivery. In fact, how and why the PS accumulates at the tumor tissue is not completely understood yet, although it is believed to be mainly a combination of receptor-mediated uptake, which internalizes the circulating PS, and the leaky neovasculature present in tumors, which fails to clear the PS from the tumor.[6] In spite of these mechanisms, many PSs tend to accumulate as well in neighboring healthy tissue and skin epithelium, causing unnecessary damage or long-lasting skin photosensitivity upon illumination as common side effects. Therefore, new agents with higher selectivity are needed.

Another current limitation of PDT is the poor penetration of light in biological tissues and skin. Blue light scarcely penetrates the tissue whereas red and near infrared (NIR) light are those with the highest penetration depth and less absorbed by biological components. Thus, the optimal wavelength range, called the optical window, is between 600-1200 nm. However, light of a wavelength longer than 800 nm typically does not have enough energy to excite the PS and further promote its reaction with molecular oxygen.[4] Therefore, the optimal window of administered light for PDT is in the range 600-800 nm.

1.1.1. Photochemical aspects

A PS is any molecule that upon light absorption can use the excitation energy to induce photophysical or photochemical reactions to another molecule.[7] In the case of PDT, PSs undergo photochemical reactions with oxygen to produce ROS.

Upon absorption of a photon from an electromagnetic wave, i.e. commonly visible light, an electron of a PS molecule is promoted to a higher-energy orbital, and the PS is said to be promoted from its ground state (^{1}PS) to an electronically excited state composed of multiple vibrational states. The excited molecule rapidly relaxes to the first excited singlet state (^{1}PS*) via vibrational relaxation or internal conversion, which are non-radiative processes. Once in ^{1}PS*, several photophysical and photochemical processes can occur (Kasha's rule). The PS can return to its ground state (^{1}PS) through internal conversion or through emission of a photon (fluorescence). Singlet states are usually very short-lived (10^{-9} to 10^{-6} s) since the spin number is preserved in both states, and according to the Spin Selection Rules, this is an allowed transition. The electron in the singlet state can also experience a change on its spin, thus undergoing intersystem crossing and populating the first excited triplet state (^{3}PS*). Now the transition from the triplet state to the singlet ground state ^{1}PS is forbidden due to the change in spin number, this being the explanation for the long lifetime of triplet states (10^{-6} to 1 s). However, the PS in its triplet state ultimately decays to the ground state, either by a radiative process (phosphorescence) or by internal conversion. In the presence of molecular oxygen or other substrates susceptible of oxidation or reduction, photochemical reactions, or the so-called Type I and Type II mechanisms, can also occur. Type I processes involve an electron transfer of the triplet state PS to another substrate, initiating a cascade of radical reactions which culminate in the formation of various types of ROS, including the hydroxyl radical ($OH^{\cdot}$) or the superoxide radical anion ($O_2^{\cdot-}$). These ROS, in turn, rapidly react with cellular macromolecules such as lipids and proteins which causes oxidative damage and the activation of cell death mechanisms. Type

II reactions comprise electron energy transfer from the triplet state PS to triplet ground state molecular oxygen ($^3O_2$) in a process called triplet-triplet annihilation, thus forming the highly reactive singlet oxygen ($^1O_2$). $^1O_2$ has been proven to be generated *in vitro* in most studies concerning photocytotoxic experiments, and hence the type II process is thought to be the main mechanism in PDT.

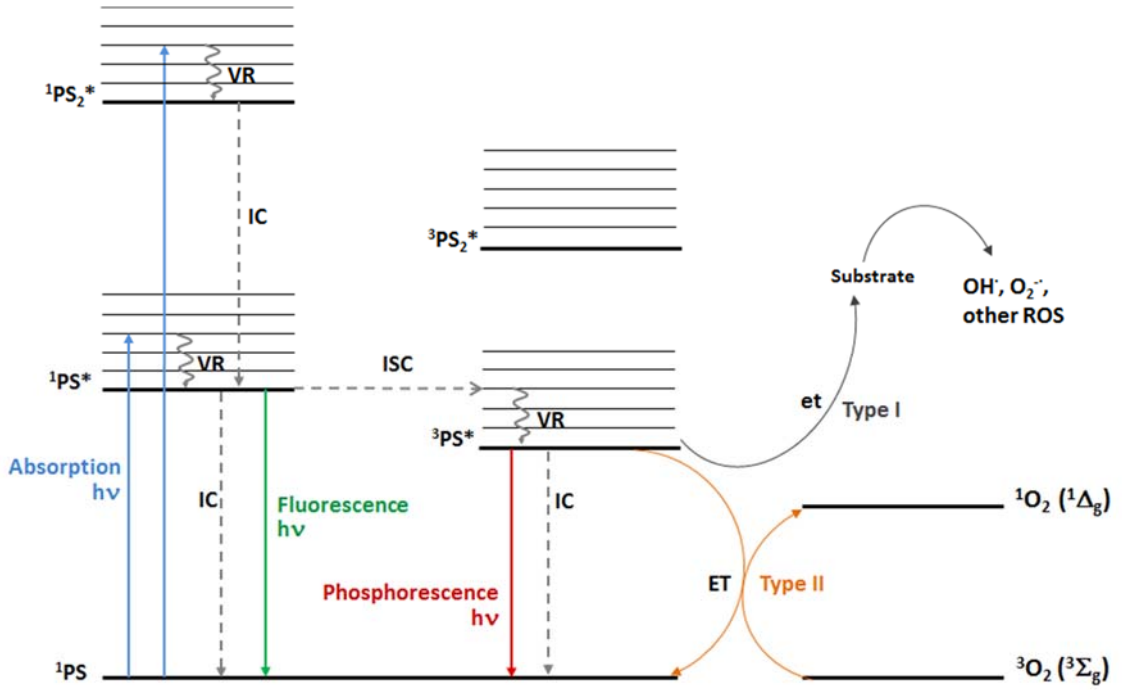

Scheme 1.1. Jablonski diagram representing the energetic states of a PS, the photophysical processes occurring upon light absorption and the Type I and Type II photochemical reactions. IC: internal conversion, ISC: intersystem crossing, VR: vibrational relaxation, et: electron transfer, ET: energy transfer.

1.1.2. Photosensitizers

PSs are commonly organic planar molecules which are aromatic or with a high degree of π-orbital conjugation. Although there are a number of distinct types of molecules that can photosensitize ROS, a vast majority are derivatives of the cyclic tetrapyrrole structure porphine,[5] for instance porphyrins, chlorins, bacteriochlorins, phthalocyanines, or porphycenes.[8] Porphine is a conjugated planar macrocycle which consists of four pyrrolic sub-units linked on opposing sides (α-positions, Figure 1.1) through four methane (CH) bridges, known as the *meso*-carbon positions (Figure 1.1). Substitutions on the porphine macrocycle may be carried out at the *meso*- or β-positions, leading to the so-called porphyrins.

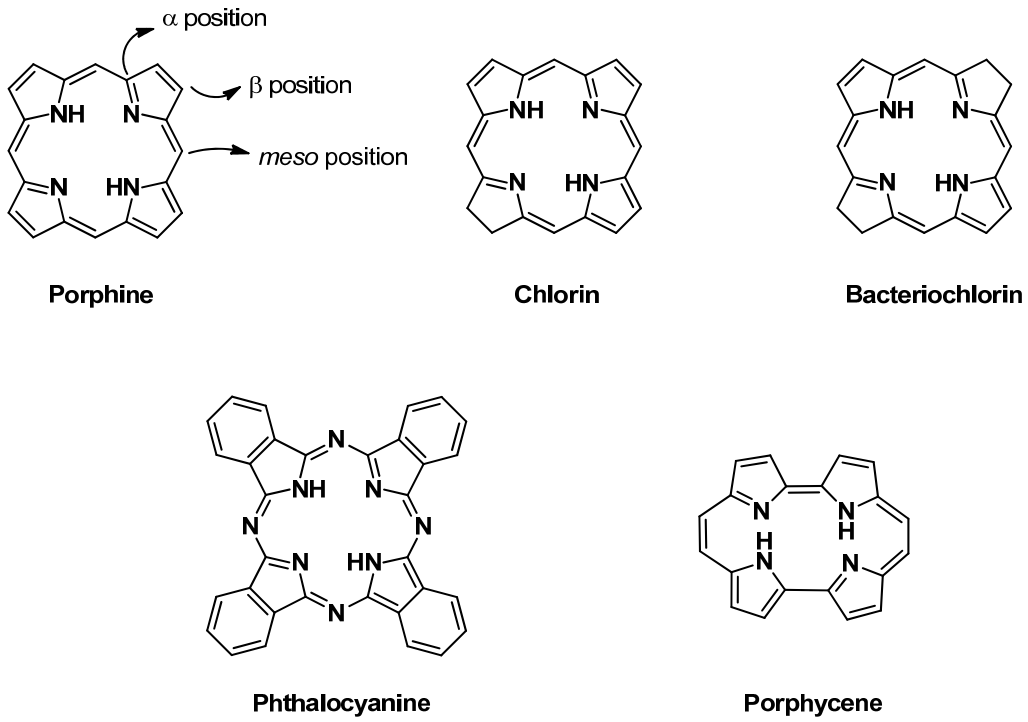

Figure 1.1. Structure of some of the existing cyclic tetrapyrrolic PSs.

The first-generation PS, hematoporphirin derivative or Photofrin®, is a mixture of porphyrin oligomers and although still largely employed, it suffers from three important disadvantages: it renders a long-lasting skin photosensitivity to patients, it has a relatively low absorbance in the red (630 nm) and it is not a pure compound but a mixture of active compounds.[9] Due to these drawbacks, many efforts have been made to synthesize second-generation PSs which could be more promising candidates for PDT. These second-generation PSs were meant to pursue the characteristics of the ideal PS, some of them being the following: [4,5,9]

- It should be a pure compound
- It should have low manufacturing costs
- Have good stability in storage
- Be water soluble
- Have a high absorption between 600-800 nm
- Have low levels of dark toxicity
- Show a relatively rapid clearance from healthy tissues (minimizing phototoxic side effects)

Although several compounds meeting some of the above features have aroused, it has been difficult to build up molecules which meet all these criteria. Even more challenging is that they become clinically approved by the Regulatory Agencies; indeed, only a few PSs have reached the market over the last 25 years after the launching of Photofrin®.[4] Therefore, despite all the efforts made by the scientific community, there are still some important limitations on the PSs developed, especially their insolubility in water at physiological pH or their lack of selectivity for targeted tissue.[5] Thus, third-generation PSs, i.e. the association of PSs to multiple-platform nanodevices or PSs direct linkage to targeting ligands are the main current strategies to overcome solubility impairment and enhance diseased tissue selectivity and are now being the focus of research.

1.1.3. Mechanisms of cell death

As already mentioned, photosensitized ROS oxidize surrounding cellular macromolecules, leading to an irreparable cellular damage which triggers tumor cell death by any of the three main pathways- apoptosis, necrosis or autophagy.[10] The type of mechanism involved in cell death depends on several factors, for instance treatment dose, cell line or subcellular localization of the PS.[11,12] The latter plays a key role in PDT since $^1O_2$ has a very short lifetime in living organisms[13,14] and ultimate cellular response largely depends on where the photochemical damage is produced, i.e. the internalized PS must be localized near its intracellular target. Charge, amphiphilicity and partition coefficients are important parameters of the PS structure that affect its main site of intracellular localization and consequently its efficiency and mechanism of cell death. For the above reasons, ascertaining the variables that determine the final subcellular localization of a PS becomes a key factor for understanding how PDT works and what ultimately determines its efficacy.[15–18] A large number of biochemical studies have demonstrated that most of the subcellular organelles, such as mitochondria, nucleus, lysosomes, plasma membrane, endoplasmic reticulum or Golgi apparatus, can become targets for PSs.[17] Moreover, i*n vivo*, tumor cell destruction is sometimes accompanied by induction of an acute local inflammatory reaction that participates in the removal of dead cells, restoration of normal tissue homeostasis, and, sometimes, in the development of systemic immunity.[4,19]

Apoptosis is a regulated cell death mechanism which can be triggered by external or internal signals and is a common cell death modality in cells treated with PDT.[4] Apoptotic cells are characterized by some morphological features, including chromatin condensation, nuclear fragmentation, pyknosis, cell shrinkage and plasma membrane blebbing. Cells are ultimately

fragmented into multiple membrane vesicles, called apoptotic bodies, which contain degraded cellular compartments. Apoptotic bodies are engulfed by phagocytes *in vivo*, which prevents inflammation and tissue destruction.[11,20] Some reports suggest, though, that in some cases PDT-induced apoptosis might stimulate the extracellular release and binding of certain heat-shock proteins (HSPs) which would subsequently trigger their association to innate immunity cells such as dendritic cells or natural killer cells. These immunity cells would in turn segregate pro-inflammatory cytokines, and altogether would propitiate the development of an anti-tumor immune response.[19] Regarding to the biochemical level, oxidation of cellular components by ROS initiates a stress response which elicits a cascade of signaling events commonly involving activation of caspases, mitochondrial damage or cytochrome c release, among many others.[11,20] Mitochondria plays a key role in regulating pro-apoptotic signals and triggering the apoptosis mechanism as a response, although some recent investigations indicate that other organelles such as lysosomes, Golgi Apparatus or endoplasmic reticulum may be important in prompting pro-apoptotic signaling cascades.[21,22]

On the contrary, necrosis has traditionally been thought as a passive, not regulated, cell death modality, although recent reports have remarked that some forms of necrosis may also occur in a regulated manner.[20,23,24] Excessive chemical or physical injury to the cell results in this cell death modality. Necrotic cells are characterized by cytoplasm swelling, destruction of organelles and uncontrolled rupture of the plasma membrane, leading to the release of intracellular contents and pro-inflammatory molecules, which leads to an acute inflammatory response.[11]

Photochemical damage of cells can also lead to cell death by autophagy. Whole organelles and intracellular proteins which need to be degraded or recycled are encapsulated by a double membrane forming the autophagosome, which ultimately fuses with a lysosome. Autophagy is in fact a cytoprotective mechanism to preserve cellular homeostasis but it can also promote cell death in response to excessive stress signals including oxidative stress caused by PDT.[4,20] Recent studies show that autophagy could both have a prodeath[25] or preservation[26] role after PDT treatment.

1.1.4. Clinical applications

The current era of PDT can be considered to begin in 1960 when R. L. Lipson and S. Schwartz observed that injection of crude preparations of hematoporphyrin led to fluorescence of neoplastic lesions visualized during surgery. Schwartz further purified the hematoporphyrin crude and obtained a more phototoxic version that he called hematoporphyrin derivative (HpD),

which was used by Lipson *et al.* for further investigations.[27] In 1978, Dougherty *et al.* conducted the first clinical trial combining HpD and red light and obtained partial or complete tumor eradication in almost all lesions treated.[28] Indeed, Dougherty and co-workers highly contributed to the development and clinical implementation of PDT. Importantly, they further purified HpD up to the launching of the first clinically approved PS known as Photofrin®,[29] which nowadays is still one of the most clinically used PSs.[4]

After the first clinical trial in 1976, numerous studies have contributed to promote PDT as a reasonable treatment option in malignant skin lesions, Barret esophagus, unresectable cholangiocarcinoma, head and neck cancer or lung cancer. However, for other tumors, only a few randomized controlled trials have been performed to date,[4] thus PDT is not yet a preferential treatment for many neoplastic lesions. This underestimated condition is likely due in part to the limitations of PDT itself: the depth of tumor destruction usually ranges from a few millimeters up to 1 centimeter due to the limited penetration of light into the tissues; and the high selectivity of this therapy makes it at the same time unviable for metastatic lesions. These drawbacks, in combination with the shortcomings of some second-generation PSs (see above), have urged scientists to explore other alternatives for rendering PDT more active and efficient, such as photochemical internalization (PCI),[30] combination of PDT with other anticancer therapies, or the use of delivery systems for PDT. Indeed, some clinically approved formulations employing nanoliposomes (Foslip® and Visudyne®)[31,32] shine some light on the near future of PDT.

1.2. Drug delivery systems in photodynamic therapy

Nanotechnology is the science, engineering and technology at the nanoscale, i.e. from 1 to some hundreds of nanometers. The concept of nanotechnology originated in 1959 when the physicist Richard Feynman gave a conference entitled “There is Plenty of Room at the Bottom”. Later in 1974, Norio Taniguchi first used the word nanotechnology, and in 1980’s Eric Drexler wrote the first book about nanotechnology. From 1990s this field has incredibly expanded and has revolutionized other areas of science, from physics to medicine.

Generally speaking, the main goal of drug vehiculization into nanocarriers or drug delivery systems is to reduce therapy associated side effects and improve bioavailability, thereby leading to a higher efficacy of the drug with a decreased overall toxicity. Additionally, nanocarriers protect the drug from premature degradation and from interactions with the biological environment in the organism, increase the circulation time of the drug in the body and also

enhance drug penetration into the diseased tissue cells.[33] Employing nanoparticles (NPs) for PDT can also have the following advantages:[34–36]

- At their reduced size, NPs have unique physicochemical properties, such as a large surface area to volume ratio. This is advantageous when the PS is transported through covalent conjugation at the surface of the NP, since the large surface area enables to construct nanocarriers with a high degree of payload
- NPs improve the aqueous solubility of the PSs
- Shape, size and surface nature of the NPs govern their biological interactions such as intracellular uptake, blood circulation times, or their clearance through reticuloendothelial system. The optimization of these parameters during synthetic procedures can result in promising delivery systems. For instance, NP surface can be modified either with certain polymers such as chitosan or poly-(ethylene glycol) (PEG) to improve their biodistribution and pharmacokinetics or with targeting moieties to enhance cellular uptake through active targeting
- They can be designed as multifunctional nanoplatforms to carry multiple components together with the PSs, such as imaging agents or chemotherapeutic drugs

As previously mentioned, many second-generation PSs with promising photophysical properties were developed although most of them suffered from a high degree of hydrophobicity and reduced tumor selectivity. The lack of aqueous solubility hinders their systemic administration and also provokes their aggregation in this media, which leads to a loss of their photophysical properties, for instance, a decrease in $^1O_2$ formation.[37] Thus, NPs have risen as an interesting option to overcome the limitations of classic PSs over last years.

A nanocarrier should meet a series of characteristics. The ideal delivery system should be biodegradable, have a small size and a high loading capacity, be stable, non-immunogenic and non-toxic, have a prolonged circulation in the body after administration, and selectively accumulate in the target area. Additionally, it was traditionally believed that the PS should be incorporated in the nanocarrier without alteration of its photophysical properties in order to be ready to generate ROS once inside the cell.[35] Although this holds true for some PSs in certain vehicles due to the improved solubility of the PS in the local environment of the nanovehicle, in other cases the photosensitizing ability of the PS becomes reduced inside the nanocarrier due to the high local concentration of the PS itself.[38] This phenomenon might actually be valuable in terms of preventing systemic phototoxicity to the patient before the nanocarrier reaches its target.

Liposomes and oil emulsions were the first delivery systems tested for the encapsulation and delivery of PSs. The first studies with entrapped Hematoporphyrin or 9-(glutamic acid glutarylamide)-2,7,12,17-tetrakis(methoxyethyl)porphycene in liposomes showed that the concentration ratio of the PS between tumor and peritumoral tissue increased by a factor of three with liposomal delivery.[39,40] Multiple studies have later evaluated the incorporation of several PSs into different types of liposomal formulations and their phototoxic activity.[41] Oil-emulsions, commonly based on the surfactant Cremophor EL (CR), were also tested for the encapsulation of PSs. Although CR emulsions have been proven to be suitable and efficient vehicles for hydrophobic PSs, they can produce acute anaphylactic reactions after their parenteral administration in some patients,[42–45] which hinders their use as delivery vehicles.

Biodegradable polymeric NPs, based on either natural or synthetic biodegradable polymers, have emerged as an alternative to liposomes and have gathered special attention as nanocarriers for antineoplastic agents as well as for PSs due to several advantages, especially their biocompatibility, their various drug release patterns depending on the characteristics of the carrier, a large variety of available materials and manufacturing processes as well as the ability to modify their surface with biological moieties to design active-targeting vehicles.[35,46] Some early investigations with hematoporphyrin, phthalocyanines or meso-tetra(hydroxyphenylchlorine) (mTHPC) entrapped in NPs of poly(isobutylcyanoacrylate) and its derivatives gave encouraging results regarding the efficiency of the PDT treatment.[35] In another study comparing two different formulations of hexadecafluoro Zn(II)-phthalocyanine in polylactide NPs or CR suspensions in EMT-6 tumor-bearing mice, PDT with polylactide NPs yielded a 100% tumor regression against only 60% with the CR emulsion, thus showing promise to replace CR emulsions.[47]

Non-biodegradable NPs have not been traditionally used as drug nanocarriers due to their inability to degrade in biological systems. Nevertheless, these systems have shown promise in PDT since the action mechanism in this therapy relies on the production and diffusion of $^1O_2$ to reach the cellular components. Therefore, non-biodegradable NPs may be suitable nanocarriers of PSs as long as they enable $^1O_2$ diffusion out of the carrier. Some of their advantages over biodegradable NPs are their simple modification of size, shape and porosity during their synthetic process, as well as their stability over temperature and pH fluctuations.[37] These nanocarriers, like biodegradable NPs, can be designed as multifunctional platforms for theranostics, since they can easily be modified on their surface to covalently link biological targeting moieties as well as to incorporate elements to enhance diagnostic imaging such as fluorescent dyes or contrast imaging agents such as magnetic NPs (iron oxide NPs). Among the

vast range of non-biodegradable NPs, some of the most studied in the PDT field have been polyacrylamide NPs,[48] silica-based NPs,[49] gold NPs,[50] fullerenes,[51] or upconversion NPs.[52] Moreover, some of these nanomaterials have significant optical properties which promote their use as PSs themselves. For instance gold NPs have unique optical properties due to their surface plasmon resonance absorption band that can be exploited to enhance the photophysical properties of the PS or can be utilized for dual therapy (phototherapy and PDT). Fullerenes are light absorbers and act as PSs *per se*. Upconversion NPs, on the other hand, are being explored as systems that may enable patient irradiation to the NIR area of the spectrum thanks to their ability to absorb NIR radiation and emit light at the visible region. Although most of them have been shown to be biocompatible, their main disadvantage is that their possible long term toxicity has not yet been evaluated, and most of them have not received FDA approval.

1.3. Poly-(*D,L*-lactide) and poly-(*D,L*-lactide-*co*-glycolide) nanoparticles as drug delivery agents for photodynamic therapy

Among the synthetic polymers, the (α-hydroxy)-polyesters polylactide (PLA), polyglycolide (PGA), and specially their copolymer poly-(lactide-*co*-glycolide) (PLGA) have generated a strong interest due to their excellent biocompatibility, biodegradability and toxicologically safe by-products. More importantly, PLGA received the US Food and Drug Administration (FDA) approval in 1999 as a delivery system for therapeutic uses.[33]

PLA, PGA and PLGA polymers are commonly synthesized by ring opening polymerization from the cyclic dimers of lactic acid and glycolic acid (lactide and glycolide rings)[53] and in the case of PLGA, copolymers with varying compositions can be obtained depending on the ratio lactide to glycolide employed. For instance, PLGA 75:25 stands for a PLGA with a composition of a 75% lactide and 25% glycolide. According to the presence of a chiral center on the lactic acid monomer, the corresponding polymer can be synthesized in its enantiomerically pure forms, namely poly-(*D*-lactide) (PDLA) or poly-(*L*-lactide) (PLLA), or the racemic form poly-(*D,L*-lactide) (PLA). The physicochemical properties of optically active PDLA and PLLA are nearly the same, except for their solid structure, since PDLA is completely amorphous while PLLA is crystalline. The methyl side group in lactic acid (Figure 1.2) renders a high hydrophobicity to this polymer. On the contrary, glycolic acid does not contain any methyl side group, which makes PGA slightly more hydrophilic and highly crystalline, similarly to PLLA. The copolymer PLGA is crystalline if it is formed from PLLA and PGA, but PDLA or PLA reduce its crystallinity.

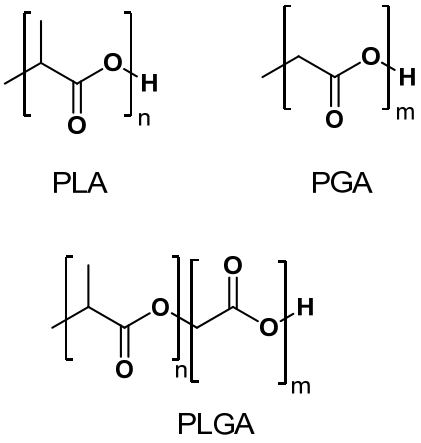

Figure 1.2. Chemical structure of the (α-hydroxy)-polyesters PLA, PGA and PLGA.

Additionally, the higher the lactide content, the higher the hydrophobicity of the copolymer.[54] Biodegradation of these polymers or its NPs *in vivo* is accomplished mainly by hydrolysis of the ester linkages, resulting in the building block monomers lactic acid and glycolic acid which are further eliminated by common metabolic pathways. The degradation rate of PLGA depends on several factors, mainly the composition of the polymer, its molecular weight, its hydrophobicity, its degree of crystallinity and its glass transition temperature (Tg). Environmental factors such as pH, temperature or ionic strength of the medium are also detrimental, although *in vivo* only significant changes would alter the degradation rate. In general, the degradation time is shorter for low molecular weight, more hydrophilic and more amorphous polymers. Exceptionally, it has been proven that PLGA 50:50 has the fastest degradation rate *in vivo* (around 50-60 days). Thus, by modifying the molecular weight and lactide to glycolide ratio, the degradation time of PLGA and consequently the release profile of the entrapped drug can be modified. Indeed, drug release depends on drug diffusion and degradation of the polymeric matrix, as well as on the nature of the delivery system (nanocapsule or nanosphere). In the case of a nanosphere, the drug is distributed/dissolved in the polymeric matrix and the release occurs by diffusion of the drug or erosion of the matrix, the main mechanism being the faster of the two. Rapid initial release or "burst" release is generally attributed to the fraction of drug which is adsorbed or weakly bound to the surface of NPs. The subsequent exponential release rate observed is probably due to the drug more internalized in the matrix.[55] In the case of a chemically conjugated drug its release is also achieved, although it has been reported to be in a time 5 fold longer than for the same system with the drug physically entrapped (25 days vs 5 days).[56]

Regarding NP internalization, a number of studies have proposed that PLGA NPs are internalized by cells via endocytosis,[57–61] an energy dependent process which is blocked at low temperatures.

Thus, the observation of a significant reduction of the internalization of NPs at 4 °C compared to 37 °C suggests that NP uptake is mediated by endocytosis.[59,62] Moreover, another study employing Raman spectral imaging as a non-invasive technique showed that HeLa cells presented intracellular PLGA inclusions after 2 h of incubation, supporting the internalization of the NPs.[63] The exact endocytic mechanism, however, is not fully known yet. Fluid phase pinocytosis or clathrin-mediated endocytosis have been suggested by some authors,[57] whereas others have observed that the endocytic process might be independent of clatrhin and caveolin proteins.[58] The intracellular fate of these NPs would naturally be the endosomal structures after the endocytic process,[62] although there is evidence that NPs may escape endo-lysosomal degradation and may be trafficked to other relevant subcellular compartments after endocytosis.[57,59,63] Moreover, it is known that uptake is influenced by the physicochemical properties of the NP itself such as its charge or its size, and that not all cell lines may follow the same internalization pathways when exposed to the same NPs.[64] Thus, some of the above results might show discrepancy due to the different cell lines and NPs tested. However, it is clear that further research is needed to better elucidate the cellular internalization process.

All the aforementioned characteristics of the polyester-based NPs, together with their ability to encapsulate hydrophilic but especially lipophilic drugs, has promoted the research on the benefits of PS incorporation into these nanodelivery systems. In a series of publications, Konan *et al.* reported the encapsulation of *meso*-tetra(4-hydroxyphenyl)porphyrin (p-THPP) in NPs of PLGA 50:50, PLGA 75:25 and PLA. They observed that polymer composition did not affect significantly the physical characteristics of NPs such as size, surface charge, drug loading or redispersibility.[65] They did observe that at the lowest concentration of p-THPP tested, 3 μg/mL, 50:50 PLGA NPs were the most efficient in inducing cell death (80%) followed by 75:25 PLGA or PLA NPs, which showed almost the same phototoxic outcome (40%). This higher efficiency of PLGA 50:50 NPs was likely due to a faster degradation rate and release for this copolymer ratio as well as its influence on the rate of carrier uptake.[66] Vargas *et al.* studied the impact of NP size on the photodynamic activity of *meso*-tetra(3-hydroxyphenyl)porphyrin (m-THPP)-loaded PLGA NPs in the chick chorioallantoic membrane (CAM) model. They observed that m-THPP was less effective in large NPs (~600 nm) than free in solution or small NPs (~100 nm). In following studies, they showed that the batch with the smallest particle size and most active *in vivo* (~100 nm) exhibited *in vitro* the highest ROS formation and the fastest m-THPP release. Absorption, fluorescence intensity and fluorescence lifetime of entrapped m-THPP varied among NP batches of different size suggesting that location and aggregation states of entrapped m-THPP was dependent on NP size.[38] McCarthy *et al.* showed that the encapsulation of meso-

tetraphenylporpholactol in PLGA NPs with a 12% drug loading also results in the quenched excited states of the PS, yet it is released and activated upon cell internalization. In cell culture, the phototoxicity caused by non-internalized NPs was minimal (9%) in contrast to the effect of internalized NPs (95%), and *in vivo* animal studies showed complete eradication of tumors.[67] These results emphasized that quenching of PS excited state inside the NP could be advantageous for preventing healthy tissue damage as long as the NPs are internalized and the PS released and reactivated. In this line, entrapment and phototoxic activity of Zn(II)-phthalocyanine (ZnPc) was also tested in PLGA NPs. It was found that once ZnPc was released from NPs to an organic solvent, its photophysical properties remained the same as for free ZnPc, although there was no report on the photophysical properties of the ZnPc entrapped into the NPs.[68] Gomes *et al.* studied the photophysical properties of an aqueous PLGA NP suspension of entrapped bacteriochlorophyll-*a* (BChl-*a*). Regarding the absorption spectrum, they reported a decrease in intensity as well as a bathochromic shift of the Q bands for entrapped BChl-*a* compared to BChl-*a* in solution, as well as a bathochromic shift in fluorescence spectrum. However, they did not attribute these spectroscopic changes to the formation of aggregates since the fluorescence quantum yield was the same for free BChl-*a* and entrapped BChl-*a*, and $^1O_2$ quantum yield, measured by indirect methods, was also comparable between both systems.[69]

Differing from the previous PSs, a study conducted by Da Silva *et al.* encapsulating 0.21% of In(III)-tetraphenylporphine (InTPP) into sub-200 nm PLGA NPs reported that InTPP was not aggregated since absorption and emission spectra of the entrapped InTPP did not show any spectroscopic differences compared to free InTPP in a non-polar solvent. It was also more efficient in inducing cell death than free InTPP in human prostate carcinoma, mainly by apoptosis. This increase was attributed to an observed higher uptake of encapsulated InTPP as well as to the aggregation state of free InTPP in culture medium, which reduces its ability to produce singlet oxygen. Zeisser-Labouèbe *et al.* studied the encapsulation of Hypericn (Hyp) in PLA NPs in various drug loadings, as well as in two types of PLGA 50:50 NPs with different PLGA molecular weight. NP size was nearly the same for all formulations, but entrapment efficiency was much higher in PLA (70% vs 20% for PLGA NPs at the same initial drug loading). Interestingly, they observed that the greater the drug loading, the lower the phototoxic effect after 1h incubation, explained by an observed faster release in the less loaded NPs and a likely increased aggregation of Hyp in highly loaded NPs.[70] In another study, they used Hyp-loaded PLA NPs in a much higher drug loading (3.7%) to study the usefulness of NPs in a rat model of ovarian cancer. The selectivity of Hyp administered with free Hyp or Hyp-loaded NPs was assessed by

fluorescence endoscopy and quantified after tissue extraction. Hyp accumulation was greater in ovarian micrometastases when administered with NPs after 24 h compared to free Hyp and it was also higher than in surrounding muscle.[71] The FDA approved 5,10,15,20-tetrakis(3-hydroxyphenyl)chlorin (m-THPC) has also been encapsulated in PLGA 50:50 NPs and its cellular internalization and phototoxicity compared to that of the free drug. It was found that mTHPC administered in PLGA NPs had the same mechanism of cell internalization, the same intracellular localization pattern as well as a similar phototoxic effect than the free drug. Nevertheless, mTHPC incorporated in PLGA NPs was advantageous since it did not produce any dark toxicity to the cultured cells.

Altogether, these variety of results show that interactions between the PS and the PLGA or PLA matrix may depend on each PS and copolymer used, and thus photophysical properties as well as photodynamic activity need to be studied for each particular case.

1.4. Targeted photodynamic therapy

1.4.1. Passive targeting

Nanoparticulate systems administered to the body with a size range of 10-500 nm can reach neoplastic cells by means of the enhanced permeability and retention (EPR) effect. This phenomenon is characterized by a leaky and more permeable vasculature and poor lymphatic drainage in tumor tissue, which enables the NPs to easily extravasate the endothelial cells of the vessels and accumulate at the interstitial space.[72]

Pharmacokinetic studies *in vivo* have shown that PLGA NPs suffer from adsorption of opsonins onto their surface likely due to the hydrophobic character of the polymer, resulting in their rapid uptake by the cells of the reticuloendothelial system (RES).[53,73,74] RES uptake of NPs depends on particle size, surface charge and especially surface hydrophobicity.[75] It has been demonstrated that coating the hydrophobic surface of such NPs with hydrophilic polymers, the most popular of which being poly-(ethylene glycol) (PEG), is efficient in preventing their rapid uptake by macrophages, and hence, in lengthening their circulation time.[76] Therefore, long-circulating PEGylated NPs are more favorable to passively accumulate in tumors than non-PEGylated counterparts thanks to their prolonged half-life in the organism.[35] The most accepted theory for this increased circulation time is that PEG reduces protein interactions on the surface of PLGA NPs thereby preventing opsonin binding.[77] Hence, PEG-modified PLA or PLGA NPs, prepared mostly by using a di-block copolymer PLA-PEG or PLGA-PEG as an additive, have been proposed

as long circulating nanodevices and have already been evaluated for PDT.[60,78,79] First studies were related to the encapsulation of $ZnPc_{16}$ into PEGylated PLA NPs or into Chremophor EL emulsions and the comparison of their photodynamic properties.[80] In other subsequent works, in addition to phototoxicity studies *in vitro* or *in vivo*, the photophysical characteristics of the PEGylated nanosystems were evaluated.[81,82] Recently, PLGA-PEG NPs encapsulating ZnPc, combined with gold NPs and an immunostimulating agent were developed as a multifunctional platform.[83] Although in all these studies the feasibility and suitability of the PEGylated nanosystems as vehicles for photodynamic therapy were demonstrated, the relevance of the photophysical properties on the characteristics of the nanosystems and their influence on the photodynamic response were not determined in detail.

1.4.2. Active targeting

An alternative strategy to convey the nanovehicles to the desired target cell is to functionalize the surface of NPs with specific ligands that bind with high affinity to certain biomolecules overexpressed or unique to diseased tissue or vasculature. A large variety of ligands have been explored including monoclonal antibodies and antibody fragments, proteins, peptides or small molecules such as folic acid or monosaccharides.[84]

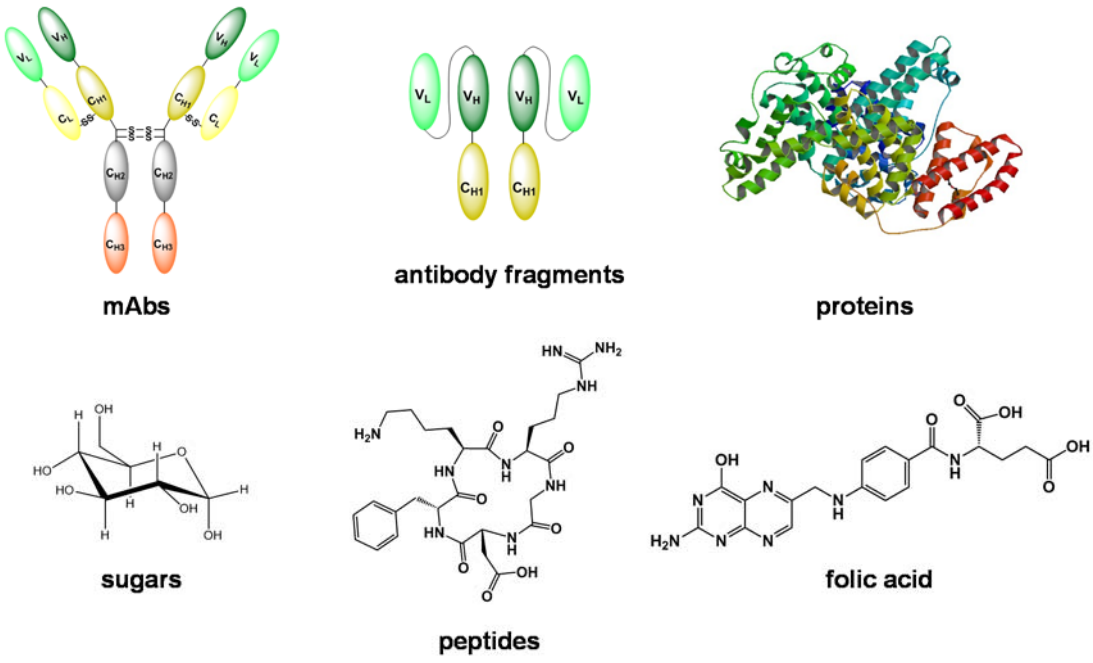

Figure 1.3. Representation of the most common ligands explored for active targeting.

The most popular approach adopted to improve PDT selectivity does not imply nanovehicles but rather the direct conjugation of PSs to monoclonal antibodies (mAbs) or antibody fragments, called photoimmunoconjugates (PICs), since these biomolecules have a high degree of specificity for its binding moiety. Despite favorable advances in the photodynamic effect of these conjugates, it has been found that obtaining well-purified and well-characterized PICs is rather problematic, mainly due to the tendency of PICs to aggregate and of the hydrophobic PSs to remain attached via non-covalent binding to the hydrophobic pockets of the antibodies.[85] mAbs can also be immunogenic, have limited half-lives, are expensive to manufacture and may vary from batch to batch, which limits their efficiency as targeting molecules.[84] Therefore, other active targeting strategies involving smaller ligands, such as aptamers, proteins, peptides or folic acid, have been studied. The direct conjugation of some PSs to these biomolecules has afforded some promising results, for instance C_{e6}-aptamer conjugates yielded a more than 500-fold increase in phototoxicity than the free C_{e6} in cells overexpressing the specific targeted antigen.[86]

Translation of the active targeting strategy to nanovehicles has resulted in several targeted delivery systems for PDT. Interestingly, most of these studies have reported an increased phototoxic effect exerted by the targeted vehicles, although it seems that its extent depends largely on the type of targeting moiety and probably the nanovehicle. For instance, folate-targeted liposomes have been reported to produce a moderate increase in the phototoxic effect (~2 fold),[87,88] whereas gold NPs conjugated with the lectin jacalin or with an anti- HER-2 mAb have shown a 5-fold photodynamic effect.[50] It is thus clear that active targeting looks promising and that research in this direction should continue in order to discover other potential targeted-nanodelivery systems. In this sense, targeted PLGA or PLA NPs have been previously reported to enhance cytotoxicity of chemotherapeutic agents, but no studies have been carried out regarding PDT, which makes them suitable for investigation.

1.5. Objectives

The main goal in this thesis is to design and study biodegradable polymer-based nanoparticles for photodynamic therapy, either passively or actively targeted. This main goal is further set in the following specific objectives:

- Development of passive targeting nanoparticle formulations for entrapping lipophilic photosensitizers and evaluation of their physicochemical, photophysical and photodynamic properties *in vitro*
- Development of biodegradable nanodelivery systems comprising a covalently linked photosensitizer and evaluation of their suitability for photodynamic therapy
- Elaboration of actively targeted biodegradable nanoparticles by conjugation of an active ligand to be exposed on the surface of nanoparticles and study of their photodynamic efficacy *in vitro*

1.6. References:

(1) World Health Organization. Global Health Observatory Data Repository http://apps.who.int/gho/data/node.main.CODWORLD?lang=en (accessed Aug 16, 2015).

(2) World Health Organization (WHO). Cancer http://www.who.int/mediacentre/factsheets/fs297/en/ (accessed Oct 15, 2015).

(3) Ferlay, J.; Soerjomataram I, I.; Dikshit, R.; Eser, S.; Mathers, C.; Rebelo, M.; Parkin, D. M.; Forman D, D.; Bray, F. Cancer Incidence and Mortality Worldwide: Sources, Methods and Major Patterns in GLOBOCAN 2012. *Int. J. Cancer* **2014**, *136*, E359–E386.

(4) Agostinis, P.; Berg, K.; Cengel, K. A.; Foster, T. H.; Girotti, A. W.; Gollnick, S. O.; Hahn, S. M.; Hamblin, M. R.; Juzeniene, A.; Kessel, D.; *et al.* Photodynamic Therapy of Cancer: An Update. *CA. Cancer J. Clin.* **2011**, *61*, 250–281.

(5) Josefsen, L. B.; Boyle, R. W. Photodynamic Therapy and the Development of Metal-Based Photosensitisers. *Met. Based. Drugs* **2008**, *2008*, 1–23.

(6) Allison, R. R.; Moghissi, K. Oncologic Photodynamic Therapy: Clinical Strategies That Modulate Mechanisms of Action. *Photodiagnosis Photodyn. Ther.* **2013**, *10*, 331–341.

(7) Wilkinson, A.; McNaught, A. D. *IUPAC. Compendium of Chemical Terminology*; M. Nic, J. Jirat, B. K., Ed.; 2nd ed.; Blackwell Scientific Publications: Oxford, 2014.

(8) Aramendia, P. F.; Redmond, R. W.; Braslavsky, S. E.; Schaffnerlf, K.; Vogel, E.; Nonell, S. The Photophysical Properties of Porphycenes: Potential Photodynamic Therapy Agents. *Photochem Photobiol* **1986**, *44*, 555–559.

(9) Castano, A. P.; Demidova, T. N.; Hamblin, M. R. Mechanisms in Photodynamic Therapy: Part One - Photosensitizers, Photochemistry and Cellular Localization. *Photodiagnosis Photodyn. Ther.* **2004**, *1*, 279–293.

(10) Kiesslich, T.; Tortik, N.; Pichler, M.; Neureiter, D.; Plaetzer, K. Apoptosis in Cancer Cells Induced by Photodynamic Treatment – a Methodological Approach. *J. Porphyr. Phthalocyanines* **2013**, *17*, 197–209.

(11) Castano, A. P.; Demidova, T. N.; Hamblin, M. R. Mechanisms in Photodynamic Therapy: Part Two: Cellular Signaling, Cell Metabolism and Modes of Cell Death. *Photodiagnosis and photodynamic therapy*, 2005, *2*, 1–23.

(12) Soriano, J.; García-Díaz, M.; Mora, M.; Sagrista, M. L.; Nonell, S.; Villanueva, A.; Stockert, J. C.; Canete, M. Liposomal Temocene (m-THPPo) Photodynamic Treatment Induces Cell Death by Mitochondria-Independent Apoptosis. *Biochim. Biophys. Acta* **2013**, *1830*, 4611–4620.

(13) Jiménez-Banzo, A.; Sagristà, M. L.; Mora, M.; Nonell, S.; Sagrista, M. L. Kinetics of Singlet Oxygen Photosensitization in Human Skin Fibroblasts. *Free Radic. Biol. Med.* **2008**, *44*, 1926–1934.

(14) Ragàs, X.; Agut, M.; Nonell, S. Singlet Oxygen in Escherichia Coli: New Insights for Antimicrobial Photodynamic Therapy. *Free Radic. Biol. Med.* **2010**, *49*, 770–776.

(15) Blázquez-Castro, A.; Stockert, J. C.; Sanz-Rodríguez, F.; Zamarrón, A.; Juarranz, A. Differential Photodynamic Response of Cultured Cells to Methylene Blue and Toluidine Blue: Role of Dark Redox Processes. *Photochem. Photobiol. Sci.* **2009**, *8*, 371–376.

(16) Dovigo, L.; Pavarina, A.; de Oliveira Mima, E.; Giampaolo, E.; Vergani, C.; Bagnato, V. Fungicidal Effect of Photodynamic Therapy against Fluconazole-Resistant Candida Albicans and Candida Glabrata. *Mycoses* **2009**, *54*, 123–130.

(17) Oliveira, C. S.; Turchiello, R.; Kowaltowski, A. J.; Indig, G. L.; Baptista, M. S. Major Determinants of Photoinduced Cell Death: Subcellular Localization versus Photosensitization Efficiency. *Free Radic. Biol. Med.* **2011**, *51*, 824–833.

(18) Tejedor-Estrada, R.; Nonell, S.; Teixido, J.; Sagrista, M. L.; Mora, M.; Villanueva, A.; Canete, M.; Stockert, J. C. An Artificial Neural Network Model for Predicting the Subcellular Localization of Photosensitisers for Photodynamic Therapy of Solid Tumours. *Curr. Med. Chem.* **2012**, *19*, 2472–2482.

(19) Garg, A. D.; Nowis, D.; Golab, J.; Agostinis, P. Photodynamic Therapy: Illuminating the Road from Cell Death towards Anti-Tumour Immunity. *Apoptosis* **2010**, *15*, 1050–1071.

(20) Galluzzi, L.; Bravo-San Pedro, J. M.; Kroemer, G. Organelle-Specific Initiation of Cell Death. *Nat. Cell Biol.* **2014**, *16*, 728–736.

(21) Liu, L.; Zhang, Z.; Xing, D. Cell Death via Mitochondrial Apoptotic Pathway due to Activation of Bax by Lysosomal Photodamage. *Free Radic. Biol. Med.* **2011**, *51*, 53–68.

(22) Moserova, I.; Kralova, J. Role of ER Stress Response in Photodynamic Therapy: ROS Generated in Different Subcellular Compartments Trigger Diverse Cell Death Pathways. *PLoS One* **2012**, *7*, e32972.

(23) Coupienne, I.; Fettweis, G.; Rubio, N.; Agostinis, P.; Piette, J. 5-ALA-PDT Induces RIP3-Dependent Necrosis in Glioblastoma. *Photochem. Photobiol. Sci.* **2011**, *10*, 1868–1878.

(24) Coupienne, I.; Fettweis, G.; Piette, J. RIP3 Expression Induces a Death Profile Change in U2OS Osteosarcoma Cells after 5-ALA-PDT. *Lasers Surg. Med.* **2011**, *43*, 557–564.

(25) Dewaele, M.; Maes, H.; Agostinis, P. ROS-Mediated Mechanisms of Autophagy Stimulation and Their Relevance in Cancer Therapy. *Autophagy* **2010**, *6*, 838–854.

(26) Reiners, J. J.; Agostinis, P.; Berg, K.; Oleinick, N. L.; Kessel, D. Assessing Autophagy in the Context of Photodynamic Therapy. *Autophagy* **2010**, *6*, 7–18.

(27) Lipson, R. L.; Baldes, E. J. The Photodynamic Properties of a Particular Hematoporphyrin Derivative. *Arch. Dermatol.* **1960**, *82*, 508–516.

(28) Dougherty, T. J.; Kaufman, J. E.; Goldfarb, A.; Weishaupt, K. R.; Boyle, D.; Mittleman, A. Photoradiation Therapy for the Treatment of Malignant Tumors Photoradiation Therapy for the Treatment of Malignant Tumors. *Cancer Res.* **1978**, 2628–2635.

(29) Dougherty, T. J.; Gomer, C. J.; Henderson, B. W.; Jori, G.; Kessel, D.; Korbelik, M.; Moan, J.; Peng, Q. Photodynamic Therapy. *J. Natl. Cancer Inst.* **1998**, *90*, 889–905.

(30) Weyergang, A.; Berstad, M. E. B.; Bull-Hansen, B.; Olsen, C. E.; Selbo, P. K.; Berg, K. Photochemical Activation of Drugs for the Treatment of Therapy-Resistant Cancers. *Photochem. Photobiol. Sci.* **2015**.

(31) Kiesslich, T.; Berlanda, J.; Plaetzer, K.; Krammer, B.; Berr, F. Comparative Characterization of the Efficiency and Cellular Pharmacokinetics of Foscan- and Foslip-Based Photodynamic Treatment in Human Biliary Tract Cancer Cell Lines. *Photochem. Photobiol. Sci.* **2007**, *6*, 619–627.

(32) Christie, J. G.; Kompella, U. B. Ophthalmic Light Sensitive Nanocarrier Systems. *Drug Discov. Today* **2008**, *13*, 124–134.

(33) Acharya, S.; Sahoo, S. K. PLGA Nanoparticles Containing Various Anticancer Agents and Tumour Delivery by EPR Effect. *Adv. Drug Deliv. Rev.* **2011**, *63*, 170–183.

(34) Paszko, E.; Ehrhardt, C.; Senge, M. O.; Kelleher, D. P.; Reynolds, J. V. Nanodrug Applications in Photodynamic Therapy. *Photodiagnosis Photodyn. Ther.* **2011**, *8*, 14–29.

(35) Konan, Y. N.; Gurny, R.; Allémann, E. State of the Art in the Delivery of Photosensitizers for Photodynamic Therapy. *J. Photochem. Photobiol. B.* **2002**, *66*, 89–106.

(36) Lucky, S. S.; Soo, K. C.; Zhang, Y. Nanoparticles in Photodynamic Therapy. *Chem. Rev.* **2015**, *115*, 1990–2042.

(37) Bechet, D.; Couleaud, P.; Frochot, C.; Viriot, M.-L. L.; Guillemin, F.; Barberi-Heyob, M. Nanoparticles as Vehicles for Delivery of Photodynamic Therapy Agents. *Trends Biotechnol.* **2008**, *26*, 612–621.

(38) Vargas, A.; Lange, N.; Arvinte, T.; Cerny, R.; Gurny, R.; Delie, F. Toward the Understanding of the Photodynamic Activity of M-THPP Encapsulated in PLGA Nanoparticles: Correlation between Nanoparticle Properties and in Vivo Activity. *J. Drug Target.* **2009**, *17*, 599–609.

(39) Jori, G.; Reddi, E.; Cozzani, I.; Tomio, L. Controlled Targeting of Different Subcellular Sites by Porphyrins in Tumour-Bearing Mice. *Br. J. Cancer* **1986**, *53*, 615–621.

(40) Reddi, E. Role of Delivery Vehicles for Photosensitizers in the Photodynamic Therapy of Tumours. *J. Photochem. Photobiol. B.* **1997**, *37*, 189–195.

(41) Jin, C. S.; Zheng, G. Liposomal Nanostructures for Photosensitizer Delivery. *Lasers Surg. Med.* **2011**, *43*, 734–748.

(42) Howrie, D. L.; Ptachcinski, R. J.; Griffith, B. P.; Hardesty, R. J.; Rosenthal, J. T.; Burckart, G. J.; Venkataramanan, R. Anaphylactoid Reactions Associated with Parenteral Cyclosporine Use: Possible Role of Cremophor EL. *Drug Intell. Clin. Pharm.* **1985**, *19*, 425–427.

(43) Wang, Y.; Wu, K.-C.; Zhao, B.-X.; Zhao, X.; Wang, X.; Chen, S.; Nie, S.-F.; Pan, W.-S.; Zhang, X.; Zhang, Q. A Novel Paclitaxel Microemulsion Containing a Reduced Amount of Cremophor EL: Pharmacokinetics, Biodistribution, and in Vivo Antitumor Efficacy and Safety. *J. Biomed. Biotechnol.* **2011**, *2011*, 854872.

(44) Bennett, C. L.; Adegboro, O. S.; Calhoun, E. A.; Raisch, D. Beyond the Black Box: Drug- and Device-Associated Hypersensitivity Events. *Drug. Healthc. Patient Saf.* **2010**, *2*, 1–5.

(45) Szebeni, J.; Alving, C. R.; Savay, S.; Barenholz, Y.; Priev, A.; Danino, D.; Talmon, Y. Formation of Complement-Activating Particles in Aqueous Solutions of Taxol: Possible Role in Hypersensitivity Reactions. *Int. Immunopharmacol.* **2001**, *1*, 721–735.

(46) Li, W.-T. Nanoparticles for Photodynamic Therapy. In *Handbook of biophotonics*; Popp, J.; Tuchin, V. V.; Chiou, A.; Heinemann, S. H., Eds.; Wiley-VCH Verlag GmbH & Co. KGaA: Weinheim, Germany, 2013.

(47) Allémann, E.; Brasseur, N.; Benrezzak, O.; Rousseau, J.; Kudrevich, S. V; Boyle, R. W.; Leroux, J. C.; Gurny, R.; Van Lier, J. E. PEG-Coated Poly(lactic Acid) Nanoparticles for the Delivery of

Hexadecafluoro Zinc Phthalocyanine to EMT-6 Mouse Mammary Tumours. *J. Pharm. Pharmacol.* **1995**, *47*, 382–387.

(48) Kuruppuarachchi, M.; Savoie, H.; Lowry, A.; Alonso, C.; Boyle, R. W. Polyacrylamide Nanoparticles as a Delivery System in Photodynamic Therapy. *Mol. Pharm.* **2011**, *8*, 920–931.

(49) Couleaud, P.; Morosini, V.; Frochot, C.; Richeter, S.; Raehm, L.; Durand, J. O. Silica-Based Nanoparticles for Photodynamic Therapy Applications. *Nanoscale* **2010**, *2*, 1083–1095.

(50) Obaid, G.; Chambrier, I.; Cook, M. J.; Russell, D. A. Cancer Targeting with Biomolecules: A Comparative Study of Photodynamic Therapy Efficacy Using Antibody or Lectin Conjugated Phthalocyanine-PEG Gold Nanoparticles. *Photochem. Photobiol. Sci.* **2015**, *14*, 737–747.

(51) Sharma, S.; Chiang, L.; Hamblin, M. Photodynamic Therapy with Fullerenes in Vivo: Reality or a Dream? *Nanomedicine* **2011**, *6*, 1813–1825.

(52) Lim, S. F.; Austin, R. H. *Upconverting Nanoparticle-Based Multi-Functional Nanoplatform for Enhanced Photodynamic Therapy: Promises and Perils*; Hamblin, M. R.; Avci, P., Eds.; 1st ed.; Elsevier, 2015.

(53) Locatelli, E.; Comes Franchini, M. Biodegradable PLGA-B-PEG Polymeric Nanoparticles: Synthesis, Properties, and Nanomedical Applications as Drug Delivery System. *J. Nanoparticle Res.* **2012**, *14*, 1316.

(54) Makadia, H. K.; Siegel, S. J. Poly Lactic-Co-Glycolic Acid (PLGA) as Biodegradable Controlled Drug Delivery Carrier. *Polymers (Basel).* **2011**, *3*, 1377–1397.

(55) Parveen, S.; Sahoo, S. K. Polymeric Nanoparticles for Cancer Therapy. *J. Drug Target.* **2008**, *16*, 108–123.

(56) Yoo, H. S.; Oh, J. E.; Lee, K. H.; Park, T. G. Biodegradable Nanoparticles Containing Doxorubicin-PLGA Conjugate for Sustained Release. *Pharm. Res.* **1999**, *16*, 1114–1118.

(57) Panyam, J.; Labhasetwar, V. Biodegradable Nanoparticles for Drug and Gene Delivery to Cells and Tissue. *Adv. Drug Deliv. Rev.* **2003**, *55*, 329–347.

(58) Qaddoumi, M. G.; Gukasyan, H. J.; Davda, J.; Labhasetwar, V.; Kim, K.-J.; Lee, V. H. L. Clathrin and Caveolin-1 Expression in Primary Pigmented Rabbit Conjunctival Epithelial Cells: Role in PLGA Nanoparticle Endocytosis. *Mol. Vis.* **2003**, *9*, 559–568.

(59) Cartiera, M. S.; Johnson, K. M.; Rajendran, V.; Caplan, M. J.; Saltzman, W. M. The Uptake and Intracellular Fate of PLGA Nanoparticles in Epithelial Cells. *Biomaterials* **2009**, *30*, 2790–2798.

(60) Rojnik, M.; Kocbek, P.; Moret, F.; Compagnin, C.; Celotti, L.; Bovis, M. J.; Woodhams, J. H.; Macrobert, A. J.; Scheglmann, D.; Helfrich, W.; *et al.* In Vitro and in Vivo Characterization of Temoporfin-Loaded PEGylated PLGA Nanoparticles for Use in Photodynamic Therapy. *Nanomedicine (Lond).* **2012**, *7*, 663–677.

(61) Lei, T.; Srinivasan, S.; Tang, Y.; Manchanda, R.; Nagesetti, A.; Fernandez-Fernandez, A.; McGoron, A. J. Comparing Cellular Uptake and Cytotoxicity of Targeted Drug Carriers in Cancer Cell Lines with Different Drug Resistance Mechanisms. *Nanomedicine* **2011**, *7*, 324–332.

(62) Konan, Y. N.; Chevallier, J.; Gurny, R.; Allémann, E. Encapsulation of P-THPP into Nanoparticles: Cellular Uptake, Subcellular Localization and Effect of Serum on Photodynamic Activity. *Photochem. Photobiol.* **2003**, *77*, 638–644.

(63) Chernenko, T.; Matthäus, C.; Milane, L.; Quintero, L.; Amiji, M.; Diem, M. Label-Free Raman Spectral Imaging of Intracellular Delivery and Degradation of Polymeric Nanoparticle Systems. *ACS Nano* **2009**, *3*, 3552–3559.

(64) Hillaireau, H.; Couvreur, P. Nanocarriers' Entry into the Cell: Relevance to Drug Delivery. *Cell. Mol. Life Sci.* **2009**, *66*, 2873–2896.

(65) Konan, Y. N.; Cerny, R.; Favet, J.; Berton, M.; Gurny, R.; Allémann, E. Preparation and Characterization of Sterile Sub-200 Nm Meso-tetra(4-Hydroxyphyenyl)poprhyrin-Loaded Nanoparticles for Photodynamic Therapy. *Eur. J. Pharm. Biopharm.* **2003**, *55*, 115–124.

(66) Konan, Y. N.; Berton, M.; Gurny, R.; Allemann, E. Enhanced Photodynamic Activity of Meso-tetra(4-Hydroxyphenyl) Porphyrin by Incorporation into Sub-200 Nm Nanoparticles. *Eur. J. Pharm. Sci.* **2003**, *18*, 241–249.

(67) McCarthy, J. R.; Perez, J. M.; Brückner, C.; Weissleder, R. Polymeric Nanoparticle Preparation That Eradicates Tumors. *Nano Lett.* **2005**, *5*, 2552–2556.

(68) Ricci-Junior, E.; Marchetti, J. M. Zinc(II) Phthalocyanine Loaded PLGA Nanoparticles for Photodynamic Therapy Use. *Int. J. Pharm.* **2006**, *310*, 187–195.

(69) Gomes, A. J.; Lunardi, C. N.; Tedesco, A. C. Characterization of Biodegradable poly(D,L-Lactide-Co-Glycolide) Nanoparticles Loaded with Bacteriochlorophyll-a for Photodynamic Therapy. *Photomed. Laser Surg.* **2007**, *25*, 428–435.

(70) Zeisser-Labouebe, M.; Lange, N.; Gurny, R.; Delie, F. Hypericin-Loaded Nanoparticles for the Photodynamic Treatment of Ovarian Cancer. *Int. J. Pharm.* **2006**, *326*, 174–181.

(71) Zeisser-Labouèbe, M.; Delie, F.; Gurny, R.; Lange, N. Benefits of Nanoencapsulation for the Hypercin-Mediated Photodetection of Ovarian Micrometastases. *Eur. J. Pharm. Biopharm.* **2009**, *71*, 207–213.

(72) Torchilin, V. Tumor Delivery of Macromolecular Drugs Based on the EPR Effect. *Adv. Drug Deliv. Rev.* **2011**, *63*, 131–135.

(73) Avgoustakis, K.; Beletsi, A.; Panagi, Z.; Klepetsanis, P.; Livaniou, E.; Evangelatos, G.; Ithakissios, D. S. Effect of Copolymer Composition on the Physicochemical Characteristics, in Vitro Stability, and Biodistribution of PLGA–mPEG Nanoparticles. *Int. J. Pharm.* **2003**, *259*, 115–127.

(74) Betancourt, T.; Byrne, J. D.; Sunaryo, N.; Crowder, S. W.; Kadapakkam, M.; Patel, S.; Casciato, S.; Brannon-Peppas, L. PEGylation Strategies for Active Targeting of PLA/PLGA Nanoparticles. *J. Biomed. Mater. Res. A* **2009**, *91*, 263–276.

(75) Alexis, F.; Pridgen, E.; Molnar, L. K.; Farokhzad, O. C. Factors Affecting the Clearance and Biodistribution of Polymeric Nanoparticles. *Mol. Pharm. 5*, 505–515.

(76) Gref, R.; Lück, M.; Quellec, P.; Marchand, M.; Dellacherie, E.; Harnisch, S.; Blunk, T.; Müller, R. "Stealth" Corona-Core Nanoparticles Surface Modified by Polyethylene Glycol (PEG): Influences of the Corona (PEG Chain Length and Surface Density) and of the Core Composition on Phagocytic Uptake and Plasma Protein Adsorption. *Colloids Surf. B. Biointerfaces* **2000**, *18*, 301–313.

(77) Owens, D. E.; Peppas, N. a. Opsonization, Biodistribution, and Pharmacokinetics of Polymeric Nanoparticles. *Int. J. Pharm.* **2006**, *307*, 93–102.

(78) Allemann, E.; Rousseau, J.; Brasseur, N.; Kudrevich, S. V; Lewis, K.; van Lier, J. E. Photodynamic Therapy of Tumours with Hexadecafluoro Zinc Phthalocynine Formulated in PEG-Coated Poly(lactic Acid) Nanoparticles. *Int. J. cancer.Journal Int. du cancer* **1996**, *66*, 821–824.

(79) Marrache, S.; Choi, J. H.; Tundup, S.; Zaver, D.; Harn, D. A.; Dhar, S. Immune Stimulating Photoactive Hybrid Nanoparticles for Metastatic Breast Cancer. *Integr. Biol. (Camb).* **2013**, *5*, 215–223.

(80) Allémann, E.; Rousseau, J.; Brasseur, N.; Kudrevich, S. V; Lewis, K.; van Lier, J. E. Photodynamic Therapy of Tumours with Hexadecafluoro Zinc Phthalocynine Formulated in PEG-Coated Poly(lactic Acid) Nanoparticles. *Int. J. Cancer* **1996**, *66*, 821–824.

(81) Li, B.; Moriyama, E. H.; Li, F.; Jarvi, M. T.; Allen, C.; Wilson, B. C. Diblock Copolymer Micelles Deliver Hydrophobic Protoporphyrin IX for Photodynamic Therapy. *Photochem. Photobiol.* **2007**, *83*, 1505–1512.

(82) Rojnik, M.; Kocbek, P.; Moret, F.; Compagnin, C.; Celotti, L.; Bovis, M. J.; Woodhams, J. H.; MacRobert, A. J.; Scheglmann, D.; Helfrich, W.; *et al.* In Vitro and in Vivo Characterization of Temoporfin-Loaded PEGylated PLGA Nanoparticles R Esearch A Rticle. *Nanomedicine* **2012**, *7*, 663–677.

(83) Marrache, S.; Choi, J. H.; Tundup, S.; Zaver, D.; Harn, D. a; Dhar, S. Immune Stimulating Photoactive Hybrid Nanoparticles for Metastatic Breast Cancer. *Integr. Biol. (Camb).* **2013**, *5*, 215–223.

(84) Singhana, B.; Slattery, P.; Melancon, M. P. *Targeted Gold Nanoshells*; Hamblin, M. R.; Avci, P., Eds.; 1st ed.; Elsevier, 2015.

(85) Planas, O.; Boix-Garriga, E.; Rodríguez-Amigo, B.; Torra, J.; Bresolí-Obach, R.; Flors, C.; Viappiani, C.; Agut, M.; Ruiz-González, R.; Nonell, S. Chapter 9: Newest Approaches to Singlet Oxygen Photosensitisation in Biological Media. In *Photochemistry: Specialist Periodical Report*; Fasani, E.; Albini, A., Eds.; Photochemistry; Royal Society of Chemistry: Cambridge, 2015; Vol. 42, pp. 233–278.

(86) Ferreira, C. S. M.; Cheung, M. C.; Missailidis, S.; Bisland, S.; Gariepy, J. Phototoxic Aptamers Selectively Enter and Kill Epithelial Cancer Cells. *Nucleic Acids Res.* **2009**, *37*, 866–876.

(87) Moret, F.; Scheglmann, D.; Reddi, E. Folate-Targeted PEGylated Liposomes Improve the Selectivity of PDT with Meta-Tetra(hydroxyphenyl)chlorin (m-THPC). *Photochem. Photobiol. Sci.* **2013**, *12*, 823–834.

(88) García-Díaz, M.; Nonell, S.; Villanueva, A.; Stockert, J. C.; Cañete, M.; Casadó, A.; Mora, M.; Sagristá, M. L. Do Folate-Receptor Targeted Liposomal Photosensitizers Enhance Photodynamic Therapy Selectivity? *Biochim. Biophys. Acta* **2011**, *1808*, 1063–1071.

CHAPTER 2

General techniques and methods

This chapter describes the common photophysical techniques, general synthetic procedures as well as analytical techniques that have been employed over this work. The general methodology for preparation of nanoparticles and the techniques and methods for their characterization are also described. Finally, general protocols of *in vitro* cell culture are also explained. Specific details will be described in the experimental section of each corresponding chapter.

2.1. Steady state optical techniques

With the goal of determining the photophysical properties of the PS embedded in the NPs, NP suspensions were appropriately diluted in water for all photophysical measurements. When the main interest was to ascertain the maintenance of the photophysical properties of the PS once released from the NP, an aliquot of the suspension was diluted in an organic solvent, typically tetrahydrofuran (THF) or dimethylsulfoxide (DMSO), which could dissolve the PS and the polymer constituting the NPs, thereby disrupting them and releasing the PS.

2.1.1. Absorbance

Absorption spectra were recorded on a double beam Varian Cary 6000i UV-vis-NIR spectrophotometer (Agilent Technologies, Santa Clara, CA, USA). In order to remove the scattering baseline when measuring the absorption spectra of PSs entrapped or conjugated to the NPs, a spectrum of a suspension of blank NPs of the same dilution was subsequently recorded. Both spectra were mathematically subtracted to yield the baseline corrected absorption spectrum of the PS.

2.1.2. Fluorescence

Fluorescence spectra were recorded in a Fluoromax 4 spectrofluorometer (Horiba Jobin Yvon, Edison, NJ, USA) exciting at the appropriate wavelength according to the PS.

Fluorescence quantum yields (Φ_F) were determined by the comparative method.[1] Fluorescence emission spectra (*F*) were collected for a set of sample and reference solutions of increasing absorbance values and the area under the spectrum was plotted against the absorption factor $(1 - 10^{-A})$. According to equation (2.1), a linear plot should be obtained the slope of which is proportional to Φ_F:

$$F = \left[\frac{\kappa}{n_r^2} I_0 \Phi_F\right] \times (1 - 10^{-A}) \qquad \text{Eq. (2.1)}$$

κ is an instrumental factor, I_0 is the radiant power of the excitation beam, and n_r is the solvent's refractive index. Thus, Φ_F for PS-loaded or –conjugated NPs was determined from the ratio of slopes measured for the NP suspensions and the proper reference.

2.2. Time-resolved optical techniques

Time-resolved optical techniques enable the detection of excited states or intermediate species upon pulsed irradiation of a sample. These species formed upon light absorption can be monitored through changes in the signal intensity of an analyzing beam (for absorption spectroscopy) or through photon emission (in the case of fluorescence or phosphorescence spectroscopy), in all cases the detection being temporally resolved.

Nowadays these techniques are usually coupled to photon counting detectors due to their better time resolution, better sensitivity and lower interference from sensitizer luminescence or scattered laser light compared to analog detectors. Photomultiplier tubes (PMTs) are detectors the response of which is based on the initiation and amplification of a pulse of electrical current when a photon strikes their surface. This principle has inspired the photon counting mode and therefore the detectors employed are commonly photomultiplier tubes (PMTs). Of the three photon counting techniques existing, namely gated photon counting (GPC), multichannel scaling (MCS) and time-correlated single photon counting (TCSPC), only the last two have been employed for the herein described experiments.[2]

2.2.1. Time-correlated single photon counting (TCSPC)

This method is common for time-resolved fluorescence measurements and it is based on the precisely timed registration of the first single photon arrival to the detector from the emitting sample. The reference for time registration is the excitation pulse. The cumulative signal obtained from repetitive cycles is a histogram of photon arrivals per time bin which represents the time decay one would have obtained from the observation of a single excitation-emission cycle (Figure 2.1). It is a prerequisite of this technique to keep the probability of registering more than one photon per cycle low, which can be accomplished by attenuating the light level arriving at the sample, or in other words, to keep the count rate at the detector equal or below 1% of the excitation rate. It must be taken into account that the measured fluorescence decay is the convolution of the “real” fluorescence decay with the instrumental response factor (IRF). Measurement of the IRF is achieved by placing some scattering medium at the sample compartment, thus no fluorescence but only some scattered excitation light will reach the detector. In order to obtain the real fluorescence decay, reconvolution by data analysis software with the measured fluorescence decay and the IRF needs to be performed.[3]

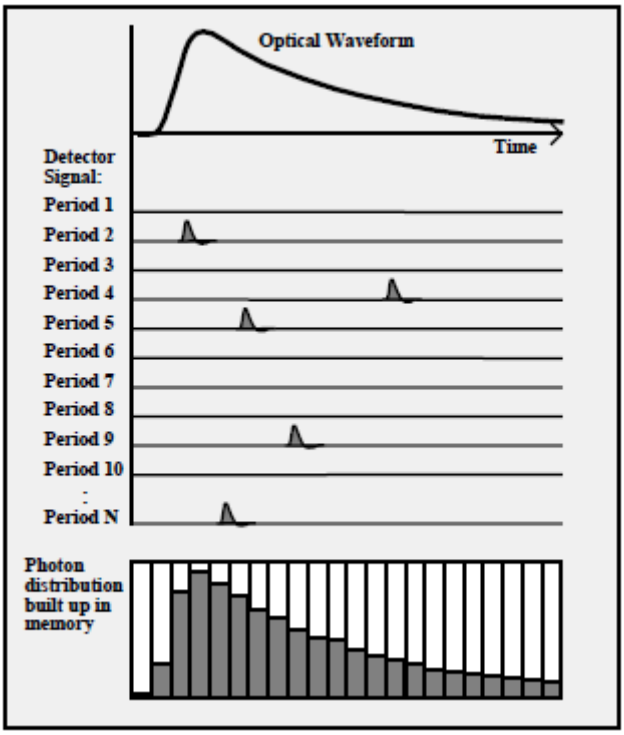

Figure 2.1. Principle of time-correlated single photon counting acquisition. From [3].

Time-resolved fluorescence decays were recorded at a specific wavelength (typically 650 nm for the compounds studied), selected by a monochromator grating, using a time-correlated single photon counting system (Fluotime 200, PicoQuant GmbH, Berlin, Germany) with a pulsed LED source emitting at 457 or 596 nm (depending on the PS studied) for excitation. Decays were analyzed using the PicoQuant FluoFit 4.5.3 data analysis software. Absorbance of the samples was kept below 0.1 at the excitation wavelength in all cases and the photon counting rate was kept below 1%. The IRF signal was measured by placing a cuvette with a suspension of Ludox® in water.

2.2.2. Time-resolved NIR phosphorescence detection (TRPD)

This method is the most commonly employed to directly observe and monitor $^1O_2$ formation and decay and subsequently to measure its lifetime (τ_Δ). It is based on the time-resolved detection of its weak phosphorescence centered at 1275 nm (Figure 2.2). In this case, the photon-counting method is MCS, in which all detected photons are counted and sorted out in the different positions of a board memory, thus the time distribution of the detected photons is obtained at once.

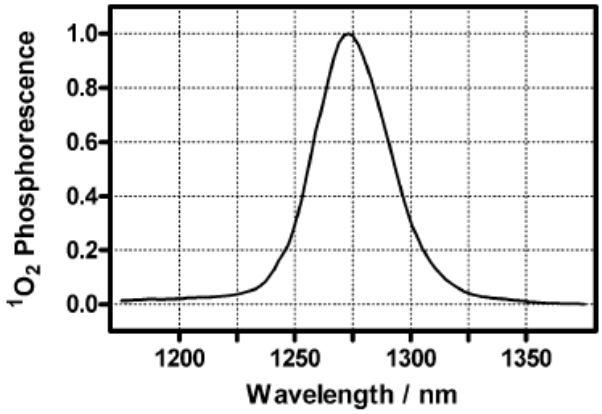

Figure 2.2. Near-infrared spectrum of $^1O_2$ phosphorescence. From [2].

$^1O_2$ phosphorescence was detected using a customized PicoQuant Fluotime 200 system described elsewhere.[2] Briefly, a diode-pumped pulsed Nd:YAG laser (FTSS355-Q, Crystal Laser, Berlin, Germany) working at 10 or 1 kHz repetition rate at 532 nm (1 μJ per pulse) was used for excitation. A 1064 nm rugate notch filter (Edmund Optics, York, UK) was placed at the exit port of the laser to remove any residual component of its fundamental emission in the NIR region. The luminescence exiting from the side of the cuvette was filtered by a cold mirror and a bandpass filter of the appropriate wavelength-1220, 1275 or 1325 nm (Spectrogon AB, Täby, Sweden). A TE-cooled Hamamatsu near IR photomultiplier (model H9170-45, Hamamatsu Photonics, Japan), sensitive from 950 to 1400 nm, was used to detect IR luminescence. The detector was operated in photon counting mode and its output sent to a multichannel scaler (PicoQuant Nanoharp 250). Photon histograms were analyzed using the PicoQuant FluoFit 4.5.3 data analysis software. For temperature-dependent measurements, an Ultraterm 6000383 (JP Selecta S.A., Abrera, Spain) thermostat was used in order to control the temperature.

The temporal profile of the time-resolved $^1O_2$ phosphorescence signals (S_t) is typically a rise-and-decay function that can be fit with the following mathematical model (Eq. 2.2):[4]

$$S_t = \sum_i S_{0_i} \times \frac{\tau_{\Delta_i}}{\tau_{\Delta_i} - \tau_{T_i}} \times \left(e^{-t/\tau_{\Delta_i}} - e^{-t/\tau_{T_i}} \right) \qquad \text{(Eq. 2.2)}$$

The subscript *i* refers to the number of independent $^1O_2$ populations in the sample. S_0 is a quantity proportional to the concentration of $^1O_2$ created by the laser pulse and τ_Δ and τ_T are the lifetimes of $^1O_2$ and $^3PS^*$, respectively.

The photosensitizer's triplet lifetime was determined, whenever possible, by fitting with Eq. 2.3 to the signal obtained at a wavelength where the triplet state of the photosensitizer emits, typically at 1110 nm:

$$I_t = \sum_i A_i \times e^{-t/\tau_{T_i}} \qquad \text{(Eq. 2.3)}$$

A_i is proportional to the concentration of excited triplet states of the photosensitizer and τ_T is the actual triplet state lifetime of the photosensitizer.

2.2.3. UV-vis nanosecond laser flash photolysis

This technique is employed to examine the absorption or emission with temporal resolution of triplet states or other photochemically generated intermediate species. In this study, it served to determine the PS triplet state kinetics by triplet-triplet absorption when information obtained from the observation of its time-resolved phosphorescence was insufficient. Several setups exist for the detection of triplet-triplet absorption, but most of them have two features in common (Figure 2.3). Firstly, any setup comprises an excitation source to produce triplet states, commonly a pulsed laser. Second, a "monitoring" light source, in this case a Xe lamp, probes the changes in absorbance at the sample.

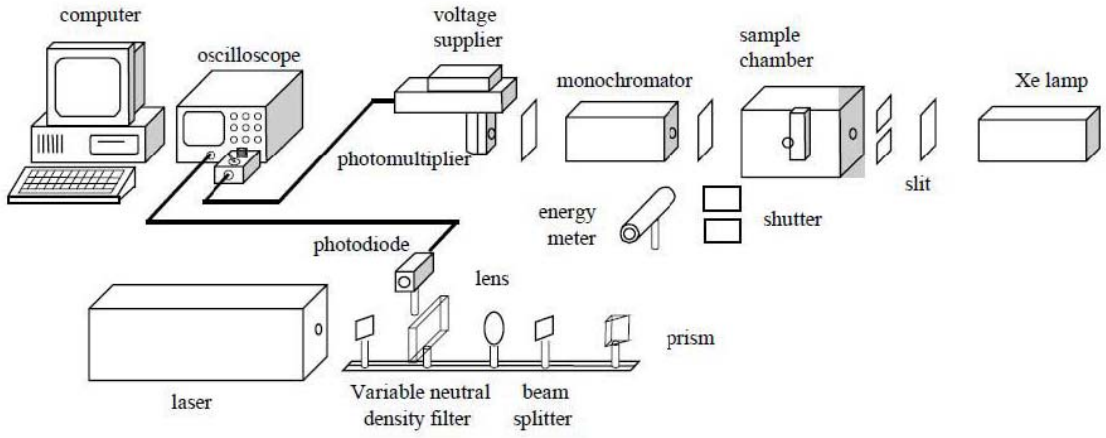

Figure 2.3. Experimental setup for UV-visible nanosecond laser flash photolysis. Adapted from [4].

Transient absorption experiments in the UV–visible (UV–vis) region were carried out using a home-built nanosecond laser flash photolysis system. In this instrument, the 2nd harmonic (532 nm) of a Continuum Surelite I-10 Nd:YAG laser (10 Hz, 5 ns pulsewidth, 0.05-1 mJ per pulse) was

directed onto the sample. Changes in the sample absorbance were detected by a Hamamatsu R928 photomultiplier in order to monitor the intensity variations of an analyzing beam produced by a 75W short arc Xe lamp (USHIO) and spectral discrimination was provided by a PTI 101 monochromator. The signal was fed to a Lecroy Wavesurfer 454 oscilloscope for digitizing (1 shot, typically) and finally transferred through a GPIB interface (National Instruments) to a PC computer for data storage and analysis. The TTL sync output of the laser was used to trigger the oscilloscope. The energy of the laser pulse was varied by controlling the Q-switch delay and measured with a pyroelectric energy meter (RJP 735 and RJ 7610) from Laser Precision Corp. The system was controlled by the in house-developed LKS software (LabView, National Instruments).

2.3. General synthetic techniques for functionalization of poly-(*D,L*-lactide) and poly-(*D,L*-lactide-*co*-glycolide) polymers

2.3.1. Conjugation of porphyrins to poly-(*D,L*-lactide-*co*-glycolide)

A cationic (hydrophilic) and a hydrophobic porphyrin were respectively conjugated to PLGA in a two-step synthetic procedure involving amide coupling chemistry in the first step and Cu(I)-catalyzed azide-alkyne cycloaddition (CuAAC) click chemistry in the second step. The reader is referred to the Experimental Section in Chapter 4 (4.2) for a detailed description of the procedures.

2.3.2. Conjugation of peptides to poly-(*D,L*-lactide)

PLA was coupled either directly (cRGD-PLA) or through a PEG spacer (cRGD-PEG-PLA) to the cyclic peptide cRGDfK (hereinafter cRGD), a ligand binding with high affinity to $\alpha_v\beta_3$ integrin receptors. Furthermore, two more polymers containing the spacer PEG were synthesized: PLA coupled to PEG with no peptide (PEG-PLA) and PLA coupled to PEG and the non-binding peptide cRADfK (hereinafter cRAD), obtaining the conjugate cRAD-PEG-PLA.

The direct conjugation between PLA and cRGD was accomplished by peptide coupling chemistry. On the contrary, the conjugation of these two moieties with the PEG as a spacer required a 5-step synthetic procedure involving peptide coupling chemistry and a metal-free azide-alkyne cycloaddition. The reader is referred to the Experimental Section in Chapter 5 (5.2) for a detailed description of the procedures.

2.4. General techniques for analysis of functionalized polymers

2.4.1. Nuclear Magnetic Resonance

Proton Nuclear Magnetic Resonance (^{1}H-NMR) spectra were recorded in a Varian Gemini 300, or 400 MHz or on a Varian Innova 500 MHz. Samples were dissolved in deuterated solvents, commonly chloroform ($CDCl_3$), DMSO (DMSO-d6) or acetone (acetone-d6) for spectra recording. Obtained spectra were analyzed by the software MestreNova 8.1. Chemical shifts (δ) are quoted in parts per million (ppm), with residual solvent peaks being used as the internal reference for chemical shifts of sample signals. In parentheses it is reported the integration, yielding the number of ^{1}H corresponding to a given signal, or in the case of polymers, a number proportional to the total amount of protons; the multiplicity of the signal, indicated as singlet (s), doublet (d), triplet (t) or multiplet (m); and the coupling constant (J, Hz), which can be calculated for systems with a defined multiplicity.

2.4.2. Ultra-High Performance Liquid Chromatography

Ultra-High Performance Liquid Chromatography (UHPLC) was performed for checking completeness of reactions and assessing qualitatively the adequacy of the purification procedure.

UHPLC was carried out with a ThermoScientific Hypersil GOLD column (50 x 2.1 mm, particle size 19 μm) in a ThermoScientific Accela system coupled to a PDA detector (PDA Accela 80 Hz detector, ThermoScientific) complementarily set at 210 and 258 nm. The mobile phase was a H_2O / ACN mixture acidified with 0.1% formic acid (Merck) in a gradient mode; an initial mixture with 2% ACN was ramped linearly up to 100% ACN from minute 0.50 to minute 5.80, and 100% ACN was kept until minute 7.50. The gradient was returned back to the initial composition in 10 seconds and kept for 1.90 min.

2.5. Preparation and characterization of nanoparticles

2.5.1. Preparation of nanoparticles by nanoprecipitation

Conventionally, two groups of techniques for NP formation have been reported: the first involves polymerization of monomers while the second is based on the dispersion of preformed polymers. Some of the techniques in the second classification group include salting-out, emulsification-diffusion, emulsification-evaporation, or nanoprecipitation. The advantage of

this second group is that physicochemical features of the NPs such as morphology, internal structure, size, drug loading and release kinetics can be modulated more easily. In this study, NPs were prepared in all cases by a modified nanoprecipitation method,[5,6] since it was found to be the most convenient in terms of the length of time needed for NP preparation, simplicity of the method and obtention of the smallest NPs. This technique consists in adding dropwise an organic phase to an aqueous phase in continuous stirring. The organic solvent employed must be miscible in water, and this phase contains the hydrophobic components of the NPs, i.e. the PLA or PLGA polymers and the PSs in the current case. The aqueous phase can be either water or an aqueous solution of a surfactant such as polyvinyl alcohol (PVA) or poloxamer, although PVA is the emulsifier most commonly used during NP formulation because the particles formed are relatively uniform, smaller in size and easy to redisperse in aqueous medium. In this method, contrary to salting-out or emulsification-diffusion, no precursor emulsion is formed during NP preparation. NP formation is explained by solvent diffusion from the organic phase into the aqueous phase, which produces polymer chain aggregation to form NPs.[7] The reader is referred to the Experimental Section of each corresponding chapter for a detailed explanation of the procedure in each particular case.

2.5.2. Characterization

NP suspensions were characterized in terms of their physicochemical properties, i.e. PS concentration, size, polydispersity index and surface charge, as well as in terms of their stability in culture medium containing 10% fetal bovine serum (FBS).

Photosensitizer concentration: Bulk PS concentration was estimated by UV-visible absorption spectroscopy or fluorescence, depending on the type and amount of incorporated PS. An aliquot of PS-loaded or PS-conjugated NPs was dissolved in an organic solvent, typically THF or DMSO (NP suspension:solvent 1:15, v/v) to disrupt NPs and dissolve the PS. This solution was stirred to ensure a complete dissolution of the polymer and the PS, and the absorption or fluorescence spectra were recorded. PS concentration was determined by comparison with standard curves obtained at the same conditions. Drug loading and entrapment efficiency were calculated as follows:

$$Drug\ loading\ \% = \frac{PS\ mass}{PLGA\ mass} \times 100 \qquad \text{Eq. (2.4)}$$

$$Entrapment\ efficiency\ \% = \frac{drug\ loading}{theoretical\ drug\ loading} \times 100 \qquad \text{Eq. (2.5)}$$

Size, polydispersity and surface charge: Size and polydispersity index of NPs were determined by dynamic light scattering (DLS) and zeta potential by laser Doppler micro-electrophoresis, using a Zetasizer Nano ZS (Malvern Instruments Ltd, Malvern, UK) at room temperature. To carry out the measures, NP suspensions were diluted (NP suspension:H_2O 1:6 v/v). Size measurements were performed at the excitation wavelength of 633 nm. To measure zeta potential, the Malvern device was calibrated with carboxy-modified polystyrene latex samples of known zeta potential.

Stability of formulations in cell culture medium: Stability of NPs was assessed in cell culture medium in presence of 10% FBS (the same concentration supplied to cultured cells). NP suspension was diluted to a final PS concentration of 10 μM in supplemented culture medium with a 10% FBS. These suspensions were incubated for various times at 37 °C at 400 rpm in a Termomixer Comfort equipped with an exchangeable thermoblock for 15 mL falcon tubes (Eppendorf AG, Hamburg, Germany). After certain time, an aliquot of 700 μL was removed, put in ice to stop the interaction, and centrifuged at 6400*xg* for 15 min, at 4 °C (Hermle Z 233 M-2 Microliter centrifuge, HERMLE Labortechnik GmbH, Germany). The pellet, containing NP aggregates, was discarded and an aliquot of the supernatant was diluted in DMSO (supernatant:DMSO 1:15, v/v) to disrupt the remaining NPs. Spectra were recorded in a Beckman DU40 UV-vis spectrophotometer (Beckman Coulter, Inc., Brea, CA, USA) or in a Synergy H1 Hybrid microplate reader (BioTek Instruments, Inc., Winooski, VT, USA) and PS concentration was determined by comparison with standard curves obtained in the same conditions.

2.6. Cell culture

2.6.1. Cell lines

Cell lines used in Chapters 3 and 4 were Human HeLa cervix adenocarcinoma cells (ATCC CCL-2). In Chapter 5 experiments were performed with Human U-87 MG glioblastoma (ECACC-89081402), which is one of the most overexpressing $\alpha_v\beta_3$ integrin receptor-cell lines.[8] Both of them are adherent and grow in monolayer up to confluence after seeding. HeLa cells were cultured with Dulbeco's Modified Eagle's Medium (DMEM)-High Glucose supplemented with 10% (v/v) FBS, 1% *L*-Glutamine, 1% (v/v) Streptomycin and 1% (v/v) Penicillin. HeLa cells were seeded in T-25 flasks and allowed to grow up to 80% confluence before subculturing. U-87 MG cells were cultured with Minimum Essential Media (MEM) (ThermoFisher, 31095-029) with *L*-Glutamine supplemented with 10% (v/v) Fetal Calf Serum (FCS), 1% (v/v) Streptomycin and 1%

(v/v) Penicillin, seeded in T-75 flasks and allowed to grow up to 80% confluence before subculturing. Both cell lines were grown at 37 °C in a humidified sterile atmosphere of 95% air and 5% CO_2.

These cell lines were maintained frozen in liquid nitrogen in CryoTubes™ (Nunc, Nalge Nunc International, IL, USA) with their corresponding supplemented culture medium with 5% DMSO as a cryoprotecting agent.

2.6.2. Cellular uptake

Cellular uptake of the PS-loaded NPs was determined by fluorescence spectroscopy of the incubated cells (Chapter 5).

U-87 MG cells were seeded in 96-well plates in a density of 10000 cells/well and allowed to grow overnight. NP suspensions were diluted in supplemented MEM to obtain a final Ppa concentration of 1 μM. Supernatant medium was discarded and the medium containing the NPs was added to the adhered cells at different time points in order to obtain different incubation times. After incubation, medium was discarded, cells were washed twice with supplemented MEM, and finally DMSO was added to dissolve cell content as well as the internalized Ppa. DMSO was employed instead of an aqueous solution of SDS 2% to ensure that NPs that might have been internalized but not completely degraded were dissolved completely and their cargo completely released for quantification. Fluorescence spectra of the samples were recorded in a SynergyMx™ or Synergy H1 Hybrid microplate reader (BioTek Instruments, Inc., Winooski, VT, USA). Fluorescence intensity was normalized by determining the protein content per each sample by the Bicinchoninic acid (BCA) assay (Thermo Scientific™Pierce™, Thermo Fisher Scientific, Inc). Briefly, this assay is based on the colorimetric quantification of the total concentration of protein in the medium. Protein reduces Cu^{2+} to Cu^{+} in alkaline medium, and one cation of Cu^{+} is chelated by two molecules of BCA, forming a water-soluble complex with strong absorbance at 562 nm. After fluorescence measurements, DMSO was discarded and SDS 2% added in order to lysate the cells. 25 μL of each sample were mixed with 200 μL of the reagent, the microplate shaken for 30 s, and incubated at 37 °C for 30 min. After this incubation time, the microplate was cooled to room temperature and the absorbance read at 562 nm on the microplate reader. Absorbance values were interpolated to a standard curve prepared with bovine serum albumin (BSA) under the same conditions. Samples were quantified in triplicate.

2.6.3. Light sources

For cell culture irradiation, three types of light sources were employed. In Chapter 3, irradiation was carried out with a Sorisa Photocare LED source (Barcelona, Spain) of a wavelength range of 530 ± 20 nm. The light intensity at the irradiation site was 5.2 mW/cm^2 measured with a LaserStar Ophir power meter (Logan, UT, USA). In Chapter 4, irradiation was carried out with a LED source of a wavelength range of 515 ± 50 nm, with a light intensity at the irradiation site of 6.6 mW/cm^2. In Chapter 5, irradiation was carried out with OSRAM L18/W67 tubular fluorescent lamps of a wavelength range of 450 ± 50 nm with a light intensity at the irradiation site of 11 mW/cm^2.

2.6.4. Photodynamic treatments *in vitro*

Reduction in cell viability as a result of the phototoxic effect of the PS delivered by different types of vehicles was determined by means of the 3-(4,5-dimethylthiazol-2-yl)-2,5-diphenyltetrazolium bromide (MTT) assay.[9]

HeLa or U-87 MG cells were seeded in 24- or 96-well plates and grown up to 70% confluence. Cells were then incubated in the dark at 37 °C for a certain time with PS-loaded NPs, usually at ranges of PS concentration between 0.1 and 10 μM in complete culture medium. Empty NPs at equivalent concentrations of the loaded ones were used as controls to ensure that photocytotoxicity was not caused by the delivery systems. Cells without any treatment were taken as controls. Subsequently, the medium was discarded, cells were washed three times with cold PBS 1x and fresh complete medium was added. Samples were irradiated at different times to achieve the intended light fluence. Cells were again incubated for 24 h in the dark and reduction in cell viability was determined by the MTT assay. Briefly, remaining cells were incubated with 0.05 mg/mL MTT (HeLa) or 0.1 mg/mL (U-87 MG) in supplemented culture medium for 3 h, after which MTT had been metabolized by viable cells to form purple crystals of formazan. Medium was discarded, crystals were solubilized with pure DMSO and formazan concentration was determined by absorption at λ_{ex}: of 562 nm. Cell viability was determined by the ratio between the absorbance of treated cells and that of non-treated cells (control, 100% viability).

2.6.5. Spectroscopic measurements of cell suspensions

Time-resolved phosphorescence detection of $^1O_2$ in cell suspensions was assessed with the system described in section 2.2.2 in order to ascertain the production of these species after delivery of PSs into the cells (Chapter 3).

HeLa cells were seeded in T-175 flasks and grown up to 70% confluence in supplemented growth medium, in the dark at 37 °C and 5% CO_2. Cells were then incubated with ZnTPP-loaded PLGA and PEG-PLGA NPs for different periods of time (2, 6 and 24 h). A bulk 5 μM concentration of ZnTPP was chosen as a good compromise between acceptable $^1O_2$ signals and avoiding particle aggregation. Cells incubated with complete medium in the absence of nanoparticles were used as control. After incubation, the medium was discarded and cells were washed three times with cold PBS 1x, scrapped and resuspended. Subsequently, the suspension was centrifuged at 1000 rpm for 5 min at 20 °C; the supernatant was discarded, and the pellet was resuspended in 1.5 mL deuterated-PBS (d-PBS). $^1O_2$ phosphorescence of these final cellular suspensions was then detected using the customized equipment described in the previous section. Afterwards, a series of control experiments were carried out in order to ensure that the signal detected was due to $^1O_2$ inside the cells: 1) detection of luminescence at 1220 and 1325 nm, where $^1O_2$ does not emit, to ensure that the 1275 nm luminescence was due to $^1O_2$; 2) addition of sodium azide (NaN_3), a known $^1O_2$ quencher,[10] to further confirm the presence of $^1O_2$; 3) after the measurements, centrifugation of cell suspensions at 5000 rpm for 12 min at room temperature followed by analysis of the supernatant luminescence at 1275 nm to demonstrate that there was no significant leakage of the PS during the measurements.

2.7. References

(1) Brouwer, A. M. Standards for Photoluminescence Quantum Yield Measurements in Solution (IUPAC Technical Report). *Pure Appl. Chem.* **2011**, *83*, 2213–2228.

(2) Jiménez-Banzo, A.; Ragàs, X.; Kapusta, P.; Nonell, S. Time-Resolved Methods in Biophysics. 7. Photon Counting vs. Analog Time-Resolved Singlet Oxygen Phosphorescence Detection. *Photochem. Photobiol. Sci.* **2008**, *7*, 1003–1010.

(3) Becker, W.; Bergmann, A.; Biscotti, G.; Rück, A. Advanced Time-Correlated Single Photon Counting Technique for Spectroscopy and Imaging in Biomedical Systems. *Springer* **2004**, *5340*, 1–9.

(4) Nonell, S.; Braslavsky, S. E. Time-Resolved Singlet Oxygen Detection. *Methods Enzymol.* **2000**, *319*, 37–49.

(5) Barichello, J. M.; Morishita, M.; Takayama, K.; Nagai, T. Encapsulation of Hydrophilic and Lipophilic Drugs in PLGA Nanoparticles by the Nanoprecipitation Method. *Drug Dev. Ind. Pharm.* **1999**, *25*, 471–476.

(6) Yallapu, M. M.; Gupta, B. K.; Jaggi, M.; Chauhan, S. C. Fabrication of Curcumin Encapsulated PLGA Nanoparticles for Improved Therapeutic Effects in Metastatic Cancer Cells. *J. Colloid Interface Sci.* **2010**, *351*, 19–29.

(7) Galindo-Rodriguez, S.; Allémann, E.; Fessi, H.; Doelker, E. Physicochemical Parameters Associated with Nanoparticle Formation in the Salting-Out, Emulsification-Diffusion, and Nanoprecipitation Methods. *Pharm. Res.* **2004**, *21*, 1428–1439.

(8) Zhang, X.; Xiong, Z.; Wu, Y.; Cai, W.; Tseng, J. R.; Gambhir, S. S.; Chen, X. Quantitative PET Imaging of Tumor Integrin alphavbeta3 Expression with 18F-FRGD2. *J. Nucl. Med.* **2006**, *47*, 113–121.

(9) Mosmann, T. Rapid Colorimetric Assay for Cellular Growth and Survival - Application to Proliferation and Cyto-Toxicity Assays. *J. Immunol. Methods* **1983**, *65*, 55–63.

(10) Wilkinson, F.; Brummer, J. G. Rate Constants for the Decay and Reactions of the Lowest Electronically Excited Singlet State of Molecular Oxygen in Solution. *J. Phys. Chem. Ref. Data* **1981**, *24*, 809–999.

CHAPTER 3

Preparation, characterization and phototoxicity studies of poly-(ethylene glycol)-coated poly-(*D,L*-lactide-*co*-glycolide) nanoparticles with occluded photosensitizers

The use of drug delivery systems for PSs to improve their solubility in aqueous medium is being extensively explored. PLGA or PEG-PLGA NPs are favorable nanocarriers thanks to their biodegradable and biocompatible properties as well as their ability to incorporate hydrophobic drugs, among others. In this chapter, we have investigated the role of the PLGA matrix as well as of the additional PEG coating on the physicochemical and specially photophysical and photobiological properties of the encapsulated PSs. We have also compared the role of the chemical nature of the PS on its photophysical properties once being in the NP suspension.

3.1. Introduction

Much attention has recently been given to PLGA NPs as delivery vehicles for PDT, since this polymer is biodegradable, biocompatible, non-immunogenic, and it has been approved by the FDA for therapeutic use.[1] Abundant literature has been published on the benefits of PS incorporation into PLGA nanodelivery systems.[2–9] NPs coated with suitable polymers such as poly-(ethylene glycol) (PEGylated NPs) show an enhanced circulation time in the body, making them more attractive as passive targeting agents.[10] These features have made PEGylated PLA or PLGA NPs attractive as nanocarriers for photosensitizing agents, and have therefore been evaluated in terms of their photodynamic activity[10] as well as in terms of their photophysical aspects.[11,12] However, the influence of the coating polymer on the photophysical properties of the encapsulated PS, on its ability to photosensitize $^1O_2$, as well as on the photodynamic response of the NPs have not been studied in detail.

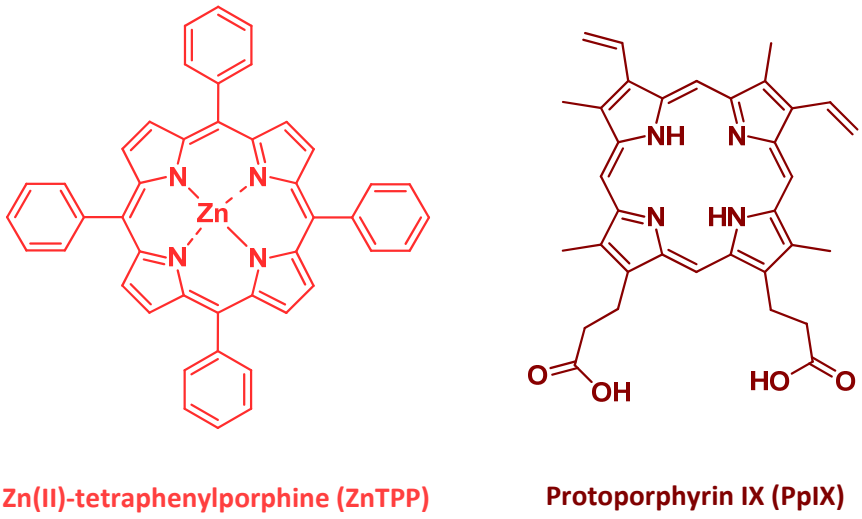

Zn(II)-tetraphenylporphine (ZnTPP) **Protoporphyrin IX (PpIX)**

Scheme 3.1. Chemical structure of the two porphyrins under study.

On the basis of these considerations, a comparative study of bare and PEG-coated PLGA NPs as delivery vehicles for Zn(II)-tetraphenylporphine (ZnTPP) (Scheme 3.1) was performed. ZnTPP was chosen since it is a model of a hydrophobic PS and its encapsulation in other delivery agents, i.e. liposomes, had been previously studied in our group.[13] Here, we evaluated (i) the physicochemical characteristics of both types of ZnTPP-loaded NPs; (ii) their spectroscopic and photophysical properties; (iii) their ability to photosensitize $^1O_2$, (iv) their photodynamic activity; (v) their effect on the subcellular localization of ZnTPP in HeLa cells; and (vi) their effect on the

cell death mechanism induced by PDT. Our results demonstrate that coating the PLGA surface with PEG leads to a faster and superior photodynamic response in HeLa cells.

Once the optimal coating was identified, PEG-coated PLGA NPs were used to encapsulate the clinically approved PS protoporphyrin IX (PpIX) (Scheme 3.1). Comparative analysis of the physicochemical and photophysical properties of the two nanosystems provided insight into the role of the PS structure on its photochemical behavior inside the PLGA NPs.

3.2. Experimental section

3.2.1. Materials

Poly-(ethylene glycol)-*block*-poly-(*D,L*-lactide-*co*-glycolide) (PEG-PLGA), with PEG M_n 5000, 5 wt% PEG (RGP d 5055) or 15 wt% PEG (RGP d 50155), and molar ratio *D,L*-lactide:glycolide 50:50, were purchased from Evonik Industries (Birmingham, AL, USA). Poly-(*D,L*-lactide-*co*-glycolide) (PLGA) RESOMER® RG 752 H (molar ratio of *D,L*-lactide:glycolide 75:25, Mw 4000-15000 Da, acid terminated) and 5,10,15,20-tetraphenyl-21*H*,23*H*-porphine zinc (ZnTPP) were purchased from Sigma-Aldrich Chemical Co. (St. Louis, MO,USA). Protoporphyrin IX was purchased from Frontier Scientific (Logan, UT, USA). The porphyrins used had a minimal purity of 99% and were used as received. Deuterium oxide (99.9%) was purchased from Solvents Documentation Synthesis (SDS, Peypin, France). All other chemicals were commercially available reagents of at least analytical grade. Milli-Q water (Millipore Bedford, Massachusetts system, resistivity of 18 MΩ cm) was used.

Fetal Bovine Serum was purchased from Lonza Ibérica S.A.U. (Barcelona, Spain). Trypsin (0.05% Trypsin-EDTA (1x)) was purchased from Life Technologies S.A. (Madrid, Spain). L-Glutamine 200 mM was purchased from PAA GmbH (Pasching, Austria). Penicillin-Streptomycin Solution 100x was purchased from Biowest (Nuaillé; France). Plasmocin™ was purchased from Nucliber S.A. (Zaragoza, Spain). Dulbecco's Modified Eagle's Medium (DMEM) with 4.5 g/L glucose, Sterile Dulbecco's phosphate-buffered saline (PBS 1x) and 3-[4,5-dimethylthiazol-2-yl]-2,5-diphenyltetrazolium bromide (MTT) were purchased from Sigma-Aldrich. The sterilized cell culture material was purchased from LabClinics S.A. (Barcelona, Spain).

3.2.2. Preparation of poly-(*D,L*-lactide-*co*-glycolide) nanoparticles

PLGA and PEG-PLGA (with 5, 10 or 15% PEG) NPs (NPs) were prepared by a modified nanoprecipitation method.[14,15] Briefly, for bare PLGA NPs, PLGA 75:25 was dissolved in acetone

at a concentration of 9 mg/mL. For PEG coated PLGA NPs (PEG-PLGA NPs) either the commercial polymers were used directly (5% or 15% PEG) or a mixture of 33% PLGA 75:25 and 67% PEG15%-PLGA 50:50 was used in order to obtain a mixture with a 10% of PEG, keeping in all cases the same final polymer concentration in acetone as for bare PLGA NPs. To obtain ZnTPP-loaded or PpIX-loaded NPs, the porphyrin was dissolved in the organic solution at a 0.8% or 1.3% (w/w) drug loading concentration, respectively, regarding total polymer mass. This solution was then injected dropwise to ultrapure water (organic phase:aqueous phase 1:2 v/v) under continuous magnetic stirring at 800 rpm for 10 min. Subsequently, acetone was removed from the colloidal suspension under reduced pressure for at least 1 h. Larger aggregates, free PLGA polymer and non-encapsulated porphyrin were removed by centrifugation at 5000 rpm (for ZnTPP-loaded NPs) or 6000 rpm (for PpIX-loaded NPs) on an Avanti J21 centrifuge (Beckman Coulter, Inc., Brea, CA, USA) and the suspensions were stored at 4 °C.

3.2.3. Physicochemical characterization of NPs

Drug concentration was estimated by UV-visible absorption spectroscopy as stated in section 2.5.3. An aliquot of ZnTPP- or PpIX-loaded NPs was dissolved in THF or DMSO, respectively (NP suspension:solvent 1:15, v/v) to disrupt NPs and extract the entrapped PS. This solution was stirred to ensure a complete dissolution of the polymer and the PS, and the absorption spectra were recorded on a Varian Cary 6000i UV-vis-NIR spectrophotometer (Agilent Technologies, Santa Clara, CA) for ZnTPP or in a Synergy H1 Hybrid microplate reader (BioTek Instruments, Inc., Winooski, VT, USA) for PpIX. Absorbance values were interpolated in a calibration curve obtained in the same conditions for each PS. Multiplication of the concentration obtained by the dilution factor yielded the total concentration of the PS in the formulation. Drug loading and entrapment efficiency were calculated as mentioned in section 2.5.3.

3.2.4. Photosensitization of HeLa cells

Photodynamic treatment in HeLa cells was carried out as explained in section 2.6.5. In this particular case, cells were incubated in the dark at 37 °C for 24 h with ZnTPP-loaded PLGA or ZnTPP-loaded PEG-PLGA NPs at ZnTPP concentrations of 1, 5 and 10 μM in complete culture medium.

3.2.5. Subcellular localization

These assays were carried out by Dr. Acedo and Dr. Villanueva at the Universidad Autónoma de Madrid and are included here for a better understanding of the photophysics and photodynamic activity results.

To determine the intracellular localization of ZnTPP encapsulated in PLGA or PEG-PLGA NPs, endocytic compartments of HeLa cells were labeled with the fluoroprobe LysoTracker Green (50 nM, Molecular Probes, Eugene, Oregon, USA) in the culture medium at 37 ºC for 30 min. Previously, cells were incubated with ZnTPP-loaded NPs at 5 μM for 24 h. After labelling, coverslips were washed with PBS and were observed in a multispectral Leica TCS SP5 confocal microscope (Wetzlar, Germany), operating with 405 nm (Argon-UV) to detect the internalized ZnTPP NPs and 488 nm (Argon) for emission of LysoTracker Green.

3.2.6. Characterization of cell death mechanisms

These assays were carried out by Dr. Acedo and Dr. Villanueva at the Universidad Autónoma de Madrid and are included here for a better understanding of the photophysics and photodynamic activity results.

Morphological changes after different photodynamic treatments were assessed by visualizing control and treated cells under phase contrast and fluorescence microscopy. HeLa cells were fixed with methanol at -20 ºC for 5 minutes, stained with Neutral red (NR; Panreac Química, Spain; 0.5% in distilled water, 2 min) for analysis of general morphology, or with Hoechst-33258 (H-33258; Sigma-Aldrich; 5 μg/ml in distilled water, 3 min) for visualization of DNA. After washing and air drying, preparations were mounted in DePeX (Serva, Heidelberg, Germany).

For indirect immunofluorescence detection of cytochrome c, cells on coverslips were fixed in formol-PBS (1:10) for 20 min at 4 ºC, washed three times with PBS (5 min each), and permeabilized with 0.5% Triton X-100. After 5 min, Triton X-100 was removed and cells were incubated in blocking solution (5% bovine serum albumin, 5% FBS, 0.02% Triton X-100 in PBS) for 30 min at room temperature. Once removed from blocking solution, 25 μl of a 1:25 solution of primary antibody (monoclonal mouse anti-cytochrome c, Invitrogen) were added to each sample and incubated at 37 ºC for 1 h. Three 5 min washings with PBS were then carried out before addition of Triton X-100 for 5 min. Incubation with secondary antibody was performed at 37 ºC for 1h (Fab specific goat anti-mouse FITC-IgG; Sigma-Aldrich). Cells were washed 3 times with PBS and counterstained using H-33258 and mounted in ProLong Gold antifade reagent.

3.3. Results

3.3.1. Physicochemical characterization of ZnTPP-and PpIX-loaded PLGA formulations

ZnTPP was encapsulated in bare or PEG-decorated PLGA NPs, following a modified nanoprecipitation method. Following studies were carried out entrapping PpIX in PEG-decorated PLGA NPs. Table 3.1 summarizes the physicochemical properties of the formulations and the incorporation efficiency of ZnTPP or PpIX in NPs.

Table 3.1. Physicochemical characteristics of PLGA NPs and ZnTPP entrapment.

Composition	Z-ave[a] (nm)	PI[b]	ζ pot[c] (mV)	Drug loading[d] (%)	E.E.[e] (%)	[PS][f] (μM)
PLGA	114 ± 5	0.10 ± 0.01	-45 ± 2	-	-	-
ZnTPP / PLGA (0.8% ZnTPP, w/w)	115 ± 4	0.10 ± 0.02	-44 ± 1	0.6 ± 0.1	73 ± 4	41 ± 2
5% PEG-PLGA	72 ± 1	0.13 ± 0.01	-32 ± 7	-	-	-
ZnTPP / 5% PEG-PLGA (0.8% ZnTPP, w/w)	71 ± 1	0.10 ± 0.01	-27 ± 1	0.6 ± 0.1	68 ± 2	43 ± 2
10% PEG-PLGA	58 ± 18	0.19 ± 0.07	-23 ± 7	-	-	-
ZnTPP / 10% PEG-PLGA (0.8% ZnTPP, w/w)	52 ± 6	0.26 ± 0.12	-19 ± 5	0.7 ± 0.1	81 ± 4	45 ± 2
15% PEG-PLGA	58 (65%) 500 (35%)	0.41 ± 0.02	-20 ± 0.3	-	-	-
PpIX / 10% PEG-PLGA (1.3% PpIX, w/w)	76 ± 6	0.20 ± 0.03	-23 ± 2	0.8 ± 0.1	60 ± 3	60 ± 3

[a] Particle size measured as Z average mean
[b] Polydispersity Index
[c] Zeta Potential
[d] Drug loading expressed as percentage of PS relative to PLGA (w/w)
[e] Encapsulation efficiency
[f] Bulk PS concentration in the NPs suspension
Values reported are the mean ± SD of at least three independent experiments.

Coating of PLGA NPs with 5% or 10% PEG resulted in a reduction of their size, in agreement with previous observations,[16] a somewhat higher polydispersity, a less-negative zeta potential, and a slightly larger encapsulation efficiency. When entrapping ZnTPP, the final entrapment efficiency (~ 70%) and ZnTPP bulk concentration were comparable for bare PLGA or PEG-PLGA NP

formulations. In the case of PpIX NPs, entrapment efficiency (~ 60%) was slightly lower than for ZnTPP. No remarkable differences in the size, PI or zeta potential were observed when encapsulating PpIX compared to ZnTPP. Finally, NPs containing 15% PEG yielded two populations of different size and were thus ruled out for further studies.

3.3.2. Stability of formulations in cell culture medium

PLGA NPs aggregate in presence of serum albumin and other plasma proteins.[17–19] Thus, a study of NP stability in cell culture medium was carried out to analyze the formation of NP aggregates due to the FBS content of the medium, and to determine the influence of PEGylation on their stability. Aliquots of ZnTPP-loaded PLGA or ZnTPP-loaded PEG-PLGA suspensions containing the same amount of ZnTPP were added to the medium containing a 10% FBS and the remaining ZnTPP in suspension was determined after defined periods of time.

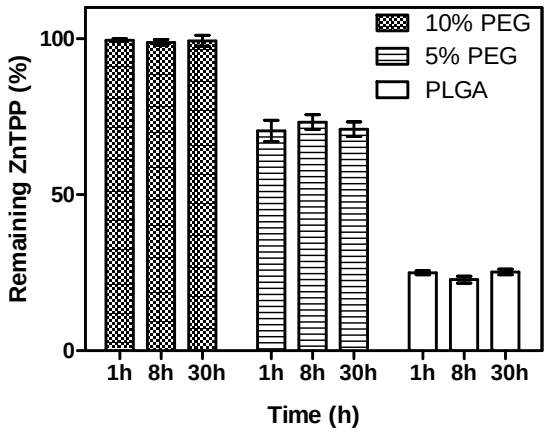

Figure 3.1. Stability of ZnTPP-loaded PLGA and PEG-PLGA NPs in cell culture medium. NP suspensions were diluted in supplemented cell culture medium (DMEM) at a concentration of 10 µM ZnTPP for various periods of time, at 37 °C. The stability was measured as the percentage of remaining ZnTPP in suspension in the incubation medium after each period of time. Results are the mean ± SD of two replicate values.

Figure 3.1 shows that all ZnTPP entrapped in PEG-PLGA NPs containing 10% PEG remains in the suspension, even after 30 h of incubation, whereas 75% of the ZnTPP initially embedded in the bare NPs precipitates already at 1 h. PEG-PLGA NPs containing 5% PEG showed intermediate results but since they were less stable than those containing 10% PEG we decided to rule them out at this stage. Hereafter the term PEG-PLGA NPs refers to NPs containing 10% PEG. The elimination of ZnTPP can be attributed to the formation of large aggregates of PLGA NPs that precipitate as a consequence of their interaction with FBS proteins. This experiment also shows

that PEGylation of the NPs protects them from FBS proteins and yields a stable formulation of the PS.

3.3.3. Absorption, steady-state and time-resolved fluorescence

Absorption and emission spectra (Figure 3.2 a, b) of aqueous suspensions of ZnTPP-loaded PLGA and ZnTPP-loaded PEG-PLGA NPs were recorded in water and in THF to compare the behavior of ZnTPP entrapped in the NPs or solubilized in the organic solvent. THF dissolves the PLGA polymer and causes the release of all the ZnTPP content into the organic solvent, where it is completely soluble.

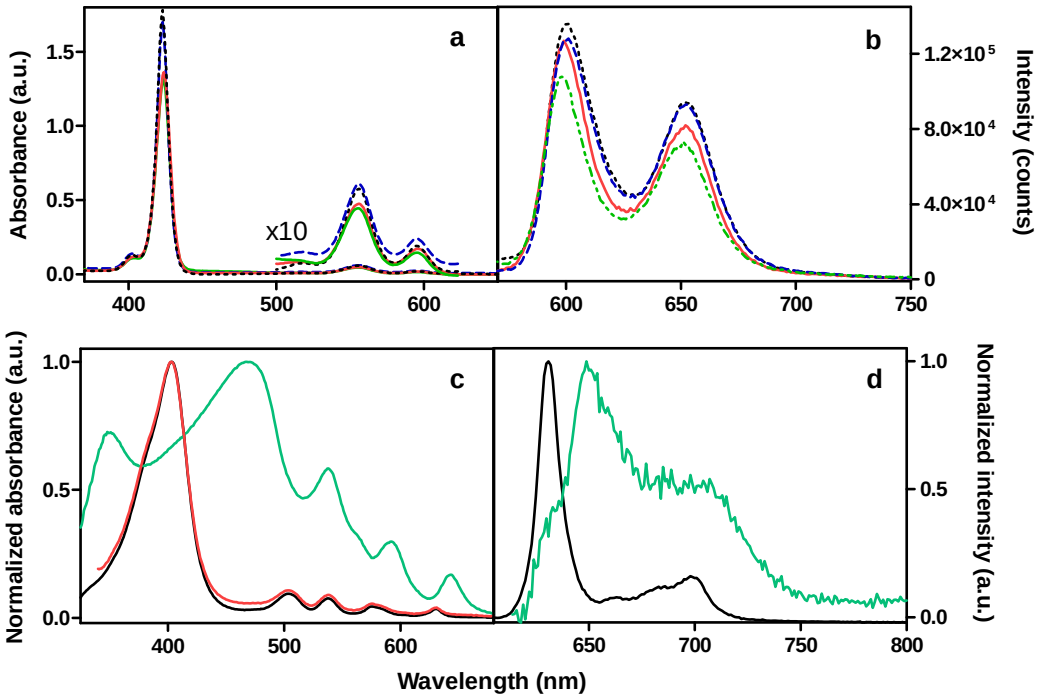

Figure 3.2. Absorption (a) and emission spectra (b) (λ_{ex}: 556 nm) of 3 μM ZnTPP in PLGA (— · · ·) and PEG-PLGA (——) NPs in aqueous suspension or PLGA (– –) and PEG-PLGA (·····) NPs dissolved in THF. Normalized absorption (c) and normalized emission spectra (d) (λ_{ex}: 591 nm) of an aqueous suspension of PpIX-loaded PEG-PLGA NPs (——), the same suspension disrupted in acetone (——) or free PpIX in acetone (——).

The spectra in the NPs were essentially identical to those in THF, which suggests that entrapped ZnTPP is largely in a monomeric state. On the contrary, the normalized absorption spectrum of aqueous suspensions of PpIX-loaded PEG-PLGA NPs (Figure 3.2 c, d) shows a remarkable blue shift for the Soret and the first Q band, a red shift for the last two Q bands as well as a remarkable difference on the relative intensities of the bands compared to the spectrum of free PpIX or

disrupted NPs in acetone. The normalized emission spectrum of PpIX in PEG-PLGA NPs (Figure 3.2 d) also shows a red shift and a different relative intensity of the bands compared to free PpIX in acetone. Therefore, unlike ZnTPP, PpIX seems to be strongly aggregated inside PEG-PLGA NPs.

The aforementioned hypotheses were confirmed by fluorescence quantum yield measurements. ZnTPP in both types of NPs showed the same fluorescence quantum yield than in toluene solution (Table 3.2). Conversely, PpIX in PEG-PLGA NPs showed a fluorescence quantum yield of 2 x 10^{-4}, which is 3 orders of magnitude lower than the value for free PpIX in methanol (0.155),[20] confirming the strong self-quenching of PpIX inside the NPs.

Fluorescence decay kinetics for ZnTPP in NPs revealed two components (Table 3.2, Figure 3.3) indicating two different populations of the excited singlet state of ZnTPP (^{1}ZnTPP*) in the nanosystems; the main component had a time constant very similar to that in organic solvents, ~ 2.0 ns.[21]

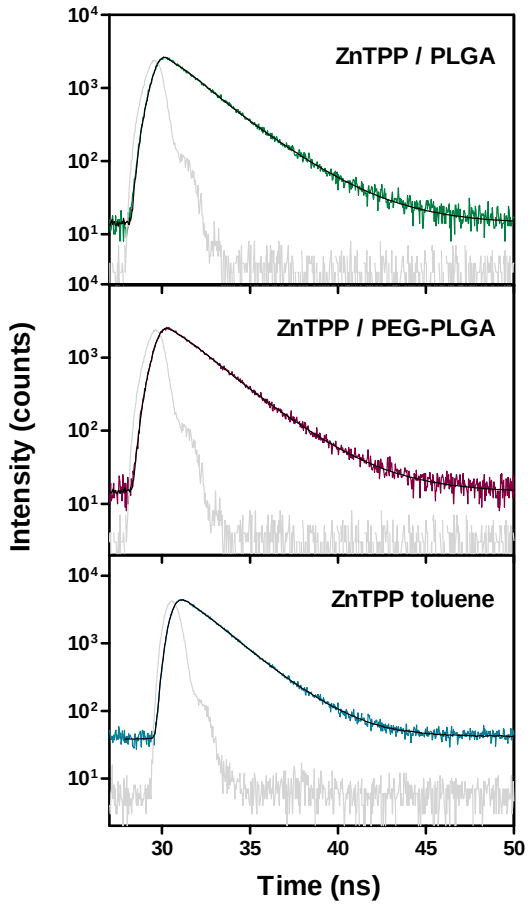

Figure 3.3. Time-Resolved Fluorescence decays of ZnTPP in PLGA or PEG-PLGA NPs and toluene. λ_{exc}: 596 nm. λ_{em}: 650 nm. Light grey line corresponds to instrumental response factor (IRF).

3.3.4. Triplet lifetime and quenching by oxygen

Laser flash photolysis experiments were used to monitor the triplet state of ZnTPP (^{3}ZnTPP*) through its time-resolved absorption at 470 nm (Figure 3.4). Data analysis revealed two and three populations of ZnTPP in bare and PEG-coated PLGA NPs, respectively. The triplet states could be quenched by oxygen with rate constants that varied for each population and for each type of NP (Table 3.2).

Table 3.2. Fluorescence quantum yields, singlet state lifetimes and their relative amplitudes, and triplet state lifetimes and their quenching rate constants by oxygen of the individual components observed in ZnTPP-loaded PLGA and PEG-PLGA NPs or PpIX-loaded PEG-PLGA NPs in water suspensions.

Sample	Φ_F	τ_{si} (ns)	A_{si} (%)	τ_{Ti} (μs)	k_{qTi}^{O2} ($M^{-1}s^{-1}$)
ZnTPP / PLGA	0.036 ± 0.005	1.7 ± 0.2	67 ± 14	77 ± 10	(3.7 ± 0.3) x 10^7
		3.1 ± 0.5	33 ± 14	209 ± 35	(1.2 ± 0.4) x 10^7
ZnTPP / PEG-PLGA	0.034 ± 0.002	1.8 ± 0.2	78 ± 14	17 ± 3	(2.7 ± 0.6) x 10^8
		3.4 ± 0.5	22 ± 14	105 ± 29	(1.2 ± 0.1) x 10^7
		-	-	286 ± 13	(4.9 ± 1.9) x 10^6
ZnTPP toluene[a]	0.033	2.0 ± 0.2	100	-	-
PpIX / PEG-PLGA[b]	(1.9 ± 0.2) x 10^{-4}	n. d.	n. d.	n. d.	n. d.

[a] ZnTPP in toluene was used as reference.[22]
[b]TMPyP in PBS was used as reference.[23]
n.d. not determined
Results are the mean ± SD of at least three independent experiments.

3.3.5. $^1O_2$ production and kinetics

Quenching of ^{3}ZnTPP* by oxygen led to the production of the cytotoxic species $^1O_2$ as unequivocally demonstrated by the observation of the specific NIR phosphorescence of this species at 1275 nm. The temporal profile of the signals (S_t, Figure 3.4) showed the typical rise-and-decay function that characterizes $^1O_2$ kinetics (Eq. 2.2). Data analysis (Table 3.3) confirmed the presence of two and three populations of ^{3}ZnTPP* and $^1O_2$ in bare and PEG-coated PLGA NPs, respectively. The ^{3}ZnTPP* lifetimes derived from NIR phosphorescence matched those from the laser flash photolysis experiments. NaN_3 had no effect on the $^1O_2$ lifetime in bare PLGA but quenched one of the $^1O_2$ populations in the PEG-coated NPs (Table 3.4).

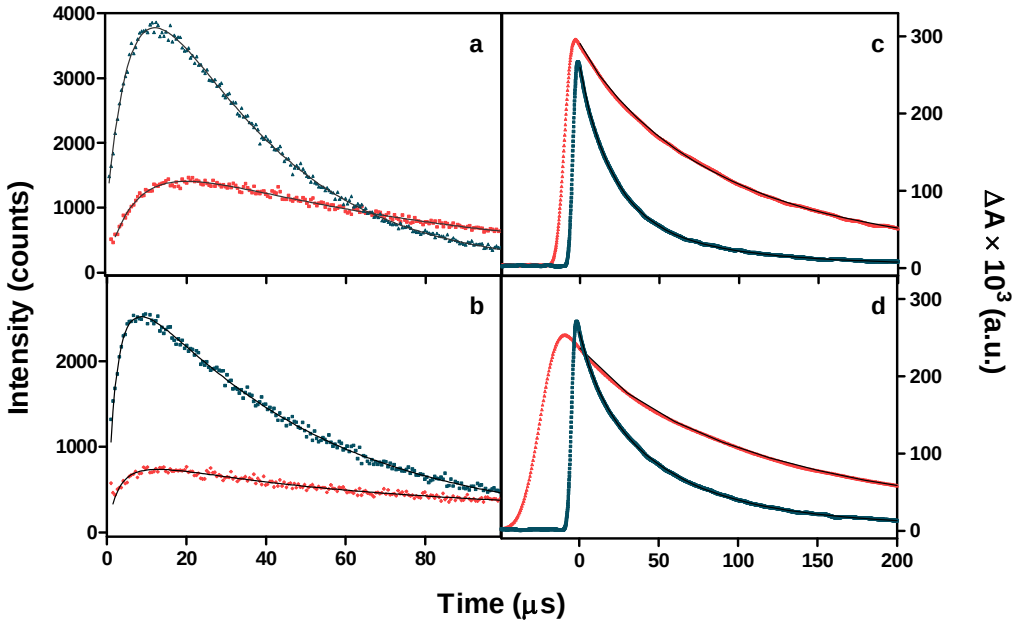

Figure 3.4. LEFT: Time-resolved $^1O_2$ phosphorescence in air (red) and in O_2 (blue) saturated aqueous suspensions of (a) PLGA or (b) PEG-PLGA NPs loaded with ZnTPP. ZnTPP was excited at 532 nm and $^1O_2$ phosphorescence was recorded at 1275 nm. RIGHT: Time-resolved triplet absorption transients at 470 nm of aqueous suspensions of ZnTPP-loaded PLGA NPs (c) and ZnTPP-loaded PEG-PLGA NPs (d), excited at 532 nm. Transients were acquired in air (red) and in O_2 (blue) saturated suspensions.

Conversely, observation of NIR time-resolved phosphorescence at 1275 nm of aqueous suspensions of PpIX-loaded PEG-PLGA NPs did not yield the characteristic rise-and-decay function of $^1O_2$ kinetics, but rather a decay function (Figure 3.5) which could be fit with Eq. 2.3, giving the following time constants: τ_1 = 0.2 ± 0.1 μs, τ_2 = 1.0 ± 0.2 μs. NIR time-resolved phosphorescence at 1110 nm also afforded a decay function, fit as well with Eq. 2.3 and giving the following parameters: τ_1 = 0.2 ± 0.1 μs, τ_2 = 0.9 ± 0.1 μs. It was thereby deduced that the decay function observed at 1275 nm was due to remaining phosphorescence of the PpIX excited triplet state (^{3}PpIX*) and that $^1O_2$ was not being photosensitized. Unsurprisingly, once the NPs were disrupted with DMSO and PpIX was released to the organic medium, the PS recovered its photosensitizing properties and $^1O_2$ formation at 1275 nm could now be observed (Figure 3.5). This function was fit with Eq. 2.2 and yielded the following time constants: τ_1 = 1.1 ± 0.1 μs, τ_2 = 6.6 ± 0.1 μs. As previously mentioned, the lifetime of 1.1 μs was assigned to the decay of ^{3}PpIX*, thus assigning τ_Δ = 6.6 ± 0.1 μs. Photosensitized $^1O_2$ by free PpIX in DMSO also yielded τ_T = 1.2 ± 0.2 μs and τ_Δ = 4.9 ± 0.2 μs, ascertaining the previous assignation for released PpIX from NPs. The fact that the experimentally obtained τ_Δ in DMSO is ~ 4 fold lower than the value described in literature (24.6 μs)[24] could be due to an increased water content in the solvent.

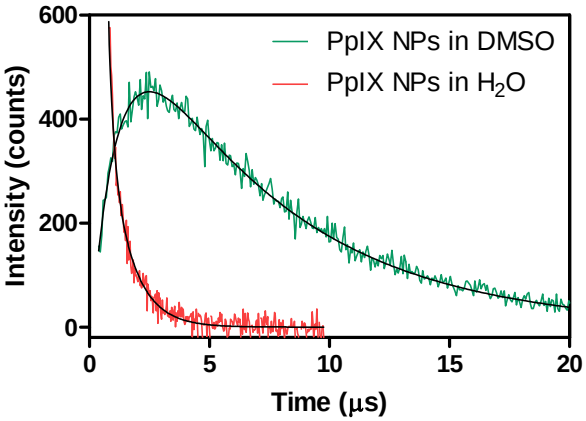

Figure 3.5. Time-resolved $^1O_2$ phosphorescence at 1275 nm of PpIX-loaded PEG-PLGA NPs in aqueous suspension or disrupted in DMSO.

Table 3.3. Time constants of $^1O_2$ luminescence of ZnTPP-loaded PLGA NPs or ZnTPP-loaded PEG-PLGA NPs under air and oxygen saturated solutions.

	ZnTPP-PLGA		**ZnTPP-PEG-PLGA**	
	air	O_2	air	O_2
$\tau_{\Delta 1}$ (μs)	5.0 ± 0.5	4.0 ± 0.1	1.6 ± 0.3	1.3 ± 0.2
τ_{T1} (μs)	92 ± 8	45 ± 3	18 ± 1	3.5 ± 0.3
$\tau_{\Delta 2}$ (μs)	14 ± 2	13 ± 2	5.0 ± 0.3	4.8 ± 0.3
τ_{T2} (μs)	219 ± 10	20 ± 1	79 ± 6	43 ± 2
$\tau_{\Delta 3}$ (μs)	-	-	12 ± 1	10 ± 1
τ_{T3} (μs)	-	-	307 ± 54	100 ± 10

Results are the mean ± SD of two independent experiments.

3.3.6. Temperature and quenching effects

The results obtained for ZnTPP-loaded NPs prompted us to investigate the effect of temperature on the kinetics of $^1O_2$ production and decay since both processes appear to be constrained by the rigidity of the PLGA NP. The decay rate constants of both ^{3}ZnTPP* and $^1O_2$ increased at higher temperatures (Figure 3.6 a; Table 3.4). At the highest temperature studied (55 °C) the two $^1O_2$ populations previously observed in bare PLGA merged, and the $^1O_2$ lifetime was close to the value commonly observed in water (~ 3 μs). Addition of NaN_3 reduced it further (Figure 3.6 c; Table 3.4). Similar observations were made in the PEG-coated NPs: increasing the temperature caused a general decrease of the ^{3}ZnTPP* and $^1O_2$ lifetimes and two of the three populations

merged at the highest temperature (Figure 3.6b, Table 3.4). Quenching by azide at this temperature caused and even more pronounced decrease of the $^1O_2$ lifetime than in the bare NPs.

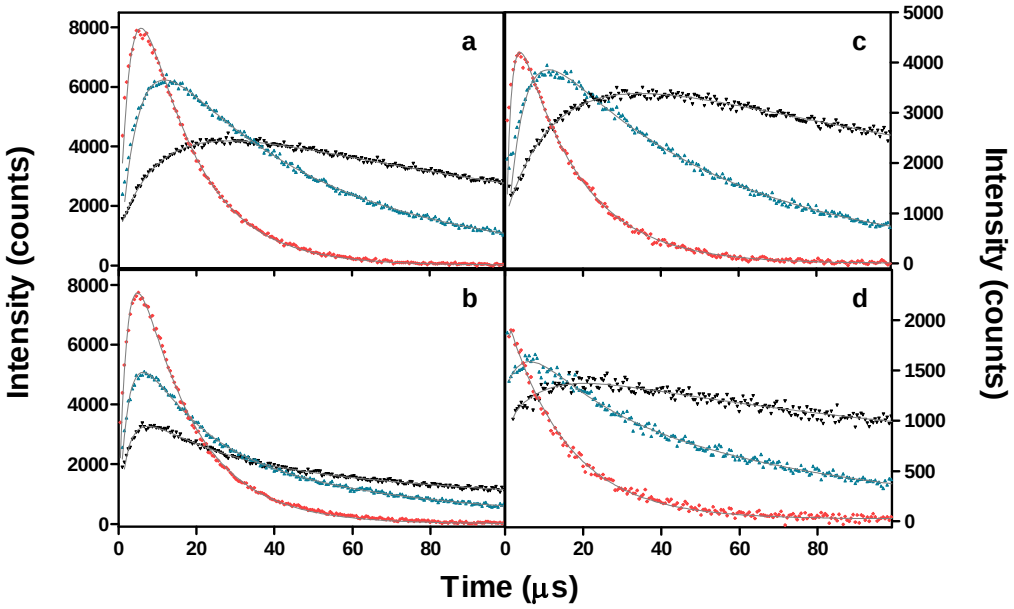

Figure 3.6. Time-resolved $^1O_2$ phosphorescence of aqueous suspensions of ZnTPP-loaded PLGA (TOP: a, c) and PEG-PLGA (BOTTOM: b, d) NPs as a function of temperature: 20 °C (black), 37 °C (blue), 55 °C (red) and of NaN_3 concentration: [NaN_3] = 0 mM (LEFT: a, b) and [NaN_3] = 10 mM (RIGHT: c, d). ZnTPP was excited at 532 nm and the luminescence was observed at 1275 nm.

Table 3.4. Time constants of $^1O_2$ luminescence transients of ZnTPP-loaded PLGA and PEG-PLGA NPs at three different temperatures and in absence and presence of NaN_3, a typical $^1O_2$ quencher.

ZnTPP-PLGA	**[NaN_3] = 0**			**[NaN_3] =10 mM**		
	20 °C	37 °C	55 °C	20 °C	37 °C	55°C
$\tau_{\Delta 1}$ (μs)	5.0 ± 0.5	4.4 ± 0.4	2.9 ± 0.5	6.0 ± 1.0	4.0 ± 0.1	1.4 ± 0.3
τ_{T1} (μs)	92 ± 8	36 ± 3	14 ± 1	110 ± 15	41 ± 5	15 ± 1
$\tau_{\Delta 2}$ (μs)	14 ± 2	4.4 ± 0.4	-	16 ± 1	4.0 ± 0.1	-
τ_{T2} (μs)	219 ± 10	78 ± 7	-	265 ± 18	99 ± 18	-
ZnTPP-PEG-PLGA	**[NaN_3] = 0**			**[NaN_3] =10 mM**		
	20 °C	37 °C	55 °C	20 °C	37 °C	55°C
$\tau_{\Delta 1}$ (μs)	1.6 ± 0.3	2.1 ± 0.4	2.7 ± 0.5	0.4 ± 0.3	0.2 ± 0.1	<0.2
τ_{T1} (μs)	18 ± 1	12 ± 1	10 ± 2	15 ± 1	8.1 ± 2.2	10 ± 2.2
$\tau_{\Delta 2}$ (μs)	5.0 ± 0.3	4.4 ± 0.7	2.7 ± 0.5	4.0 ± 1	5.3 ± 0.6	<0.2
τ_{T2} (μs)	79 ± 6	37 ± 4	22 ± 4	91 ± 14	49 ± 4	22 ± 4
$\tau_{\Delta 3}$ (μs)	12 ± 1	4.4 ± 0.7	-	12 ± 1	5.3 ± 0.6	-
τ_{T3} (μs)	307 ± 54	97 ± 14	-	356 ± 50	116 ± 2	-

Results are the mean ± SD of two independent experiments.

3.3.7. $^1O_2$ in HeLa cells

Cells incubated with ZnTPP-loaded PLGA NPs, either bare or coated with PEG, showed clear $^1O_2$ phosphorescence signals at 1275 nm (Figure 3.7).

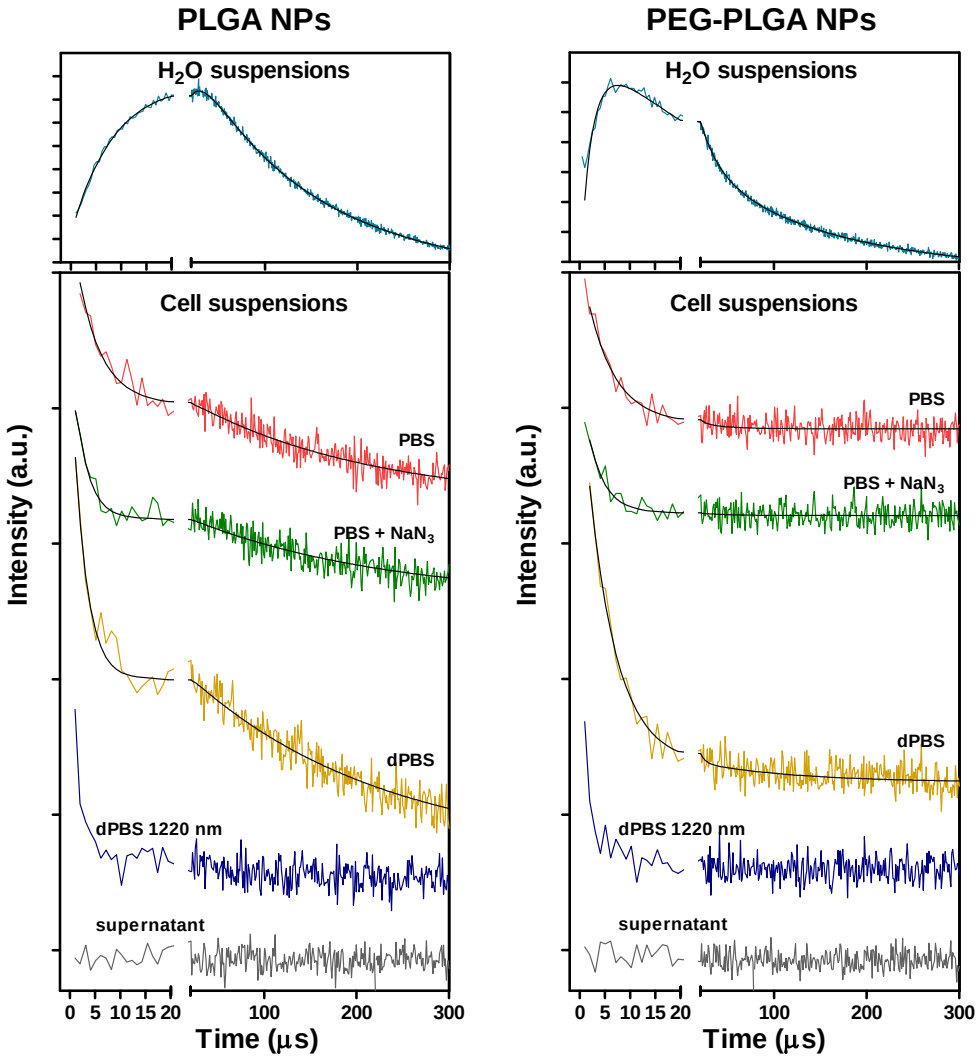

Figure 3.7. Time-resolved $^1O_2$ phosphorescence of ZnTPP-loaded PLGA (LEFT) and PEG-PLGA (RIGHT) NPs in aqueous suspensions (TOP) and in HeLa cell suspensions (BOTTOM) after 24 h incubation. ZnTPP was excited at 532 nm and $^1O_2$ phosphorescence was recorded at 1275 nm. The signal at 1220 nm, where $^1O_2$ shows almost no emission, was recorded to measure light scattering by cells. All measurements were taken at 20 °C; dPBS stands for D_2O-based PBS.

Control experiments confirmed that the signals were due to $^1O_2$ and that they originated in the cells since the luminescence showed a maximum at 1275 nm and no signal could be observed from the supernatant obtained by centrifugation of the suspensions. Analysis of the $^1O_2$ kinetics revealed important differences with respect to the aqueous suspension of the NPs. For bare PLGA, only one of the previously observed two $^1O_2$ populations could now be detected and it

showed similar kinetics as in aqueous suspensions. Moreover it could not be quenched by 10 mM NaN_3 and the only effect of solvent deuteration was to slightly increase its intensity. In contrast, cells incubated with PEG-coated NPs failed to show the long emission tail and the short-lived decay component could be quenched by azide. In this case also, deuteration allowed the observation of a longer-lived emission (Figure 3.7 RIGHT).

3.3.8. Photosensitization of HeLa cells

HeLa cells were incubated in the dark with various concentrations of ZnTPP-loaded PLGA and PEG-PLGA NPs for 24 h. Afterwards cells were exposed to various fluences of LED green light and cell viability was assessed 24 h after treatment. Cell death was observed in a concentration- and light fluence-dependent manner (Figure 3.8, Panel A).

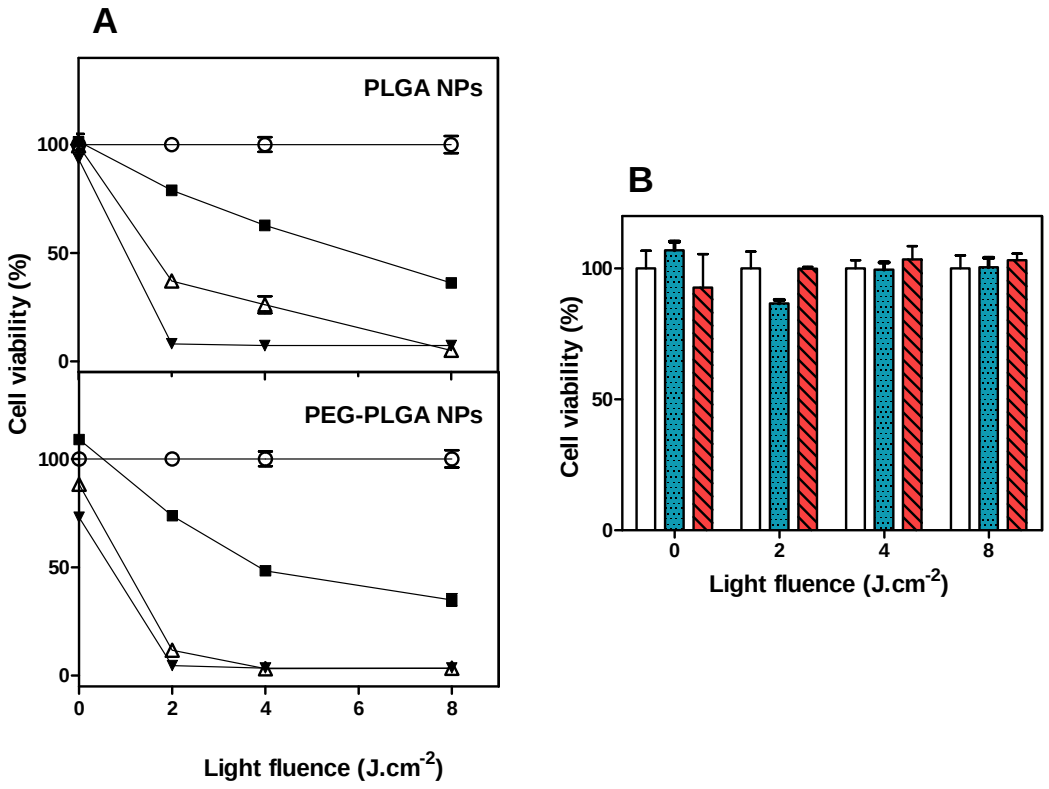

Figure 3.8. Panel A. HeLa cells viability (expressed in percentage) after incubation with ZnTPP-loaded PLGA or PEG-PLGA NPs at various concentrations and subsequent irradiation at various light fluences. ZnTPP concentrations are 1 μM (■), 5 μM (Δ) and 10 μM (▼). Plain circles (O) represent cell controls incubated only with complete growth medium. Panel B. HeLa cells viability as a function of light fluence after incubation with empty PLGA (blue dotted bars) or PEG-PLGA (red lined bars) NPs. In both cases, the concentration of NPs in incubates was equivalent to that delivered at 10 μM ZnTPP. White bars represent cell controls exposed to light without NPs.

ZnTPP delivered in PEGylated NPs was more phototoxic than in bare PLGA, particularly at low light fluences. On the other hand, it also showed a slightly higher dark cytotoxicity. Light alone or in combination with empty NPs was devoid of any detectable cytotoxicity (Figure 3.8, Panel B).

The results below (Subsections 3.3.9. and 3.3.10.) were obtained by Dr. Acedo and Dr. Villanueva at the Universidad Autónoma de Madrid and are included here for a better understanding of the photophysics and photodynamic activity results shown above.

3.3.9. Subcellular localization

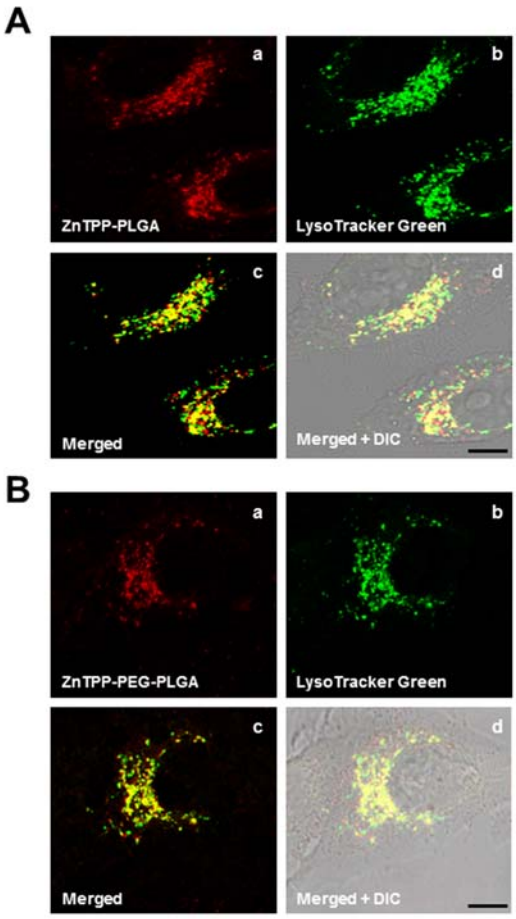

Figure 3.9. Panel A. (a) Live imaging HeLa cells showing the localization of ZnTPPdelivered by PLGA NPs, (b) lysosomes labelling with LysoTracker Green, (c) merged image. Yellow in the overlay images (a and b) appears where the red fluorescence of ZnTPP colocalizes with the green fluorescence of LysoTracker Green, (d) and overlap of UV and green channels with differential interference contrast (DIC) image of the same cells. Panel B. Same instrument settings were used to acquire images after incubation of the cells with ZnTPP delivered by PEG-PLGA NPs by confocal microscopy. Scale bar = 10 µm.

ZnTPP delivered in PLGA or PEG-PLGA NPs showed similar intracellular localization in lysosome-like structures (Figure 3.9). Co-localization studies performed in non-fixed HeLa cells using LysoTracker Green, a marker for lysosomes, confirmed that ZnTPP entrapped in both types of NPs was specifically accumulated in lysosomes.

3.3.10. Mechanism of cell death

Apoptotic cell death induced by PDT treatments was confirmed by two methods: analysis of morphological alterations[25] and cellular distribution of cytochrome c.

Morphological changes

Photodynamic treatments on HeLa cells with ZnTPP-loaded PLGA or PEG-PLGA NPs at 5 μM ZnTPP and 4 $J.cm^{-2}$ light fluence resulted in apoptotic pattern of cell death morphology, revealed by neutral red and Hoechst-33258 (H-33258) staining (Figure 3.10). After photodynamic treatment with ZnTPP-loaded PLGA but specially with ZnTPP-loaded PEG-PLGA, cells showed significant morphological changes depending on the time elapsed after the end of treatment (6 and 24 h). As shown in Figure 3.10, a significant number of cells have undergone apoptosis 6 h after ZnTPP-loaded PEG-PLGA photodynamic treatment, as deduced from the cell shrinkage, chromatin condensation, and nuclear fragmentation, which are typical apoptotic features. At 24 h most cells have undergone apoptosis and only scarce cells remain alive. Cells treated with ZnTPP-loaded NPs but not irradiated, as well as cells irradiated without preincubation with NPs, presented similar morphology to control HeLa cells (data not shown).

Detection of cytosolic cytochrome c

Immunofluorescence techniques showed that cytochrome c was confined to mitochondria in control cells (Figure 3.11). However, photoactivated ZnTPP-loaded PEG-PLGA triggered release of cytochrome c from the mitochondria to the cytosol and the majority of cells displayed diffuse cytochrome c cytoplasmic staining and condensed and fragmented nuclei (Figure 3.11, a''-d'').

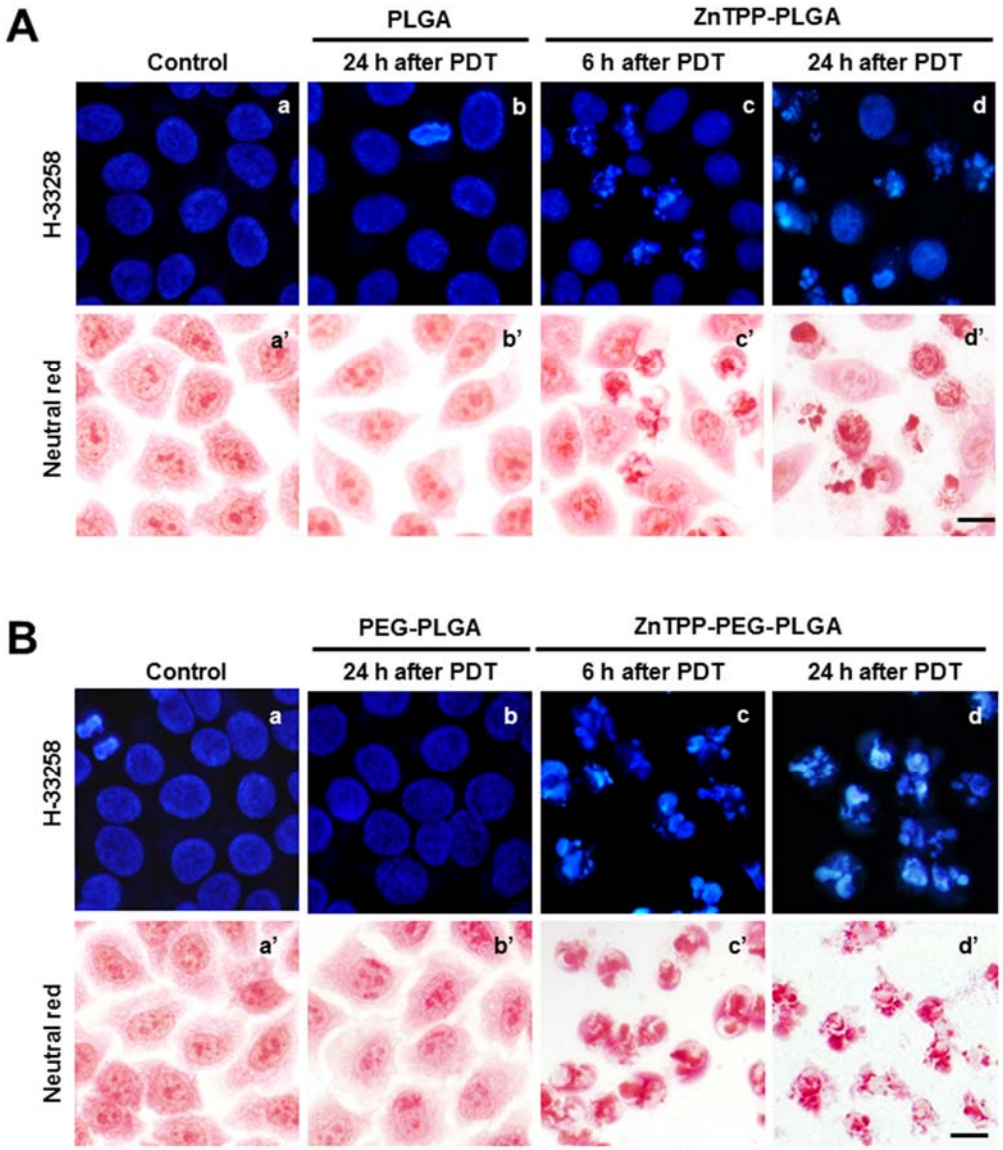

Figure 3.10. Morphology of cells treated with PDT by ZnTPP-loaded PLGA (Panel A) and ZnTPP-loaded PEG-PLGA (Panel B) NPs, after neutral red or H-33258 staining. (a-a') HeLa control cells morphology. (b-b') Cells incubated 24 h with empty PLGA or PEG-PLGA NPs followed by green light irradiation (4 $J.cm^{-2}$) and observed 24 h later. (c-d and c'-d') Cells incubated 24 h with 5 μM ZnTPP entrapped in PLGA or PEG-PLGA NPs followed by green light irradiation (4 $J.cm^{-2}$) and observed 6 and 24 h later, respectively. Note that ZnTPP-loaded PEG-PLGA induced apoptotic cell death more effectively than ZnTPP-loaded PLGA. Most of HeLa cells displayed the morphological features of apoptosis (cell shrinkage and chromatin fragmentation) after 24 h PDT-treatment. Scale bar = 10 μm.

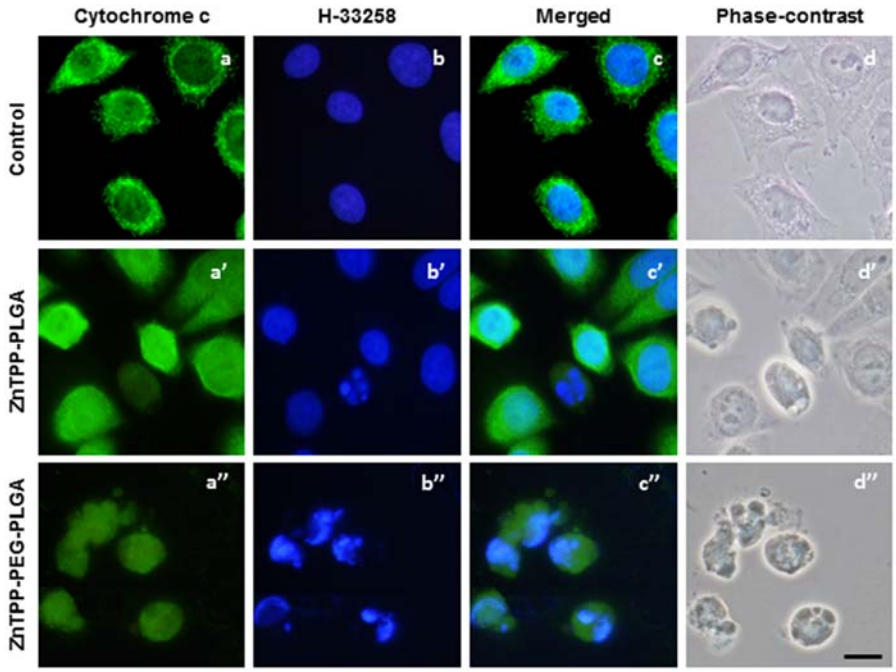

Figure 3.11 HeLa cells visualized by cytochrome c immunofluorescence (green) and DNA counterstaining with H-33258 (blue), overlap images and corresponding phase-contrast of HeLa cells. (a-d) Control cells showing mitochondrial cytochrome c. (a'-d') Cells 24 h after PDT treatment with ZnTPP-loaded PLGA and green light irradiation (4 J.cm^{-2}) show cytochrome c release to cytosol only in cells with condensed and fragmented chromatin. (a''-d'') The same PDT treatment with ZnTPP-loaded PEG-PLGA led to diffuse cytoplasmic cytochrome c staining with condensed and fragmented chromatin 24 h after irradiation. Scale bar = 10 μm.

3.4. Discussion

We have investigated the photodynamic activity of the model PS ZnTPP delivered to cancer cells using bare or PEGylated PLGA NPs. Additionally, we have entrapped the clinically approved PpIX in PEGylated PLGA NPs and we have compared the photophysical properties of the two entrapped PSs

PLGA NPs, prepared by a modified nanoprecipitation method, had a diameter of around 100 nm and a pronounced negative zeta potential, consistent with the terminal carboxylic groups of the polymer. Coating their surface with 5% or 10% PEG chains led to a decrease in their size, as previously observed,[16,26] and to a less negative zeta potential. However, increasing the PEG content to 15% produced highly heterogeneous NP populations (Table 3.1). No significant differences in size were reported when any of both PSs were encapsulated.

Bare PLGA NPs aggregated and precipitated when added to culture medium containing 10% FBS,[17–19,26] whereas 10% PEG coating conferred stability to the suspension (Figure 3.1). These results rule out bare PLGA NPs as drug carriers for *in vivo* PDT.

Absorption and fluorescence spectra as well as fluorescence quantum yields of ZnTPP in both types of NPs were similar to those in THF or toluene solution (Figure 3.2), indicating that ZnTPP is not appreciably aggregated in the core of the NPs. These results are in contrast to those obtained for PpIX; shifts and different relative intensities in the spectra of encapsulated PpIX indicate a strong aggregation of this PS inside the NPs, which is confirmed by its extremely low fluorescence quantum yield. Similarly to the case of PpIX, *meso*-tetrahydroxyphenyl porphyrin (m-THPP) in PLGA shows large red shifts and an important reduction of intensities.[6] This indicates that the chemical properties of the PS exert a profound influence on its interaction with PLGA.

Time-resolved fluorescence and triplet-triplet absorption revealed different populations of ZnTPP in the NPs (Table 3.2). Thus, two different populations were identified in bare PLGA whereas in PEG-PLGA a third population could also be detected. The long triplet lifetimes observed in aerated suspensions indicate that ^{3}ZnTPP* is largely shielded from oxygen in the NPs. The rate constants for oxygen quenching (Table 3.2) were 1-3 orders of magnitude lower than in aqueous solutions[27] depending on the specific ^{3}ZnTPP* population and type of NP. This would indicate that each population occupies a different region inside the NPs.

Despite such shielding, ZnTPP is able to produce $^1O_2$ and we find different populations for this species as well, which is in agreement with a heterogeneous microenvironment within the NPs. The fact that NaN_3, a water-soluble $^1O_2$ quencher, is unable to reduce the $^1O_2$ lifetime in bare PLGA, indicates that $^1O_2$ is confined within these NPs. Although NaN_3 is a small anion that can readily enter the cell from the extracellular medium[28] our results indicate that it is not able to enter the NPs, probably due to electrostatic repulsion by their negative surface charge. The situation is slightly different for PEGylated NPs, in which the zeta potential is less negative and we see quenching of the third population. We therefore tentatively assign this population to $^1O_2$ molecules at the PLGA/PEG interface. Increasing the temperature reduced the differences between the different populations, which ultimately merged into a single one that decayed with the typical lifetime in aqueous solutions ($\sim$ 3 μs)[27] and that was amenable to azide quenching (Table 3.4, Figure 3.6). This likely reflects the decrease in PLGA rigidity at higher temperatures, which facilitates the diffusion of ZnTPP, O_2 and $^1O_2$. In line with these observations, in films of poly-(lactide) (PLA) an increase in oxygen permeability with temperature has also been observed.[29] Conversely, PpIX entrapped in PEGylated PLGA NPs fails to produce $^1O_2$ (Figure 3.5),

which is another confirmation of the self-quenched state of PpIX inside the NPs. Nevertheless, once PpIX is released from the NPs it recovers its photosensitizing ability, as demonstrated in Figure 3.5. This observation points out that it may not be indispensable to keep the PS photoactive inside its vehicle to produce a phototoxic effect, as long as the PS is released to the cells before light irradiation.

A key question is whether or not the NPs are internalized or release their cargo at the cell surface. Chernenko *et al*.[30] proposed that PLGA NPs are internalized and completely digested by HeLa cells within 6 h but this conclusion has been challenged by others.[31] Furthermore, many publications support the hypothesis of an endocytosis-mediated uptake of the intact NPs[3,32–35] while others advocate for delivery of their cargo via extracellular release or contact-based transfer.[31,36,37] The kinetics of $^1O_2$ production and decay in HeLa cells yielded a number of striking findings (Figure 3.7). Firstly, the decay of the phosphorescence signal was, in the case of bare PLGA, essentially as long as in aqueous suspensions, even after 24 h of incubation. However, a fast and more accessible decay component was also observed in the early part of the signal, which is demonstrated by the shortening of the early component in the presence of azide, the increase of the signal intensity upon solvent deuteration, and by the induction of cell mortality (Figures. 3.8 and 3.10). This suggests that a large fraction of $^1O_2$ molecules is still confined within the NP, implying that bare NPs hold their cargo, or at least a substantial fraction of it, even after 24 h, while another is nevertheless outside the NP and leads to the fast decay component. This, together with the observation that $^1O_2$ signals resemble so much those in aqueous suspensions of the NPs indicate that a substantial fraction of $^1O_2$ molecules are still within the NPs while another is nevertheless outside of it. This observation, however, does not resolve the question as to whether the NP has been internalized or not (but see Chapter 4). Notice that laser light scattered by the cells decays much faster (Figure 3.7), as demonstrated by the signal at 1220 nm where $^1O_2$ has almost no emission.

The situation for PEGylated NPs is much different. The slow decay observed in aqueous suspensions is no longer detectable, which indicates the faster release of ZnTPP in this case, confirmed by the quenching effect of azide, the signal enhancement upon solvent deuteration (Figure 3.7), and the faster appearance of dead cells after PDT treatments (Figure 3.10). This finding is consistent with the observations reported by Avgoustakis *et al.*, who studied the *in vitro* degradation and drug release of a series of PLGA-mPEG polymers with various PLGA:PEG compositions and observed that both the rate of NP degradation and drug release at 37 °C increased with PEG content.[38] In another work comparing free and encapsulated temoporfin in PLGA or PEG-PLGA NPs, Rojnik *et al.* also observed a faster temoporfin release for PEGylated

NPs than for PLGA NPs.[39] Again, these results do not clarify whether the NPs have been internalized or have released their cargo at the cell surface.

The photodynamic activity of ZnTPP delivered by PLGA NPs was evaluated *in vitro* against HeLa cells. ZnTPP was more effective when encapsulated into PEG-PLGA NPs (Figures 3.8 and 3.10), which is consistent with the results of $^1O_2$ production. The inactivation process led to a significant percentage of apoptotic morphology 24 h after irradiation, characterized by cell shrinkage, chromatin condensation and nuclear fragmentation with apoptotic body formation (Figure 3.11).

Internalization of ZnTPP was demonstrated by confocal fluorescence microscopy. ZnTPP was mainly located in the acidic endo-lysosomal compartment independently of the delivery vehicle used, as evidenced by its co-localization with Lyso Tracker Green (Figure 3.9).[40,41] The same localization has been previously observed for ZnTTP delivered using liposomes.[13] Lysosomes are the final destination for many macromolecules and PSs taken up by endocytosis from the extracellular space and from the cell surface.[42] Once again, the results are inconclusive as to whether NP internalization or ZnTPP release occurs first.

After the photodynamic treatments, cytochrome c was released from the mitochondrial compartment to the cytosol in cells with condensed and fragmented chromatin (Figure 3.11). This increase in mitochondrial membrane permeability must therefore be held responsible for the initiation of apoptotic cell death processes.[43,44] All these results together indicate that treatment with 5 μM ZnTPP entrapped in NPs for 24 h followed by irradiation (4 J.cm^{-2}) induced massive apoptotic cell death (> 90%), PEG-PLGA NPs being a more effective vehicle than bare PLGA NPs.

3.5. Conclusions

In this chapter, we have investigated the physicochemical and biological aspects of the use of PLGA NPs as delivery vehicles for the model hydrophobic photosensitizer ZnTPP in photodynamic killing of HeLa cells. 10% PEG coating confers higher stability to the PLGA NPs in the presence of serum proteins, thereby enabling its use *in vivo*. ZnTPP molecules are distributed between two and three different compartments within bare and PEG-coated NPs, respectively. As a result, $^1O_2$ is confined within the NP in the case of bare PLGA, however coating with PEG facilitates its release to the external medium, as does rising the temperature. In agreement with these observations, ZnTPP delivered with PEG-coated PLGA NPs acts faster and more efficiently

in inducing cell death upon exposure to light. ZnTPP delivered by both types of PLGA NPs localizes in lysosomes and kills cells mainly by apoptosis.

On the other hand, we have also evaluated the physicochemical and photophysical properties of the clinically approved PS PpIX entrapped in PEGylated PLGA NPs. Unlike ZnTPP, PpIX is strongly aggregated inside these NPs, which completely inhibits $^1O_2$ production. However, release of PpIX reestablishes its photosensitizing activity.

The reported results indicate that the chemical nature of the PS likely affects its interaction with the NP material, and thus, affects its photophysical activity. We can also conclude that PEG-PLGA NPs show high potential as delivery agents for PDT.

3.6. References

(1) Panyam, J.; Labhasetwar, V. Biodegradable Nanoparticles for Drug and Gene Delivery to Cells and Tissue. *Adv. Drug Deliv. Rev.* **2003**, *55*, 329–347.

(2) Gomes, A. J.; Lunardi, C. N.; Tedesco, A. C. Characterization of Biodegradable poly(D,L-Lactide-Co-Glycolide) Nanoparticles Loaded with Bacteriochlorophyll-a for Photodynamic Therapy. *Photomed. Laser Surg.* **2007**, *25*, 428–435.

(3) Konan, Y. N.; Berton, M.; Gurny, R.; Allemann, E. Enhanced Photodynamic Activity of Meso-tetra(4-Hydroxyphenyl) Porphyrin by Incorporation into Sub-200 Nm Nanoparticles. *Eur. J. Pharm. Sci.* **2003**, *18*, 241–249.

(4) Konan, Y. N.; Cerny, R.; Favet, J.; Berton, M.; Gurny, R.; Allémann, E. Preparation and Characterization of Sterile Sub-200 Nm Meso-tetra(4-Hydroxyphyenyl)poprhyrin-Loaded Nanoparticles for Photodynamic Therapy. *Eur. J. Pharm. Biopharm.* **2003**, *55*, 115–124.

(5) Allemann, E.; Konan, Y.; Gurny, R.; Boch, R. E.; Alleman, E. Compositions and Methods for Delivery of Photosensitive Drugs. US 2004/0047913 A1, 2004.

(6) Vargas, A.; Lange, N.; Arvinte, T.; Cerny, R.; Gurny, R.; Delie, F. Toward the Understanding of the Photodynamic Activity of M-THPP Encapsulated in PLGA Nanoparticles: Correlation between Nanoparticle Properties and in Vivo Activity. *J. Drug Target.* **2009**, *17*, 599–609.

(7) Vargas, A.; Eid, M.; Fanchaouy, M.; Gurny, R.; Delie, F. In Vivo Photodynamic Activity of Photosensitizer-Loaded Nanoparticles: Formulation Properties, Administration Parameters and Biological Issues Involved in PDT Outcome. *Eur. J. Pharm. Biopharm.* **2008**, *69*, 43–53.

(8) Vargas, A.; Pegaz, B.; Debefve, E.; Konan-Kouakou, Y.; Lange, N.; Ballini, J.-P.; van den Bergh, H.; Gurny, R.; Delie, F. Improved Photodynamic Activity of Porphyrin Loaded into Nanoparticles: An in Vivo Evaluation Using Chick Embryos. *Int. J. Pharm.* **2004**, *286*, 131–145.

(9) Zeisser-Labouebe, M.; Lange, N.; Gurny, R.; Delie, F. Hypericin-Loaded Nanoparticles for the Photodynamic Treatment of Ovarian Cancer. *Int. J. Pharm.* **2006**, *326*, 174–181.

(10) Allemann, E.; Rousseau, J.; Brasseur, N.; Kudrevich, S. V; Lewis, K.; van Lier, J. E. Photodynamic Therapy of Tumours with Hexadecafluoro Zinc Phthalocynine Formulated in PEG-Coated Poly(lactic Acid) Nanoparticles. *Int. J. cancer.Journal Int. du cancer* **1996**, *66*, 821–824.

(11) Li, B.; Moriyama, E. H.; Li, F.; Jarvi, M. T.; Allen, C.; Wilson, B. C. Diblock Copolymer Micelles Deliver Hydrophobic Protoporphyrin IX for Photodynamic Therapy. *Photochem. Photobiol.* **2007**, *83*, 1505–1512.

(12) Rojnik, M.; Kocbek, P.; Moret, F.; Compagnin, C.; Celotti, L.; Bovis, M. J.; Woodhams, J. H.; MacRobert, A. J.; Scheglmann, D.; Helfrich, W.; *et al.* In Vitro and in Vivo Characterization of Temoporfin-Loaded PEGylated PLGA Nanoparticles R Esearch A Rticle. *Nanomedicine* **2012**, *7*, 663–677.

(13) García-Díaz, M.; Nonell, S.; Villanueva, A.; Stockert, J. C.; Cañete, M.; Casadó, A.; Mora, M.; Sagristá, M. L. Do Folate-Receptor Targeted Liposomal Photosensitizers Enhance Photodynamic Therapy Selectivity? *Biochim. Biophys. Acta* **2011**, *1808*, 1063–1071.

(14) Barichello, J. M.; Morishita, M.; Takayama, K.; Nagai, T. Encapsulation of Hydrophilic and Lipophilic Drugs in PLGA Nanoparticles by the Nanoprecipitation Method. *Drug Dev. Ind. Pharm.* **1999**, *25*, 471–476.

(15) Yallapu, M. M.; Gupta, B. K.; Jaggi, M.; Chauhan, S. C. Fabrication of Curcumin Encapsulated PLGA Nanoparticles for Improved Therapeutic Effects in Metastatic Cancer Cells. *J. Colloid Interface Sci.* **2010**, *351*, 19–29.

(16) Gref, R.; Lück, M.; Quellec, P.; Marchand, M.; Dellacherie, E.; Harnisch, S.; Blunk, T.; Müller, R. "Stealth" Corona-Core Nanoparticles Surface Modified by Polyethylene Glycol (PEG): Influences of the Corona (PEG Chain Length and Surface Density) and of the Core Composition on Phagocytic Uptake and Plasma Protein Adsorption. *Colloids Surf. B. Biointerfaces* **2000**, *18*, 301–313.

(17) Armstrong, T. I.; Davies, M. C.; Illum, L. Human Serum Albumin as a Probe for Protein Adsorption to Nanoparticles: Relevance to Biodistribution. *J. Drug Target.* **1997**, *4*, 389–398.

(18) Chang, J.; Paillard, A.; Passirani, C.; Morille, M.; Benoit, J.-P.; Betbeder, D.; Garcion, E. Transferrin Adsorption onto PLGA Nanoparticles Governs Their Interaction with Biological Systems from Blood Circulation to Brain Cancer Cells. *Pharm. Res.* **2012**, *29*, 1495–1505.

(19) Karmali, P. P.; Simberg, D. Interactions of Nanoparticles with Plasma Proteins: Implication on Clearance and Toxicity of Drug Delivery Systems. *Expert Opin. Drug Deliv.* **2011**, *8*, 343–357.

(20) Lozovaya, G. I.; Masinovsky, Z.; Sivash, A. A. Protoporphyrin IX as a Possible Ancient Photosensitizer: Spectral and Photochemical Studies. *Orig. Life Evol. Biosph.* **1990**, *20*, 321–330.

(21) Karolczak, J.; Kowalska, D.; Lukaszewicz, A.; Maciejewski, A.; Steer, R. P. Photophysical Studies of Porphyrins and Metalloporphyrins: Accurate Measurements of Fluorescence Spectra and Fluorescence Quantum Yields for Soret Band Excitation of Zinc Tetraphenylporphyrin. *J. Phys. Chem. A* **2004**, *108*, 4570.

(22) Strachan, J.-P.; Gentemann, S.; Seth, J.; Kalsbeck, W. A.; Lindsey, J. S.; Holten, D.; Bocian, D. F. Effects of Orbital Ordering on Electronic Communication in Multiporphyrin Arrays. *J. Am. Chem. Soc.* **1997**, *119*, 11191–11201.

(23) Dosselli, R.; Tampieri, C.; Ruiz-González, R.; De Munari, S.; Ragàs, X.; Sánchez-García, D.; Agut, M.; Nonell, S.; Reddi, E.; Gobbo, M. Synthesis, Characterization, and Photoinduced Antibacterial Activity of Porphyrin-Type Photosensitizers Conjugated to the Antimicrobial Peptide Apidaecin 1b. *J. Med. Chem.* **2013**, *56*, 1052–1063.

(24) Wilkinson, F.; Brummer, J. G. Rate Constants for the Decay and Reactions of the Lowest Electronically Excited Singlet State of Molecular Oxygen in Solution. *J. Phys. Chem. Ref. Data* **1981**, *24*, 809–999.

(25) Rello, S.; Stockert, J. C.; Moreno, V.; Gamez, A.; Pacheco, M.; Juarranz, A.; Cañete, M.; Villanueva, A. Morphological Criteria to Distinguish Cell Death Induced by Apoptotic and Necrotic Treatments. *Apoptosis* **2005**, *10*, 201–208.

(26) Avgoustakis, K.; Beletsi, A.; Panagi, Z.; Klepetsanis, P.; Livaniou, E.; Evangelatos, G.; Ithakissios, D. S. Effect of Copolymer Composition on the Physicochemical Characteristics, in Vitro Stability, and Biodistribution of PLGA–mPEG Nanoparticles. *Int. J. Pharm.* **2003**, *259*, 115–127.

(27) Redmond, R. W.; Gamlin, J. N. A Compilation of Singlet Oxygen Yields from Biologically Relevant Molecules. *Photochem. Photobiol.* **1999**, *70*, 391–475.

(28) Snyder, J. W.; Skovsen, E.; Lambert, J. D. C.; Poulsen, L.; Ogilby, P. R. Optical Detection of Singlet Oxygen from Single Cells. *Phys. Chem. Chem. Phys.* **2006**, *8*, 4280–4293.

(29) Auras, R.; Harte, B.; Selke, S. Effect of Water on the Oxygen Barrier Properties of Poly (ethylene Terephthalate) and Polylactide Films. *J. Appl. Polym. Sci.* **2004**, *92*, 1790–1803.

(30) Chernenko, T.; Matthäus, C.; Milane, L.; Quintero, L.; Amiji, M.; Diem, M. Label-Free Raman Spectral Imaging of Intracellular Delivery and Degradation of Polymeric Nanoparticle Systems. *ACS Nano* **2009**, *3*, 3552–3559.

(31) Xu, P.; Gullotti, E.; Tong, L.; Highley, C. B.; Errabelli, D. R.; Hasan, T.; Cheng, J.-X.; Kohane, D. S.; Yeo, Y. Intracellular Drug Delivery by Poly(lactic-Co-Glycolic Acid) Nanoparticles, Revisited. *Mol. Pharm.* **2009**, *6*, 190–201.

(32) Cartiera, M. S.; Johnson, K. M.; Rajendran, V.; Caplan, M. J.; Saltzman, W. M. The Uptake and Intracellular Fate of PLGA Nanoparticles in Epithelial Cells. *Biomaterials* **2009**, *30*, 2790–2798.

(33) Danhier, F.; Vroman, B.; Lecouturier, N.; Crokart, N.; Pourcelle, V.; Freichels, H.; Jérôme, C.; Marchand-Brynaert, J.; Feron, O.; Préat, V. Targeting of Tumor Endothelium by RGD-Grafted PLGA-Nanoparticles Loaded with Paclitaxel. *J. Control. Release* **2009**, *140*, 166–173.

(34) Lei, T.; Srinivasan, S.; Tang, Y.; Manchanda, R.; Nagesetti, A.; Fernandez-Fernandez, A.; McGoron, A. J. Comparing Cellular Uptake and Cytotoxicity of Targeted Drug Carriers in Cancer Cell Lines with Different Drug Resistance Mechanisms. *Nanomedicine* **2011**, *7*, 324–332.

(35) Reix, N.; Parat, A.; Seyfritz, E.; Van der Werf, R.; Epure, V.; Ebel, N.; Danicher, L.; Marchioni, E.; Jeandidier, N.; Pinget, M.; *et al.* In Vitro Uptake Evaluation in Caco-2 Cells and in Vivo Results in Diabetic Rats of Insulin-Loaded PLGA Nanoparticles. *Int. J. Pharm.* **2012**, *437*, 213–220.

(36) Chen, H.; Kim, S.; Li, L.; Wang, S.; Park, K.; Cheng, J. Release of Hydrophobic Molecules from Polymer Micelles into Cell Membranes Revealed by Förster Resonance Energy Transfer Imaging. **2008**, *105*.

(37) Sunoqrot, S.; Bae, J. W.; Jin, S.-E.; M Pearson, R.; Liu, Y.; Hong, S. Kinetically Controlled Cellular Interactions of Polymer-Polymer and Polymer-Liposome Nanohybrid Systems. *Bioconjug. Chem.* **2011**, *22*, 466–474.

(38) Avgoustakis, K.; Beletsi, A.; Panagi, Z.; Klepetsanis, P.; Karydas, A. G.; Ithakissios, D. S. PLGA-mPEG Nanoparticles of Cisplatin: In Vitro Nanoparticle Degradation, in Vitro Drug Release and in Vivo Drug Residence in Blood Properties. *J. Control. Release* **2002**, *79*, 123–135.

(39) Rojnik, M.; Kocbek, P.; Moret, F.; Compagnin, C.; Celotti, L.; Bovis, M. J.; Woodhams, J. H.; Macrobert, A. J.; Scheglmann, D.; Helfrich, W.; *et al.* In Vitro and in Vivo Characterization of Temoporfin-Loaded PEGylated PLGA Nanoparticles for Use in Photodynamic Therapy. *Nanomedicine (Lond).* **2012**, *7*, 663–677.

(40) García-Díaz, M.; Kawakubo, M.; Mroz, P.; Sagristà, M. L.; Mora, M.; Nonell, S.; Hamblin, M. R. Cellular and Vascular Effects of the Photodynamic Agent Temocene Are Modulated by the Delivery Vehicle. *J. Control. Release* **2012**, *162*, 355–363.

(41) Tamietti, B. F. P.; Machado, A. H. A.; Maftoum-Costa, M.; Da Silva, N. S.; Tedesco, A. C.; Pacheco-Soares, C. Analysis of Mitochondrial Activity Related to Cell Death after PDT with AlPCS(4). *Photomed. Laser Surg.* **2007**, *25*, 175–179.

(42) Bonifacino, J. S.; Traub, L. M. Signals for Sorting of Transmembrane Proteins to Endosomes and Lysosomes. *Annu. Rev. Biochem.* **2003**, *72*, 395–447.

(43) Liu, L.; Zhang, Z.; Xing, D. Cell Death via Mitochondrial Apoptotic Pathway due to Activation of Bax by Lysosomal Photodamage. *Free Radic. Biol. Med.* **2011**, *51*, 53–68.

(44) Moserova, I.; Kralova, J. Role of ER Stress Response in Photodynamic Therapy: ROS Generated in Different Subcellular Compartments Trigger Diverse Cell Death Pathways. *PLoS One* **2012**, *7*, e32972.

CHAPTER 6

General discussion

A general discussion of the entire work presented as well as a brief discussion about the future research in photodynamic therapy is comprised in this chapter.

6.1. General discussion

The results presented along the previous chapters deal with the study of biodegradable polymeric NPs as delivery vehicles for PDT. Specifically, we have explored the (α-hydroxy)-polyesters PLGA and PLA and their copolymers with PEG to form nanodelivery systems for photosensitizing agents. We have pursued: i) a better understanding of the role of both the PS and the delivery system itself on the physicochemical and photophysical properties of the PS-loaded NP suspensions; ii) the adequacy of formulating biodegradable NPs with conjugated PSs; iii) the use of active targeting strategies to enhance PS accumulation and phototoxicity in tumor cells.

Although a vast range of 2nd generation PSs with improved photophysical properties respect to Photofrin® have been developed, many of them still suffer from a low aqueous solubility or a poor selectivity for tumor tissue, therefore being indispensable their association to nanodelivery systems for their administration.[1] Among the numerous nanovehicles under study, we have chosen PLGA and PLA NPs due to their interesting properties such as their biodegradability and biocompatibility, their ability to encapsulate hydrophobic drugs, the possibility to modify their surface to introduce targeting moieties, and their approval by the FDA for therapeutic use.[2]

On a first basis we have compared bare PLGA and PEG-coated PLGA NPs as passive targeting systems for PDT. We have fist evaluated their stability in biological medium, and have observed, in agreement with previous reports,[3] that PEGylated NPs are more stable than bare PLGA NPs in a medium with a high content of proteins since PEG chains prevent protein adsorption at the surface of the NP.[4] It is thus clear that non-PEGylated NPs remain as a system for proof-of-concept studies, but PEGylation is unavoidable for *in vivo* use.

In order to evaluate the role of the vehicle on the properties of the PS-loaded NP suspensions, we compared the physicochemical, photophysical and phototoxic properties of PLGA and PEG-PLGA NPs when the model hydrophobic PS ZnTPP was physically entrapped. The inclusion of the PEG-PLGA copolymer to the formulation lead to a reduction of the NP size by the half up to ~50 nm, pointing out that micellar structures might be formed for this specific blend,[5] and it also increased the zeta potential of the PEGylated NP suspensions. ZnTPP was incorporated mainly in monomeric form in both types of NPs, although multiple populations of the excited singlet and triplet states denoted various locations of ZnTPP in the NPs. Time-resolved detection of $^1O_2$ by its NIR phosphorescence provided uncontestable evidence of the lack of ZnTPP aggregation once inside the NPs and enabled us to gain insight in the characteristics of these polymeric nanoparticle systems. We have found that PLGA and PEG-PLGA NPs are systems within which

O_2 diffusion is hampered and $^1O_2$ is largely confined (Scheme 6.1), as evidenced by the long triplet state and $^1O_2$ lifetimes. PEGylation of the NP results in an additional yet more accessible $^1O_2$ population. Due to this hampered diffusion and the presence of multiple populations of excited states, we have found that the best model to describe $^1O_2$ formation and decay kinetics is represented by Eq. 2.2, which takes into account each population of excited states forming $^1O_2$, representing the microheterogenous character of these NPs. These findings are opposed to what had been observed for micellar suspensions by Lee & Rodgers,[6] where the observed $^1O_2$ lifetime was an average of that in the various compartments due to a fast $^1O_2$ diffusion between them (Scheme 6.1). Despite the confinement of $^1O_2$ in PLGA or PEG-PLGA polymeric NPs, both induced HeLa cell death by apoptosis after photodynamic treatment, although PEGylated NPs induced a faster and superior mortality in agreement with the observation of faster $^1O_2$ kinetics in HeLa cells for ZnTPP delivered by PEGylated NPs.

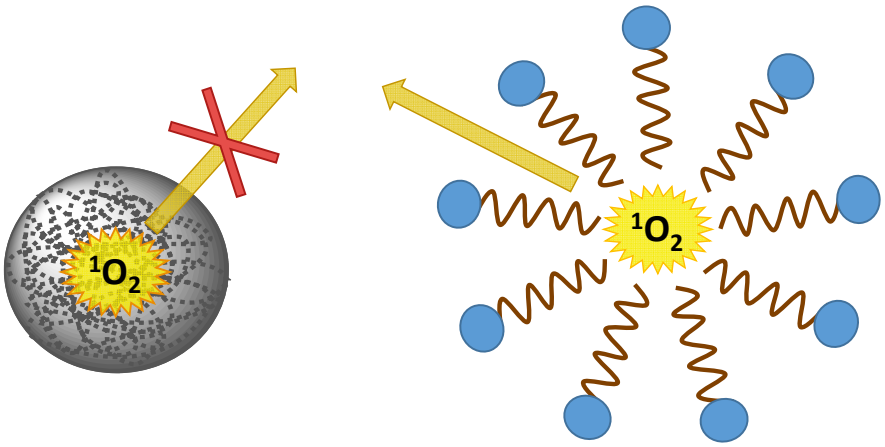

Scheme 6.1. Representation of the diffusion of $^1O_2$ in PLGA NPs or micelles.

In order to assess the suitability of a certain nanocarrier system for PDT, it is also important to understand how the photophysical properties of the PS may become altered upon encapsulation.[7] Besides the metallated ZnTPP, we have also incorporated in PEGylated NPs the clinically approved free-base porphyrin PpIX, as well as the hydrophobic chlorin Ppa. Although ZnTPP is still photophysically active once embedded into the NPs, both the free-base PpIX and Ppa become completely aggregated. A similar pattern had been previously observed for the encapsulation of metallated and free-base porphyrins into liposomes,[8] concluding that the presence of the metal central ion in the porphyrin structure prevented the formation of large aggregated supramolecular structures and consequently favored a higher percentage of encapsulation in the lipid bilayers. This observation seems to hold true for our polymeric

nanostructures, since PpIX and Ppa also presented a lower entrapment efficiency than ZnTPP. Moreover, some previous studies of free-base porphyrins encapsulated in PLGA or PLA NPs had also shown certain aggregation of the encapsulated PS.[9] Notwithstanding, another group has reported the incorporation of PpIX into polymeric micelles of PCL-PEG, and they have found no appreciable aggregation of this PS inside such micelles.[10] The reason of this difference could be the higher hydrophobic nature of the PCL polymer. Altogether, the reported results indicate that the chemical structure of the PS and also of the nanocarrier exert a profound effect on the final physicochemical properties of the NP suspension.

Delivery vehicles in PDT initially emerged as a means of overcoming water solubility and aggregation of the hydrophobic PSs. Therefore, it has traditionally been thought that an adequate nanocarrier for a PS should preserve the photophysical activity of the embedded PS, i.e. its capacity of photosensitizing $^1O_2$.[11] We have shown, though, that in the case of physically entrapped PSs in biodegradable PEG-PLGA or PEG-PLA NPs, the aggregated PpIX and Ppa recover its monomeric form and photosensitizing properties once released from the NP to an organic solvent. Given that a large number of cellular structures have lipidic regions, it is plausible that these PSs will exist as monomers inside the cells. Indeed, Ppa delivered by PEG-PLA NPs induces an important phototoxic effect in U-87 MG cells, corroborating that the key step is the intracellular delivery of the PS in monomeric form. Indeed, some approaches such as molecular beacons to keep the PS inactive until it reaches its intracellular target are currently under study,[12] which supports the idea that the aggregation of the PS inside a biodegradable nanocarrier might in fact be advantageous to avoid undesired phototoxicity until the nanocarrier reaches its target.

The aim of synthesizing PS-conjugated NPs responded to a double objective: on one hand, the exploration of a methodology that had not been previously reported for the encapsulation of PSs in biodegradable PLGA NPs; on the other hand, deepening on the role of the chemical nature of the PS on its location in the NP and its influence on the properties of the NP suspension. Conjugation of the hydrophobic ZnTPP and the hydrophilic ZnTriMPyP to PLGA was accomplished by CuAAC, and NPs with various percentages of the conjugates with the copolymer PEG-PLGA could be obtained. Both PSs remained mainly in monomeric form in the NPs and were able to photosensitize $^1O_2$, yet its kinetics of formation and decay were remarkably different: the hydrophilic ZnTriMPyP showed fast $^1O_2$ production and kinetics according to its location at the external surface of the NP, whilst ZnTPP showed slower $^1O_2$ kinetics as previously observed for ZnTPP-loaded PEG-PLGA NPs, confirming its localization inside the PLGA core. Despite the ability of both PSs to generate $^1O_2$, we were unable to induce any phototoxicity in

HeLa cells *in vitro*. This striking finding drove us to the conclusion that PEG-PLGA NPs might not be internalized by HeLa cells and therefore, would be unable to deliver their cargo when the PSs are covalently conjugated to the NP (Scheme 6.2). Numerous publications have addressed the internalization of PLGA or PEG-PLGA NPs, the vast majority of them suggesting that PLGA or PEG-PLGA NPs are internalized by endocytosis.[13–16] However, a thorough analysis of these reports evidences that most of these studies have relied on the assumption that the physically entrapped fluorophore used to track the NP would remain entrapped during cell internalization and would be indicative of the NP fate inside the cell, without considering that the fluorophore might actually leak from the NP and follow an independent pathway of internalization. Therefore, it may be advisable to covalently conjugate the fluorophore labels to the NPs to be sure that the fluorophore remains attached to the NP and reports its trafficking. Two publications have addressed this issue comparing the uptake of PLGA and PEG-PLGA NPs with conjugated or physically entrapped fluorophores;[17,18] they have observed no intracellular fluorescence when the NPs are covalently labeled, emphasizing the absence of internalization of PLGA or PEG-PLGA NPs, and have proposed a contact-based transfer between the NP and the cellular membrane as the mechanism of drug delivery to the cell.

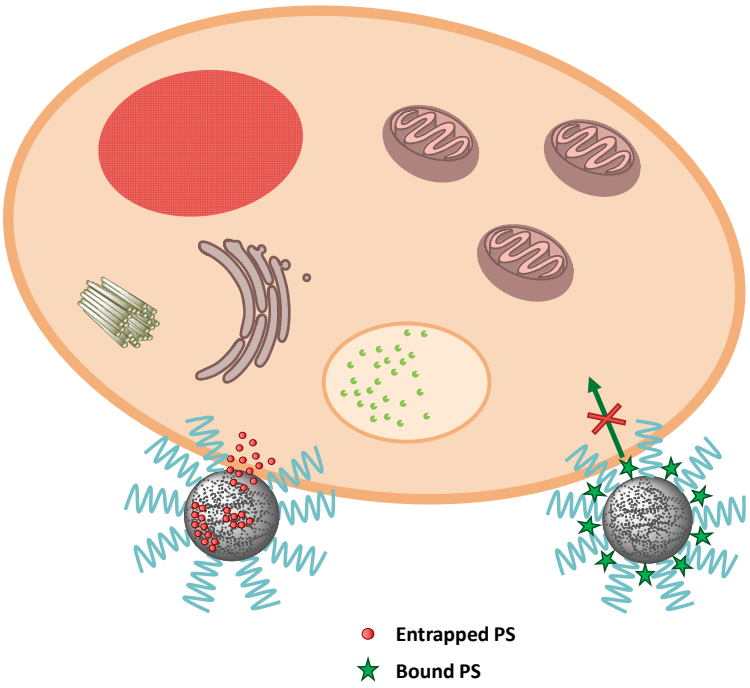

Scheme 6.2. Representation of the release of the cargo of PEG-PLGA NPs into a cell. An entrapped PS is released at the cell surface, whereas a bound PS does not cross the cellular membrane.

In the light of these observations, our own results also suggest that neither PLGA nor PEG-PLGA NPs are internalized by cells (Scheme 6.2). On one hand, the lack of phototoxicity for PS-conjugated PEG-PLGA NPs would clearly support this notion since such NPs do indeed release $^1O_2$. In the case of ZnTPP-loaded NPs, the lysosomal subcellular localization of ZnTPP as well as the different $^1O_2$ formation and decay kinetics when HeLa cells were incubated with bare PLGA or with PEG-PLGA NPs confirm internalization of the PS. Taken together, both observations are consistent with a model in which the NPs stick to the cell membrane and release the entrapped PS there, which is subsequently internalized. However, if the PS is covalently bound to the NP it cannot be uptaken by the cell (Scheme 6.2).

Another desired feature of drug delivery systems is to enhance accumulation of the drug in the diseased tissue while avoiding drug distribution in healthy organs. Active targeting of the nanocarriers with moieties that selectively bind to overexpressed receptors in diseased tissue is an area in continuous expansion.[19] With the objective of enhancing not only drug delivery but also the phototoxic response in cancer cells, we have evaluated a series of cRGD-targeted PLA NPs incorporating the chlorin Ppa. The conjugation of the peptide through a PEG spacer is vital to enhance cellular internalization of Ppa respect to non-targeted NPs. Although cRGD-PEG-PLA NPs show a higher intracellular concentration of Ppa compared to the controls, the phototoxicity induced by the targeted NPs in receptor positive U-87 MG cells was comparable to that of non-targeted NPs. This observation could be attributed to a possibly different subcellular localization of the PS in the two cases.[20] Alternatively, one may suggest that receptor-mediated endocytosis internalizes the NP as a whole, in which the PS remains entrapped in a photoinactive form owing to aggregation until it is (slowly) released. A modest increased internalization of the drug or PS delivered by cRGD-targeted NPs has also been reported by other authors,[21–24] indicating that non-specific internalization mechanisms of the NPs or the drug are competing with the receptor-mediated internalization of the targeted NPs. Overall, cRGD-targeted PEG-PLA NPs are promising delivery systems for PDT although they need further optimization.

6.2. Future perspectives

Almost 30 years after the first PDT clinical trial with Photofrin®, PDT has largely evolved as a treatment modality but there is still much research to do in order to situate it among the preferential anticancer treatments.

Numerous 2nd generation PSs improving many of the drawbacks of hematoporphyrin derivative have been developed over the years, yet meeting all the characteristics of the ideal PS is rather rare. 3rd generation PSs have been designed with the main goals of overcoming aqueous solubility and enhancing selectivity for the diseased tissue. Although relevant advances have been made in this field, resulting in clinically approved formulations (Foslip® and Visudyne®),[25,26] further optimization is needed for developing therapeutics with enhanced selectivity for tumor tissue or vasculature.

The work carried out in this thesis evidences the importance of a thorough characterization and understanding of the physicochemical and photophysical features of 3rd generation PSs as well as of its internalization mechanisms and drug release to the cell, and further research should consider to do a step forward in the elucidation of these mechanisms for PLGA or PLA NPs, either bare or PEGylated. Targeted NPs should also be better characterized regarding their uptake mechanism as it might depend on the target receptor,[27] and the optimization of the vehicles might consider trying to avoid their non-specific internalization. Future work is also necessary to ascertain if the comparable phototoxicity achieved by non-targeted vehicles despite their lower drug delivery is due to a different subcellular localization of the PS or if there are other processes involved.

Additional selectivity of the delivery systems seems to be linked to the development of activatable PSs, which comprise the use of scaffolds for quenching the photophysical properties of the PS but which become degraded in contact with specific enzymes present in the target tissue.[12,28] Similarly, the development of photo-triggered nanocarriers[29] which can become activated by a photo-isomerization[30] or by light-to-heat conversion in gold NPs[31] are only a few examples of this innovative and expanding field.

Another strategy to improve PDT efficacy is its combination with other anticancer therapies. One of the most relevant approaches is PCI, a treatment modality that exploits the damage exerted by a PS in lysosomal membranes to translocate other drugs from the endo/lysosomes to the cytosolic space. Various studies have reported the benefits of this therapy in multi-drug resistance cancerous cell lines,[33] pointing out that PCI may become a promising anticancer therapy in the near future.

6.3. References

(1) Josefsen, L. B.; Boyle, R. W. Photodynamic Therapy and the Development of Metal-Based Photosensitisers. *Met. Based. Drugs* **2008**, *2008*, 1–23.

(2) Acharya, S.; Sahoo, S. K. PLGA Nanoparticles Containing Various Anticancer Agents and Tumour Delivery by EPR Effect. *Adv. Drug Deliv. Rev.* **2011**, *63*, 170–183.

(3) Avgoustakis, K.; Beletsi, A.; Panagi, Z.; Klepetsanis, P.; Livaniou, E.; Evangelatos, G.; Ithakissios, D. S. Effect of Copolymer Composition on the Physicochemical Characteristics, in Vitro Stability, and Biodistribution of PLGA–mPEG Nanoparticles. *Int. J. Pharm.* **2003**, *259*, 115–127.

(4) Owens, D. E.; Peppas, N. a. Opsonization, Biodistribution, and Pharmacokinetics of Polymeric Nanoparticles. *Int. J. Pharm.* **2006**, *307*, 93–102.

(5) Letchford, K.; Burt, H. A Review of the Formation and Classification of Amphiphilic Block Copolymer Nanoparticulate Structures: Micelles, Nanospheres, Nanocapsules and Polymersomes. *Eur. J. Pharm. Biopharm.* **2007**, *65*, 259–269.

(6) Lee, P. C.; Rodgers, M. A. J. Singlet Molecular Oxygen in Micellar Systems. 1. Distribution Equilibria between Hydrophobic and Hydrophilic Compartments. *J. Phys. Chem.* **1983**, *87*, 4894–4898.

(7) Bechet, D.; Couleaud, P.; Frochot, C.; Viriot, M.-L.; Guillemin, F.; Barberi-Heyob, M. Nanoparticles as Vehicles for Delivery of Photodynamic Therapy Agents. *Trends Biotechnol.* **2008**, *26*, 612–621.

(8) Postigo, F.; Mora, M.; de Madariaga, M. A.; Nonell, S.; Sagrista, M. L. Incorporation of Hydrophobic Porphyrins into Liposomes: Characterization and Structural Requirements. *Int. J. Pharm.* **2004**, *278*, 239–254.

(9) Vargas, A.; Lange, N.; Arvinte, T.; Cerny, R.; Gurny, R.; Delie, F. Toward the Understanding of the Photodynamic Activity of M-THPP Encapsulated in PLGA Nanoparticles: Correlation between Nanoparticle Properties and in Vivo Activity. *J. Drug Target.* **2009**, *17*, 599–609.

(10) Li, B.; Moriyama, E. H.; Li, F.; Jarvi, M. T.; Allen, C.; Wilson, B. C. Diblock Copolymer Micelles Deliver Hydrophobic Protoporphyrin IX for Photodynamic Therapy. *Photochem. Photobiol.* **2007**, *83*, 1505–1512.

(11) Konan, Y. N.; Gurny, R.; Allémann, E. State of the Art in the Delivery of Photosensitizers for Photodynamic Therapy. *J. Photochem. Photobiol. B.* **2002**, *66*, 89–106.

(12) Liu, T. W. B.; Chen, J.; Zheng, G. Peptide-Based Molecular Beacons for Cancer Imaging and Therapy. *Amino Acids* **2011**, *41*, 1123–1134.

(13) Panyam, J.; Labhasetwar, V. Biodegradable Nanoparticles for Drug and Gene Delivery to Cells and Tissue. *Adv. Drug Deliv. Rev.* **2003**, *55*, 329–347.

(14) Qaddoumi, M. G.; Gukasyan, H. J.; Davda, J.; Labhasetwar, V.; Kim, K.-J.; Lee, V. H. L. Clathrin and Caveolin-1 Expression in Primary Pigmented Rabbit Conjunctival Epithelial Cells: Role in PLGA Nanoparticle Endocytosis. *Mol. Vis.* **2003**, *9*, 559–568.

(15) Cartiera, M. S.; Johnson, K. M.; Rajendran, V.; Caplan, M. J.; Saltzman, W. M. The Uptake and Intracellular Fate of PLGA Nanoparticles in Epithelial Cells. *Biomaterials* **2009**, *30*, 2790–2798.

(16) Rojnik, M.; Kocbek, P.; Moret, F.; Compagnin, C.; Celotti, L.; Bovis, M. J.; Woodhams, J. H.; Macrobert, A. J.; Scheglmann, D.; Helfrich, W.; *et al.* In Vitro and in Vivo Characterization of

Temoporfin-Loaded PEGylated PLGA Nanoparticles for Use in Photodynamic Therapy. *Nanomedicine (Lond).* **2012**, *7*, 663–677.

(17) Chen, H.; Kim, S.; Li, L.; Wang, S.; Park, K.; Cheng, J. Release of Hydrophobic Molecules from Polymer Micelles into Cell Membranes Revealed by Förster Resonance Energy Transfer Imaging. **2008**, *105*.

(18) Xu, P.; Gullotti, E.; Tong, L.; Highley, C. B.; Errabelli, D. R.; Hasan, T.; Cheng, J.-X.; Kohane, D. S.; Yeo, Y. Intracellular Drug Delivery by Poly(lactic-Co-Glycolic Acid) Nanoparticles, Revisited. *Mol. Pharm.* **2009**, *6*, 190–201.

(19) Danhier, F.; Pourcelle, V.; Marchand-Brynaert, J.; Jérôme, C.; Feron, O.; Préat, V. Targeting of Tumor Endothelium by RGD-Grafted PLGA-Nanoparticles. *Methods Enzymol.* **2012**, *508*, 157–175.

(20) Conway, C. L.; Walker, I.; Bell, A.; Roberts, D. J. H.; Brown, S. B.; Vernon, D. I. In Vivo and in Vitro Characterisation of a Protoporphyrin IX-Cyclic RGD Peptide Conjugate for Use in Photodynamic Therapy. *Photochem. Photobiol. Sci.* **2008**, *7*, 290–298.

(21) Danhier, F.; Vroman, B.; Lecouturier, N.; Crokart, N.; Pourcelle, V.; Freichels, H.; Jérôme, C.; Marchand-Brynaert, J.; Feron, O.; Préat, V. Targeting of Tumor Endothelium by RGD-Grafted PLGA-Nanoparticles Loaded with Paclitaxel. *J. Control. Release* **2009**, *140*, 166–173.

(22) Liu, P.; Qin, L.; Wang, Q.; Sun, Y.; Zhu, M.; Shen, M.; Duan, Y. cRGD-Functionalized mPEG-PLGA-PLL Nanoparticles for Imaging and Therapy of Breast Cancer. *Biomaterials* **2012**, *33*, 6739–6747.

(23) Wang, Z.; Chui, W.-K.; Ho, P. C. Design of a Multifunctional PLGA Nanoparticulate Drug Delivery System: Evaluation of Its Physicochemical Properties and Anticancer Activity to Malignant Cancer Cells. *Pharm. Res.* **2009**, *26*, 1162–1171.

(24) Selvestrel, F.; Moret, F.; Segat, D.; Woodhams, J. H.; Fracasso, G.; Echevarria, I. M. R.; Baù, L.; Rastrelli, F.; Compagnin, C.; Reddi, E.; *et al.* Targeted Delivery of Photosensitizers: Efficacy and Selectivity Issues Revealed by Multifunctional ORMOSIL Nanovectors in Cellular Systems. *Nanoscale* **2013**, *5*, 6106–6116.

(25) Kiesslich, T.; Berlanda, J.; Plaetzer, K.; Krammer, B.; Berr, F. Comparative Characterization of the Efficiency and Cellular Pharmacokinetics of Foscan- and Foslip-Based Photodynamic Treatment in Human Biliary Tract Cancer Cell Lines. *Photochem. Photobiol. Sci.* **2007**, *6*, 619–627.

(26) Christie, J. G.; Kompella, U. B. Ophthalmic Light Sensitive Nanocarrier Systems. *Drug Discov. Today* **2008**, *13*, 124–134.

(27) Hillaireau, H.; Couvreur, P. Nanocarriers' Entry into the Cell: Relevance to Drug Delivery. *Cell. Mol. Life Sci.* **2009**, *66*, 2873–2896.

(28) Gabriel, D.; Zuluaga, M. F.; Lange, N. On the Cutting Edge: Protease-Sensitive Prodrugs for the Delivery of Photoactive Compounds. *Photochem. Photobiol. Sci.* **2011**, *10*, 689–703.

(29) Rai, P.; Mallidi, S.; Zheng, X.; Rahmanzadeh, R.; Mir, Y.; Elrington, S.; Khurshid, A.; Hasan, T. Development and Applications of Photo-Triggered Theranostic Agents. *Adv. Drug Deliv. Rev.* **2010**, *62*, 1094–1124.

(30) Barhoumi, A.; Kohane, D. S. *Light-Controlled Nanoparticulate Drug Delivery Systems*; Hamblin, M. R.; Avci, P., Eds.; Elsevier, 2015.

(31) Kah, J. C. Y.; Yeo, E. L. L.; He, S.; Engudar, G. *Gold Nanorods in Photomedicine*; Hamblin, M. R.; Avci, P., Eds.; Elsevier, 2015.

(32) Kelkar, S. S.; Reineke, T. M. Theranostics: Combining Imaging and Therapy. *Bioconjug. Chem.* **2011**, *22*, 1879–1903.

(33) Weyergang, A.; Berstad, M. E. B.; Bull-Hansen, B.; Olsen, C. E.; Selbo, P. K.; Berg, K. Photochemical Activation of Drugs for the Treatment of Therapy-Resistant Cancers. *Photochem. Photobiol. Sci.* **2015**.

CHAPTER 7

Conclusions

Conclusions

1. Poly-(*D,L*-lactide-*co*-glycolide) (PLGA) nanoparticles have been scrutinized as potential vehicles for hydrophobic photosensitizers in photodynamic therapy. Addition of the copolymer poly-(ethylene glycol)-poly-(*D,L*-lactide-*co*-glycolide) (PEG-PLGA) enhances their stability in biological medium, increases the permeability of the nanoparticle to oxygen, the release of the photosensitizer into the cell, and the phototoxic effect exerted by the photodynamic drug on HeLa cancer cells.

2. Unlike other vehicles, singlet oxygen generated within PLGA and to a lesser extent, within PEG-PLGA nanoparticles, remains confined within it, which keeps the photodynamic drug harmless until it is released from the nanoparticles. Therefore fulfilment of the phototoxic potential of the drug requires its previous release from the nanoparticles.

3. The chemical structure of the photosensitizer determines its state inside the PLGA nanoparticles. Thus, metallated porphyrins are entrapped in monomeric form, whereas free-base porphyrins and chlorins aggregate within the nanoparticle, which further prevents their phototoxicity while incorporated. Notwithstanding, their photosensitizing ability is restored when they are released from the nanoparticles.

4. Comparison of the phototoxicity results obtained with covalently-bound and occluded photosensitizers indicates that the nanoparticles are not internalized by HeLa cells but release the entrapped cargo at the cell surface for subsequent internalization. PS molecules covalently bound to the nanoparticle do not enter the cells.

5. Surface modification of PEG-PLA nanoparticles with the peptide cRGDfK is a successful strategy to promote a higher internalization of entrapped PSs in cells that overexpress $\alpha_v\beta_3$ receptors, however there is no parallel increase in phototoxicity.

List of abbreviations

ACN	Acetonitrile
CR	Cremophor EL
CuAAC	Cu(I)-catalyzed azide-alkyne cycloaddition
EDC	1-ethyl-3-(3-dimethylaminopropyl)carbodiimide
DCM	Dichloromethane
DMF	Dimethylformamide
DMSO	Dimethyl sulfoxide
FBS	Fetal Bovine Serum
NIR	Near-infrared
NHS	*N*-hydroxysuccinimide
DBCO-NH_2	Dibenzocyclooctyne-amine
DIPEA	*N,N*-diisopropylethylamine
dPBS	D_2O-based PBS
HpD	Hematoporphyrin derivative
Hyp	Hypericin
NP	Nanopartice
NaN_3	Sodium azide
PpIX	Protoporphyrin IX
Ppa	Pyropheophorbide a
PCI	Photochemical internalization
PDT	Photodynamic therapy
PEG	Poly-(ethylene glycol)
PLGA	Poly-(*D,L*-lactide-*co*-glycolide)
PLA	Poly-(*D,L*-lactide)
PGA	Poly-(glycolide)

PS	Photosensitizer
RES	Reticuloendothelial system
ROS	Reactive oxygen species
TEA	Triethylamine
TFA	Trifluoroacetic acid
Tg	Glass transition temperature
THF	Tetrahydrofuran
TMPyP	5,10,15,20-tetrakis(*N*-methyl-4-pyridyl)-21*H*,23*H*-porphine
TriMPyP	5-phenyl-10, 15, 20-tri-(*N*-methyl-4-pyridyl)-21*H*,23*H*-porphine
UHPLC	Ultra-High Performance Liquid Chromatography
ZnTriMPyP	5-[4-Azidophenyl]-10,15,20-tri-(*N*-methyl-4-pyridinium)porphyrinato zinc (II) trichloride
ZnTPP	Zn(II)-tetraphenylporphine
^{1}H-NMR	Proton nuclear magnetic resonance
$^1O_2$	Singlet oxygen

List of publications:

- Boix-Garriga, E.; Acedo, P.; Casadó, A.; Villanueva, A.; Stockert, J. C.; Cañete, M.; Mora, M.; Sagristá, M. L.; Nonell, S. *Poly(D,L-lactide-co-glycolide) nanoparticles as delivery agents for photodynamic therapy: enhancing singlet oxygen release and phototoxicity by surface PEG coating.* Nanotechnology, 2015, 26, 365104 (16pp). DOI: 10.1088/0957-4484/26/36/365104
- Planas, O.; Boix-Garriga, E.; Rodríguez-Amigo, B.; Torra, J.; Bresolí-Obach, R.; Flors, C.; Viappiani, C.; Agut, M.; Ruiz-González, R.; Nonell, S. (2015). *Newest approaches to singlet oxygen photosensitisation in biological media.* In Photochemistry, 42, 233–278. Fasani, E.; Albini, A. (Ed.). RSC, Cambridge. Print ISBN: 978-1-84973-956-6. DOI: 10.1039/9781782624547-00233
- Boix-Garriga, E.; Rodríguez-Amigo, B.; Planas, O.; Nonell, S. (2015). *Properties of Singlet Oxygen.* In Singlet Oxygen: Applications in biosciences and nanosciences, Chapter 2. Nonell, S.; Flors, C. (Ed.) RSC Publishing. ISSN: 2041-9716 (In press)

Communications in Schools and Congresses:

- Boix, E.; Nonell, S.; Sagristá, M.L.; Mora, M. *Preparation, characterization and in vitro photodynamic activity of ZnTPP loaded PLGA nanoparticles.* 2nd Photobiology School of the European Society for Photobiology, Bressanone (Italia), June 18-23, 2012
- Boix, E.; Nonell, S.; Sagristá, M.L.; Mora, M. *Influence of polyethyleneglycol side chains on oxygen and drug permeability of PLGA nanoparticles*. 15th Congress of the European Society for Photobiology, Liège (Belgium), September 2–6, 2013
- Boix-Garriga, E.; Nonell, S.; Sagristá, M.L.; Mora, M. *Singlet oxygen generation by Zn(II)-tetraphenylporphine in poly(D,L-lactide-co-glycolide) nanoparticles: temperature and polyethyleneglycol side-chain effects.* XXV IUPAC Symposium on Photochemistry, Bordeaux (France), July 13-18, 2014
- Boix-Garriga, E.; Lange, N.; Nonell, S.; Sagristá, M.L.; Mora, M. *PLA targeted nanoparticles for photodynamic therapy.* 16th Congress of the European Society for Photobiology, Aveiro (Portugal), August 31–September 4, 2015